The copyright of this thesis vests in the author. No quotation from it or information derived from it is to be published without full acknowledgement of the source. The thesis is to be used for private study or non-commercial research purposes only.

Published by the University of Cape Town (UCT) in terms of the non-exclusive license granted to UCT by the author.

University of Cape Town

RECONSTRUCTION OF INDUSTRIAL PIPING INSTALLATIONS FROM LASER POINT CLOUDS USING PROFILING TECHNIQUES

By

Willard T. Mapurisa

March 2009

Supervisor: Dr George Sithole

University of Cape Town

Submitted to the University of Cape Town in fulfilment of the requirements for a MSc Degree in Engineering

Department of Geomatics

ABSTRACT

As-built models of industrial piping installations are essential for planning applications in industry. Laser scanning has emerged as the preferred data acquisition method of as built information for creating these three dimensional (3D) models. The product of the scanning process is a cloud of points representing scanned surfaces. From this point cloud, 3D models of the surfaces are reconstructed .Most surfaces are of piping elements e.g. straight pipes, t-junctions, elbows, spheres.

The automatic detection of these piping elements in point clouds has the greatest impact on the reconstructed model. Various algorithms have been proposed for detecting piping elements in point clouds. However, most algorithms detect cylinders (straight pipes) and planes which make up a small percentage of piping elements found in industrial installations. In addition, these algorithms do not allow for deformation detection in pipes. Therefore, the work in this research is aimed at the detection of piping elements (straight pipes, elbows, t-junctions and flange) in point clouds including deformation detection.

An efficient way of detecting piping elements is to first segment the point cloud. This reduces the overall time required for detecting and classifying elements. A segmentation algorithm is therefore proposed. The segmentation algorithms works by detecting discontinuities encountered where piping elements are connected. The discontinuities are introduced by flanges or abrupt changes in radius. A variation of the scan line based segmentation is employed whereby scan planes, referred to as profiles, are recreated on the point set in many different directions. By identifying changes in curvature along profiles, segments are defined. This segmentation approach allows for the detection of most piping elements including flanges.

The detection algorithm is based on detecting ellipses in point clouds. The ellipses are formed from the intersection of profiles and piping elements. Most piping elements result from Boolean operations on basic geometric shapes namely cylinders, spheres, cones and tori. These primitives form ellipses when they intersect with planes. This is the concept used in the algorithm. These ellipses have properties that are then used in determining the parameters for the primitives. For most geometric primitives, the

University of Cape Town

centres of the ellipses lie on the axis of the primitive. The minor axis of the ellipse can be used to approximate the radius of the primitive. By stacking profiles in such that they are contiguous on a point set and detecting ellipses, the axis of primitives are traced out by the ellipse centres. This gives the position and orientation of the primitives' axis. The radius is then approximated using the minor axes of the ellipse. Deformations in pipes cause the ellipse centres to deviate from the axis. Identifying the deviations in centres from the axis, deformations are also detected.

The results from the detection are a set of centres representing the position and orientation of the primitives' axis, and a radius value for each primitive. The radii values for the primitives are then used in the classification of the piping elements which they constitute. The results from the research can be used for various applications. This includes selecting CSG models based on the classification, approximating initial estimates for surface fitting, detecting deformations in pipes, clash detections and solving path problems in piping installations.

University of Cape Town

Plagiarism Declaration

1. I know that plagiarism is wrong. Plagiarism is using another's work and to pretend that it is my own

2. I have used the Harvard convention for citation and referencing. Each significant contribution to, and quotation in, this project, from the work, or works of other people has been attributed and has been cited and referenced.

3. This project is my own

4. I have not allowed, and will not allow, and will not allow anyone to copy my work with the intention of passing it off as his or her own work.

University of Cape Town

Signed: _____

Willard T Mapurisa

University of Cape Town

March, 2009

ACKNOWLEDGEMENT

Firstly, I would like to thank my supervisor, Dr George Sithole, for offering me the opportunity to conduct this research. Through the constructive advice and guidance, I was able to carry out my research.

Secondly, I would like to thank GeoSystems Africa for providing the data that was used in the research.

I would like to thank my family and close friends who were there to support and encourage me through tough times.

I would also like to thank the Geomatics staff for their support.

University of Cape Town

Contents

University of Cape Town

University of Cape Town

LIST OF FIGURES

University of Cape Town

University of Cape Town

University of Cape Town

University of Cape Town

LIST OF TABLES

University of Cape Town

University of Cape Town

1. Introduction

1.1 Background

Planning applications for industrial piping installations require accurate as-built Computer Aided Design (CAD) models. These applications, which include upgrading, safety standard concern and maintenance work, result in frequent modification of existing installations. Accurate, up to date CAD models of the installations are therefore required. The three dimensional (3D) CAD models are reconstructed using data acquired by three main techniques namely field survey methods, close range photogrammetry and in recent years Laser Scanning.

Data acquired by Laser Scanning is a cloud of 3D points and usually numbers in the millions. These point samples represent scanned surfaces. Most surfaces found in installations are of piping elements which are mainly elbows, t-junctions, straight pipes and flanges. From the point cloud, the 3D models of the surfaces are then reconstructed. Because of the large data size produced from the scanning process, the reconstruction process must be automated.

Before a model is reconstructed, the point data is pre-processed. This pre-processing includes tasks such as registration and noise filtering. Multiple scans are usually required for a single object. These scans are brought into the same reference frame in the registration process. In noise filtering, outliers are identified and removed from the point cloud. Segmentation and detection/fitting is then carried out on the processed data. In segmentation, points from similar surfaces are identified and given the same label. Detection is carried out on the segments in order to identify the type of surface represented by each of the segments. The final model is then generated based on the detection results.

Segmentation and detection have the greatest impact on the resulting model. The correctness of a model depends on the results from these two processes. Errors carried over from detection and segmentation procedures will affect the quality of a model.

University of Cape Town

This research will therefore be focused on the segmentation and detection of piping primitives for modelling purposes.

Various algorithms have been presented that reconstruct piping installations. However, the area remains one of ongoing research. The main concern in this research is increasing automation of the reconstruction process. This is the main motivation of research

1.2 Brief history

Before the advent of laser scanning, as-built information was acquired by manual tape measurements, tachometry and surveying through the use of theodolites. This information was stored as two dimensional (2D) plan drawings. Frequent revamp and modifications of piping installations result in out of date plans (Tangelder et al., 1999). Updating the drawings was time consuming because the data acquisition methods were slow. This resulted in industries shutting down for long periods in order to implement changes to piping installations. In addition to the measurement methods mentioned above, photogrammetry was also used to acquire as-built data (Veldhuis and Vosselman, 1998). However, it was mainly used for 3D point measurement (van den Heuvel, 2000, p. 853).

After the introduction of CAD in the 1950s, drawings were stored in a digital environment. Consequently, editing and updating was now easier even though the drawings were still presented in a 2D format. CAD capabilities were further enhanced with the introduction of 3D wireframes. Three dimensional CAD models of piping installations could now be reconstructed on a CAD system. The advancement in the field of CAD led to the integration with photogrammetry (van den Heuvel, 2000, p.853). CAD models of piping installations could now be built using a combination of CSG models and images (Tangelder et al., 1999; Vosselman, 2001). This integration led to further research into better modelling techniques. Various techniques for reconstruction from images and CAD models have been presented. Typical examples are presented in Tangelder et al. (2000, 2003). Trends in CAD based photogrammetric measurements are presented by van den Heuvel (2000).

University of Cape Town

As a result of the advances in modelling systems, the need for accurate pipe models increased .The process of planning applications was made easier increasing productivity. The introduction of Laser Scanning led to better reconstruction techniques due to the geometric information provided by the scanners. Data collection was now fast and models could be produced in real time.

Laser scanning is now being integrated with existing techniques in order to obtain more accurate models (Rabbani et al., 2004). However, better reconstruction techniques for modelling piping installations are still being sought. This is the major motivating factor for research in this area.

1.3 Previous work

Considerable work has been done in the reconstruction of piping installations from point clouds. Most of the work has been focused on segmentation and detection of geometric primitives[1] (Rabbani and van den Heuvel, 2004; Rabbanni et al., 2005; Schnabel et al., 2007; Chaperon and Goulette, 2001; Werghi et al. 1999). This is because the accuracy of the reconstructed model depends on the segmentation and detection processes. According to Rabbanni et al. (2005), detection algorithms can be classified into two: the first class requires segmentation before detection. In the second, the point cloud is processed without segmentation. Detection methods which require segmentation generally use surface fitting methods for object detection (Lukacs et al., 1997; Werghi et al., 1999). Methods which do not require prior segmentation generally employ robust fitting methods which are the Hough Transform (Rabbani and van den Heuvel, 2004; Rabbanni et al. 2005) or Random Sample Consensus (RANSAC) based techniques (Chaperon et al. 2001; Schnabel, Wahl and Klein, 2007; Holies and A.Fischler, 1981). Hough based techniques generally detect cylinders and planes while RANSAC techniques iteratively searches for points which best fits the required primitive. A more detailed discussion on existing segmentation and detection algorithms is given in chapter 3.

[1] These primitives are usually cylinders, cones, tori and spheres

University of Cape Town

1.4 Research methods and objectives

The objective of this research is to come up with an algorithm that semi-automatically or automatically detects piping elements in a point cloud. These piping elements are mainly straight pipes, pipe bends or elbows, t-junctions and flanges. The piping elements usually result from Boolean operations on cylinders, cones, spheres and tori. The algorithm must be robust and able to work with different types of point sets of industrial installations. In order to come up with the algorithm, the research was subdivided into three parts as listed below.

i. Study of current detection algorithms

ii. Design and implementation of the detection algorithm

iii. Quantitative analysis of algorithm.

1.4.1 Study of current detection algorithms

The first part of the research involves a study of the processes involved in reconstruction with the main focus on detection. Firstly, the processes are discussed together with current algorithms used. The aim is to identify the impact of each stage on the final reconstruction. Problem areas with current detection algorithms are also identified in this study which is outlined in Chapter 3. From this study, areas of improvements are identified.

1.4.2 Design and implementation of the detection algorithm

The study in Chapter 3 identifies the problems with current detection algorithms. A new detection algorithm is developed focusing on the problem areas identified. The algorithm proposed is based on some existing and new techniques. The steps involved in this design are discussed in the sub sections below.

Segmentation of Terrestrial Laser scanner Pipe Data

An efficient way of detecting piping elements is to first segment the data. This eliminates the task of continuously searching for piping elements in a point set. The different piping elements are presented as segments and fitting is done to the required segments. This also eliminates the need of carrying out point by point classification as points are classified as a cluster. This reduces the execution time of the algorithm.

University of Cape Town

Therefore, the detection algorithm proposed will incorporate a segmentation algorithm. Some detection algorithms do not require a prior segmentation of the point cloud. The downside is that more time is taken in the detection process (e.g. Hough transform).

Piping installations consist of connected piping elements. The main challenge with segmentation of pipe data is establishing the different piping elements' segments. Most algorithms use a surface or curve fitting approach in defining the different segments (Luckas, Martin and Marshall, 1998; Attene, Falcidieno and Spagnuolo, 2006; Rabbanni et al, 2006). Another approach is to use surface discontinuity in defining segments. The assumption used is that discontinuities are encountered at segment boundaries. This is the approach used and is discussed in chapter 4.

Detection

The aim of the detection procedure is to obtain higher level information about the pipe segments. The purpose of detection is to identify piping elements from the segmented point cloud. Some algorithms detect one of the elements which are usually straight pipes (cylinders) (Chaperon and Goulette, 2001; Rabbanni and Van Den Heuvel, 2005). Other algorithms employ an iterative approach in order to detect the required primitives (e.g. RANSAC based techniques). Detecting most piping elements efficiently with no iterations would reduce the time required for the detection process. Therefore, a detection algorithm is discussed in Chapter 5 for detecting piping elements.

University of Cape Town

1.4.3 Quantitative analysis of algorithm

To assess the effectiveness of the algorithm, test data is applied. The outcome together with the quality of results is outlined in chapter 6.

1.5 Scope of research

The work in this paper is aimed at the reconstruction of industrial piping installations from laser scanned point clouds with a high degree of accuracy and reliability. An algorithm for semi-automatic or automatic detection of piping primitives from point

clouds must be developed. The results of the work should be an improvement on some of the problems cited. These are:

- Some reconstruction algorithms can only detect certain kinds of piping elements which accounts for a small percentage of piping elements. Most algorithms detect cylinders only (Chaperon and Goulette, 2001; Rabbanni and Van Den Heuvel, 2005). Even though some detect various elements, they do so one at a time (RANSAC based methods) which slows down the process.

- Most reconstruction algorithms do not allow for the detection of deformations in pipes. The algorithms assume piping elements are free of deformations (Schnabel, Wahl and Klein, 2007; Chaperon and Goulette, 2001).

- Alghorithms which employ surface or curve fitting require the estimation of parameters. These parameters are usually estimated using point normals (Pottmann et al., 2003; Liu, Pottmann and Wang, 2005). This can be a challenge when dealing with noisy data.

The algorithm proposed must therefore be able to

a) Detect all piping elements constructed from Boolean operations on four basic geometric shapes (spheres, cylinders, tori, cones)

b) Detect deformation in pipes

c) Work well in the presence of noise.

University of Cape Town

1.5.1 Assumptions about the data

Point distribution and density differ in point clouds. Assumptions must be carefully made such that they apply to all point sets. The following assumptions have been made about the data:

i. Registration of the point set has been done correctly and is accurate.
ii. Points are unstructured i.e. the arrangement of points does not form any repeating pattern.

1.6 Contribution to knowledge

The research done in the development of a new detection algorithm contributes to the field of Terrestrial Laser Scanning in the following ways:

- Segmentation algorithm – The segmentation algorithm employed uses the concept of scan line segmentation. The main advantage of the algorithm is that is does not require structured data. Scan planes can be recreated in any direction as opposed to fixed scan line direction which is usually formed in parallel lines. This allows the capture of the surface form in any direction. By analysing the form of points in scan planes, surface segments extents can be identified. Curvature is used in defining segment boundaries. The approach works on most types of point clouds and can work with 3D point data. Most scan line based algorithms work on range images and 2.5D data. The segmentation algorithm is discussed in Chapter 4.

- Detection algorithm –The detection algorithm detects most piping elements composed of any of the four geometric primitives namely cylinders, tori, spheres and cone. No information prior to the detection is needed for the algorithm. Deformations are also detected.

1.7 Outline of thesis

The thesis consists of 7 chapters. The contents of Chapter 2 to 6 have been discussed. The final chapter summarises the objectives and the results obtained. The aspects of the research that require further work are also discussed in this chapter.

University of Cape Town

2. Principles of Laser Scanning

2.1 Introduction

This chapter briefly looks at laser scanning. The aim is to understand the resulting point structure from the scanning process and its effect on segmentation and detection. Firstly, laser scanning and its core principles are briefly discussed. Next, errors encountered in the scanning process are outlined. The effects of these errors on point cloud structure are also outlined. Finally, the effects of point cloud structure on segmentation and detection are briefly discussed.

2.2 Laser scanning

Photogrammetry stands as one of the main techniques that have contributed most to the developments in 3D modelling. With better image analysis techniques being introduced, the capabilities of Photogrammetry are increasing (van den Heuvel, 2000; (Tangelder, Vosselman and van den Heuvel, 2000). The integration with other techniques has resulted in more accurate modelling techniques. However, cheaper and faster accurate methods for modelling are being sought.

In the last few decades, Laser scanning has emerged as a strong complementary tool for as-built modelling. Laser scanning is the process of obtaining three dimensional data about real world objects through the use of a laser scanner. The product of the scanning process is a cloud of points termed a point cloud. Laser scanning allows for the capture of data at sub-millimetre accuracy. Laser scanning has the following advantages:

- Vast amounts of acquired data
- Fast and cost effective
- Wide variety of applications (medicine to entertainment)
- Explicit 3D information at data acquisition

Laser scanning dates back to about thirty years but its application in 3D modelling became popular in the last two decades. The increasing use of laser technology has

University of Cape Town

introduced many research areas in relation to applications of laser scanning. These applications include deformation monitoring, heritage preservation, engineering design and topographic mapping. Examples of applications of Laser Scanning are presented by Marc et al. (2000), Bruce (2005), Chow (2007) and Norbet and Ralf (2004).

2.2.1 The Laser Scanning Process

The laser scanning process begins with selecting the object to be scanned. The scanner is setup next to the object with the object in the field of view. The scanner to object distance must be well within maximum measuring range of the scanner. The scanner then sweeps across the object in the field of view from a selected starting point making point measurements. The point spacing (resolution) depends on the range of the object from the scanner, the set angle of increment of the scanner as it sweeps across the object and the radius of the laser dot.

For large objects, a single scan is insufficient to provide point data of the entire object thus multiple scans of the object are taken from different viewpoints. These scans are then brought into the same frame of reference in the registration process.

Laser scanning comes with its problems that require careful attention. Surface reflectivity of the object affects the measuring process. Surfaces with low or high reflectivity result in less accurate distance measurements. The overall effect is a high percentage of outliers in the point cloud (Sotoodeh, 2006: p 299). Fidera et al. (2004), present a paper on the effects of reflectivity of surfaces on laser scanning.

2.2.2 Point Measurement

The distance d is used in determining point positions. If the scanner position $Sc\ \{X, Y, Z\}$ is known together with angles Θ and Φ, the position of the point p in figure 2-1 can be determined as follows:

$$Xp = X + d\cos\theta \tag{2.1}$$

University of Cape Town

$$Yp = Y + d\sin\theta \tag{2.2}$$

$$Zp = h + d\sin(90 - \emptyset) \tag{2.3}$$

Where X_p, Y_p, Z_p are coordinates for point P.

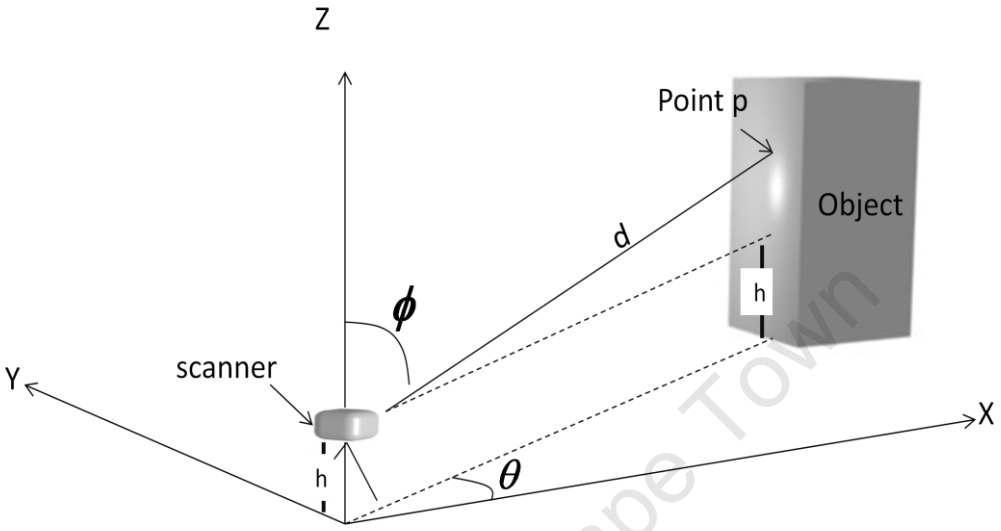

Figure 2-1 Point Measurement

University of Cape Town

2.2.3 Types of Laser Scanners

Various types of laser scanners exist, each employing different measurement principles. Most common types of terrestrial laser scanners are Triangulation Scanners and Time-based Scanners. These scanners employ laser in the measuring process. The measured entity is the distance (range) between the scanner and object which is then used in calculating point positions as explained in section 2.2.2. The distance measurement technique is generally used in the classification of these scanners. A brief description of scanner types is given below.

a) Triangulation Scanners

The principles of triangulation are applied in determining the range of the object. This is illustrated in figure 2-2.

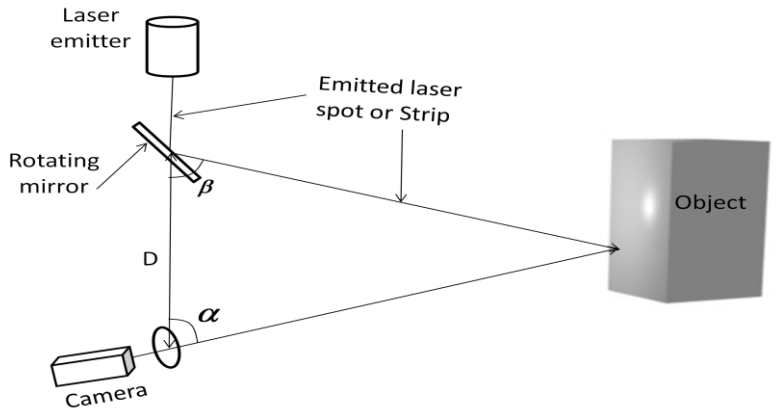

Figure 2-2 Triangulation Scanner

A laser emitter is mounted a fixed distance D from a CCD camera, figure 2-2. This distance is referred to as the base. Laser light or laser pattern (strip) is emitted towards an object at a known angle β using a rotating mirror. The camera is then used to track the location of the emitted beam on the object. The angle α is determined by the location of the beam on the object. Using this known information, the distance can be determined using triangulation methods. Triangulation-based scanners have a limited range, refer to table 2.1, and are mainly used in industrial applications where higher degrees of accuracy is required (e.g. reverse engineering). With triangulation scanners, micrometer accuracy can be achieved.

University of Cape Town

Table 2-1 Summary of Laser scanner Measurement Technology (Fröhlich and Mettenleiter, 2004)

Measurement technology	**Range [m]**	**Accuracy[mm]**
Time of flight (Time Based)	< 1000	< 20
Phase shift Method (Time Based)	<100	<10
Triangulation	<5	<1

b) Time based scanners.

Time-based scanners have the longest range of up to several hundreds of meters (refer to table 2.1) and are more suitable for open environments. This makes them suitable for measuring large objects (buildings, monuments and aeroplanes). Time based scanners measure the return time of an emitted laser pulse. This time is measured using two common techniques namely the time-of-flight and phase shift method. Time based scanners can be further classified according to these two techniques which are discussed below.

Time of flight method

The measured entity in this method is the time taken by a laser beam to travel from the scanner to the object and back to a detector on the scanner. Using this time and the known speed of light, the range can be calculated. The scanner measures a time $2t$, which is the time taken by the beam to get to the object and back to the receiver. The distance d is given by:

$$d = t.c \tag{2.4}$$

c is the speed of light.

Phase shift method

Modulated laser light is emitted by the scanner towards the target object. When the detector senses the reflected laser light from the object the difference $\Delta\varphi$ in phase between the emitted and received laser signal is measured. This phase difference is then used to calculate a time delay t. The time delay is given by

$$t = \frac{\Delta\varphi}{2\pi f} \tag{2.5}$$

The distance is then calculated using equation 2.4.

University of Cape Town

2.2.4 Components of a laser scanning system

The main components of a laser scanning system are:

i. A Laser scanner usually mounted on a tripod. The choice of scanner depends on the object to be scanned
ii. Computer- for controlling the data acquisition process
iii. Data storage unit for storing data. This can either be an external storage source or the computer.
iv. Global Positioning System (GPS) to establish ground control, and cameras for capturing images of the object. These are optional accessories. Some scanners have mounted cameras to capture photographs of the scene. Other survey methods besides GPS can also be used to establish ground control.

2.3 Errors in laser scanning

Certain prevailing conditions during laser scanning have a direct as well as indirect effect on the geometric accuracy of the point set. Various types of errors are encountered in laser scanning. The most common sources of errors are:

- Environmental
- Object related
- Instrumental
- Methodological

These errors or outliers in the point set are termed scan noise. Noise reduces the geometric accuracy of the point set hence producing less accurate models. The effects of outliers are reduced through filtering algorithms or employing robust detection methods, for example RANSAC or Hough Transform based detection. Some filtering algorithms have been proposed by (Sotoodeh. 2006; Schall et al. 2005; Ohtake et al. 2005). A discussion of the errors encountered follows.

University of Cape Town

2.3.1 Environmental errors

Laser scanners have recommended operating conditions for accurate measurements. Environmental conditions vary depending on location and this always introduces errors even if the scanner is properly configured for the selected area. Various errors resulting from changes in the environment are discussed below.

a) Temperature

Every scanner has a recommended temperature range that supports its efficient functioning. Even in the recommended temperature range, errors are encountered (Boehler et al. 2003: p. 3). Internal heating of instrument parts during use can introduce deviations in the measurements due to expansion of these parts. Temperature changes do not only affect scanners but errors can result from scanning heated objects. With heated objects, the background radiation from the object reduces the Signal-to-Noise ratio which in turn reduces the instrument precision (Theory and practice on Terrestrial Laser Scanning, 2003)

b) Variations atmospheric conditions

Pressure variations, together with temperature variations affect the propagation speed of light and this introduces errors. The errors introduced by these variations are small since the scanners have a limited measuring range usually less than 1000m. The errors are generally encountered over longer distances; however these errors become evident over short ranges in the presence of steam or dust (Boehler et al. 2003).

c) Interfering radiation

Scanning is usually done in the presence of other light sources. This illumination source will produce its own radiation. If the radiation from the illuminating source is stronger than the signal being used for measurement, then errors are encountered. This ambient radiation will be able to pass through the receiver signal filters and affect the accuracy of the measurements (Boehler et al, 2003: p3).

d) Distortions from motion

Moving objects in the surrounding areas usually cause vibrations. Scanning large objects can take up to 30 minutes and during this time the scanner is susceptible to these vibrations (Theory and practice on Terrestrial Laser Scanning, 2003: p 34). This

University of Cape Town

results in the displacement of the scanner position. The resulting points will no longer have the same reference point.

2.3.2 Object-related errors

Point measurements in laser scanning depend on light reflected from the object being scanned. This means that the object must be able to reflect sufficient ambient radiation from the scanner. This is not always the case as different objects are made up of different materials resulting in variations in reflectivity. The structure of the object also affects the measurement process. Object related errors are as a result of the factors discussed below.

a) Surface reflectivity

For sufficient point data to be captured the object being scanned must be able to reflect sufficient light back to the scanner. This implies that the reflectivity of the surface must be high. White coloured surfaces will reflect a stronger signal than dark coloured surfaces. Consequently, dark coloured surfaces are less accurately recorded. Surface reflectivity varies due to object colour. The errors encountered in scanning different objects therefore, vary. The spectral characteristics of the laser light being used in relation to object material also cause errors. A more detailed discussion is found in Boehler et al, (2003).

Refraction

The optical properties of a surface and the laws of reflection can also introduce errors in the distance measurement process. Light incident on a surface at a low angle of incidence is not in its entirety, reflected back to the scanner. Some of the light is refracted to another surface where it is then reflected back to the scanner. This is referred to as multi-path effect, see figure 2-4 (a).

University of Cape Town

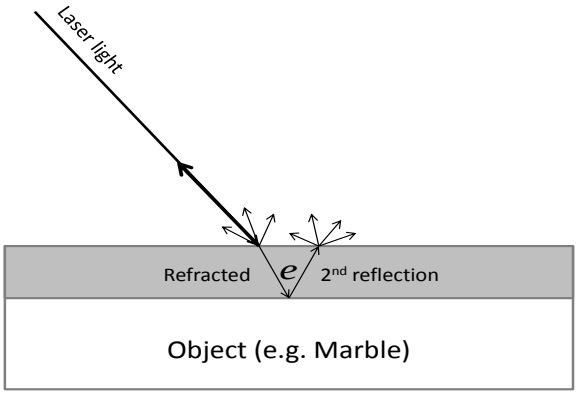

Figure 2-3 Effects of semi coated material **(**Theory and practice on Terrestrial Laser Scanning, 2003: p.33)

The same applies for materials that have semi transparent coatings. The laser beam is refracted and reflected within the material. Errors are introduced in the form of an addition constant *e*; refer to figure 2-3. Wood and marble are examples of such material (Theory and practice on Terrestrial Laser Scanning, 2003: p.33)

.

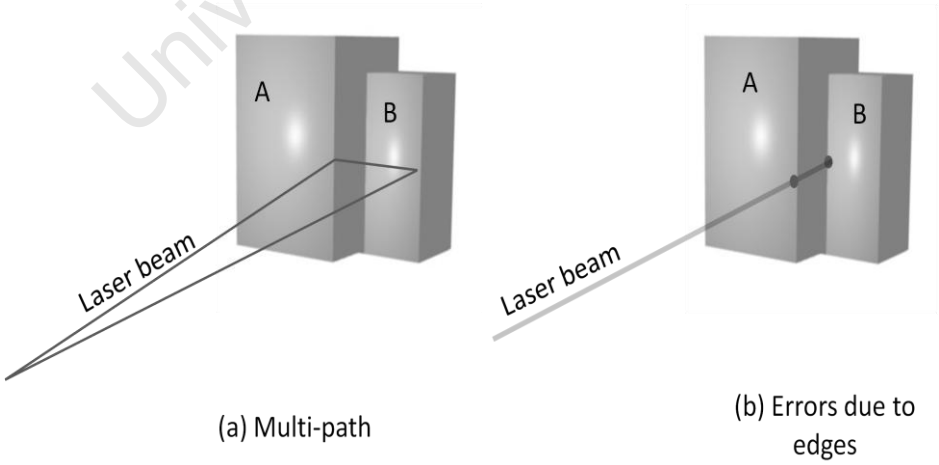

Figure 2-4 Errors in scanning

University of Cape Town

b) Edge effects

Edges are usually difficult to capture during scanning. When the laser beam hits the edge of object A, figure 2-4 (b), the beam is separated into two and the other part of the beam is reflected off object B. The result is a distance measurement dependent on the average time taken by the split beam. This results in a displaced point representing object A. Sotoodeh (2006) presents a detailed explanation on the effect of edges in scanning. The edge effect illustrated in figure 2-4 (b) can be reduced by using a laser beam with a smaller diameter. Another problem when scanning is that the edge is not captured; refer to figure 2-5. Points can only be captured near the edge and not the edge itself.

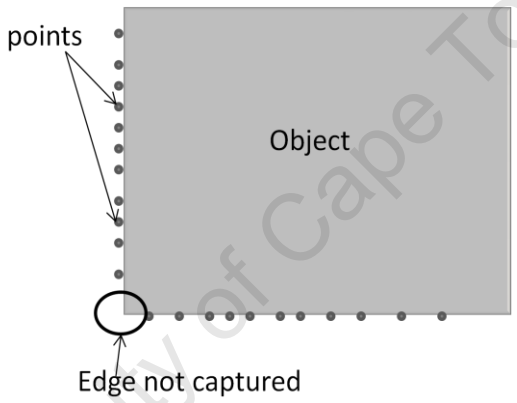

Figure 2-5 Errors introduced by edges

University of Cape Town

2.3.3 Instrumental Errors

These errors emanate from scanner design. Scanners are manufactured under different conditions. The parts used in the construction of these scanners are different hence the errors vary according to scanner type. Heated parts as a result of surrounding temperature will cause slight deviations in the distance measurements. These variations will depend on scanner type and material for constructing the parts.

2.3.4 Methodological Errors

Methodological errors usually result from the selected survey technique and partly due to the lack of experience on part of the user. Careful attention to resolution and scanner type is required before scanning an object. Setting an incorrect resolution for an object can result in under or over-sampling.

The type of scanner must be selected according to the size of object to be scanned Using a scanner whose range is almost equal to the object range can result in less accurate and sometimes no measurement hence increased noise or insufficient data captured.

2.4 Scan Characteristics and Point Distribution

Scan Characteristics

For range data, the point spacing is usually in range of 1mm to 5cm. The distance between the scanner and the object has the greatest effect on the resulting point structure. For a single scanner setup, objects closer to the scanner will have a higher resolution than objects further away. The point spacing will not be constant for the entire scan. Similar objects positioned at different distances from the scanner will have different resolutions. This is illustrated with the figure 2-6.

University of Cape Town

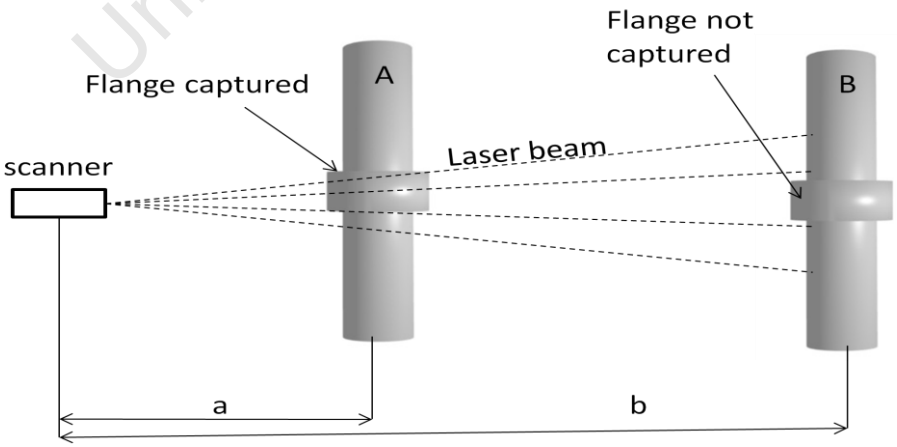

Figure 2-6 Effect of object range on resolution

More points are measured on pipe A than pipe B since distance *a* is less than distance *b*. As the scan for pipe B will have a lower resolution, some detail will not be measured, such as the flange on pipe B.

The errors discussed in section 2.3 also have a direct effect on the structure of the point set. As a result of these errors, points will not lie exactly on the surface but deviate from their true surface positions. This will result in inconsistent point spacing across the object and loss of scan line information.

Point distribution and densities

Point sets become unstructured after the registration process because of overlapping areas from different scans. This results in varying point densities across the entire point set. Occlusions and clustering of the pipe surfaces, in most cases, result in piecewise representations of scanned surfaces as only those surfaces visible in the field of view are scanned. The distribution and densities of points need to be considered in designing a robust reconstruction algorithm.

2.5 Discussion

This section discusses the overall effects of the resulting point structures and outliers on reconstruction. The focus is on segmentation. For some segmentation algorithms, the demarcation of segment boundaries relies on identifying discontinuities in surfaces or detecting edges. These discontinuities in piping primitives are usually introduced by flanges or plane surfaces that are connected to piping elements. These discontinuities are at times not captured as a result of the point distribution and resolution. If flanges are not captured as illustrated in figure 2-6 with pipe B, the result is under-segmentation since the discontinuity is not easily discernible, see figure 2-7. The flanges in figure 2-7 (a) and (b) are not easily discernible as a result of outliers and edge errors in the data.

University of Cape Town

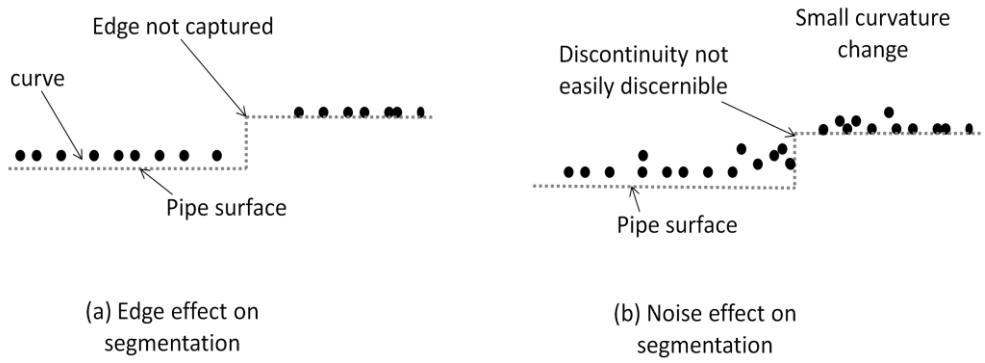

Figure 2-7 Effects of scanning errors on segmentation

Most detection algorithms therefore, employ methods of implementation that perform well in the presence of noise (RANSAC or Hough Transform) or use noise filtering algorithms prior to segmentation and detection. Noise cannot be entirely eliminated but the amount of erroneous points can be reduced. Some errors are difficult to model due to their random nature, therefore, cannot be eliminated. Errors will always exist in the point set and this must be considered in the design of a reconstruction algorithm. The effects of point distribution and densities as well as noise on detection are discussed in chapter 5.

The next chapter looks at the processing of point data for reconstruction. The main focus is on detection of piping elements. This will help in identifying problem areas and areas of improvement with current detection algorithms.

University of Cape Town

3. Reconstruction

3.1 Introduction

From a point cloud, the shape and characteristics of objects must be extracted. This process is commonly referred to as reconstruction. For a model to be reconstructed, the data goes through a series of processes. In this chapter, the processes involved from data acquisition to representation of the detected piping primitives are discussed. Each process is discussed together with current algorithms employed. Focus is on detection with the aim of identifying problems areas with current algorithms. An analysis of the detection methods is also given.

University of Cape Town

3.2 The Reconstruction Process

The reconstruction process entails a series of steps that are carried out from data acquisition to the reconstructed 3D model. The main processes involved from the data acquisition stage are mainly registration, filtering or structuring, segmentation, detection and representation. An illustration of the processes and the hierarchy is shown in figure 3.1. Each step is elaborated on in the succeeding sections.

The data does not necessarily go through all the steps shown in figure 3.1. The purpose of the reconstructed model and algorithms employed in the different stages determine the processing required for the data. For example, if a 3D model is required only for visual perception then points are usually rendered to a 3D polygonal mesh without segmentation or detection. Conversely, segmentation and detection is required for reconstructing piping installations were information concerning the types of scanned piping elements and their parameters is required. Another example is some detection algorithms do not require a prior segmentation. Detection is carried out on raw[1] point clouds. A typical example is presented by (Rabbanni and van den Heuvel, 2005) where detection of cylinders and planes is done without a prior segmentation.

[1] Raw point cloud refers to a point set after registration before any other processing is carried out.

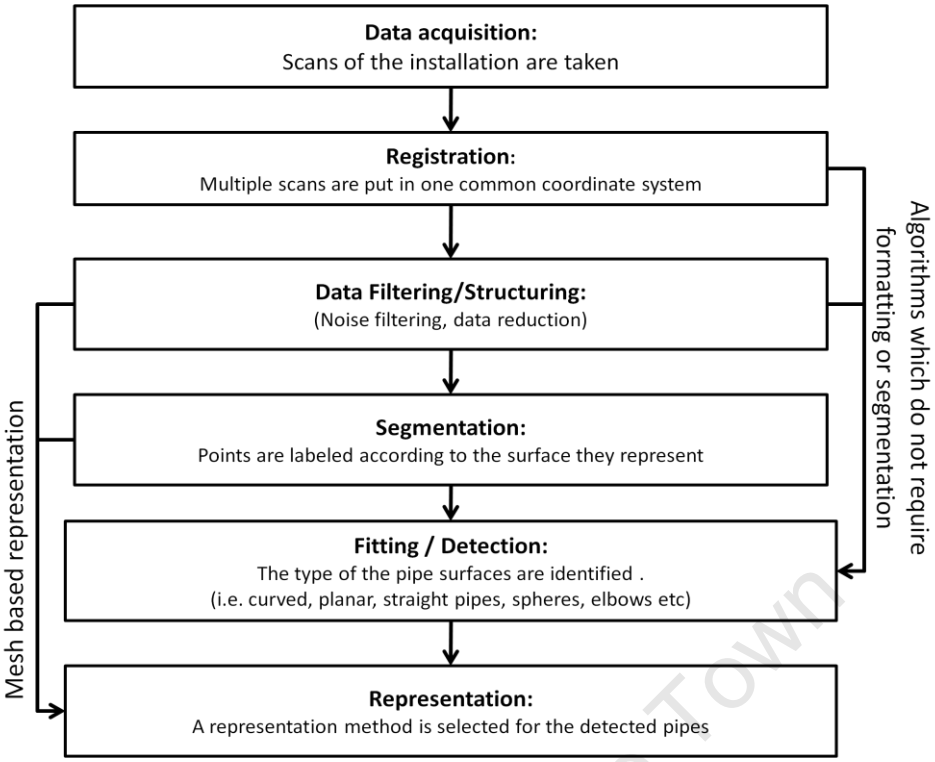

Figure 3-1 Data processing

3.2.1 Data acquisition

This is the process of acquiring 3D point data of objects. A single scanner setup is not sufficient to record point data of objects as a result of complexity, size and occlusions. Multiple scans of the object are therefore taken from different viewpoints. Figure 3-2 shows examples of scans of a piping installation. A single object scan can result in millions of points being collected.

Figure 3-2 Point cloud data of Pipes

University of Cape Town

3.2.2 Registration

Since multiple scans of a single object are taken, these scans are each in their own coordinate system. The scans are then brought into one common frame of reference in the registration process. Registration is defined as the process of finding a set of transformation parameters that when applied to scans taken from different viewpoints, brings the scans into one frame of reference. Registration of point clouds must be done correctly to ensure successful reconstruction. Errors in the registration process will propagate significantly to the final 3D model. Many algorithms exist for point cloud registration, each based on different principles. The most common algorithms are Iterative Closest Point (ICP) (Besl & McKay 1992) and Chen and Medioni's method (Chen et al, 1992). Many variations to these algorithms have been proposed as improvements to the original algorithms (Sharp, Lee and Wehez, 2000). Other algorithms include (Acka, 2003; Wendt, 2004; Kang, Zlatanova and Gorte, 2007). Bae (2006) classifies registration algorithms as either being point to point based or point to surface based.

Point to Point based algorithms

Point to point based algorithms minimise the distance between corresponding point pairs in different overlapping scans. The basic concept for these algorithms is coming up with matching point pairs from different point sets. The transformation parameters from one point set to the other are then calculated based on this matching.

The **ICP** is one of the most common point to point based algorithms in the registration of multi-view scans. The ICP was developed by Besyl and Mckay in 1992. The ICP assumes that for any overlapping surfaces in two different point sets C_1 and C_2, the closest point to any point in C_1 from C_2 is a good estimate of the corresponding point of C_1 in C_2. The first stage in the ICP is to establish these corresponding point pairs. A set of transformation parameters are then calculated using the corresponding pairs. This is achieved by minimising the sum of the squared distance between corresponding point pairs (Bae et al., 2004: p 222). In the ICP algorithm, an initial alignment has to be provided first before the algorithm is implemented. There has to be sufficient overlap between scans. Basic survey methods or images can be used in the initial alignment process. Many variants to the ICP have

University of Cape Town

been proposed with the aim of improving the process of establishing corresponding point pairs. Other algorithms that are point to point based and variants of the ICP are the Iterative Closest Point Using Invariant Features (ICPIF) (Sharp, Lee and Wehez, 2000), and the Iterative Closest Compatible Point (ICCP) which was later improved in the Random Sampled ICCP (RSICCP) in Godin et al (2001).

Point to Surface based algorithms

Point to surface based algorithms have the same concept as point to point based algorithms. The main difference between the two is that in the later, distances between points and their corresponding surfaces are minimised. Measures like curvature, normal vectors (Chen et al, 1992) and surface kinematics (Pottman et al, 2004) are usually used in establishing point to surface correspondence.

The most popular of point to surface based algorithms is Chen and Medioni's method, (1992). This method is based on the assumption that the normal vectors of points and their corresponding surface normals are similar.

Bae (2006) presents a variant of Chen and Medioni's method, the Geometric Primitive ICP with Random Sample Consensus (GP-ICPR). The GP-ICPR uses geometric primitives like change in geometric curvature and normal vectors of surfaces to establish correspondence. The advantage of this method is that no good initial alignment is assumed. Examples of other point to surface based algorithms are Pottmann et al. (2004), Witzgall et al. (2002) where points are matched to a triangulated surface, and Mitra et al. (2004).

3.2.3 Data Structuring

The number of points in a point cloud orders in the millions. Some algorithms cannot handle these large point sets. Besides algorithms failing to handle this data, it is more efficient for those that handle this data to deal with a minimal subset of points which allows for accurate reconstruction (Amenta, Bern and Kamvysselis, 1998). Other algorithms require the detection and removal of outliers through filtering. Consequently, data reduction or filtering is required. Data reduction is usually referred to as point cloud simplification and is common in mesh based techniques (Amenta, Bern and Kamvysselis, 1998).

University of Cape Town

Data Reduction/Filtering

Data reduction can be defined as the process of extracting a subset of points P_1 from an input point set P of size N with the resulting point set size $N_1 < N$. With data reduction/filtering, redundant points and outliers are removed while maintaining sufficient point density for faithful reconstruction. The result is a point set that allows for efficient memory use and reduced execution time in some algorithms. The main challenge in data reduction is density control of the resulting point set P_1. In some algorithms, points are sampled according to complexity of surfaces to maintain the correct point density in complex surfaces. An example is the crust algorithm where a higher point density is maintained in complex areas of an object and fewer points for other areas (Amenta et al, 1998). Examples of point cloud simplification algorithms can be found in (Moenning et al., 2004; Amenta et al., 1998; Vieira et al., 2003).

Data reduction and outlier detection can be performed independently of one another. For example, some algorithms may handle the large data set but perform poorly in the presence of noise. As a result, only outlier detection is required. Examples of noise filtering algorithms are presented by Sotoodeh (2006) and Papadimitriou et al. (2003).

University of Cape Town

Data formatting

Some segmentation algorithms are designed to deal with structured[2] point data especially in scan line based segmentation (Jiang et al. 1994; Natonek 1998). The result of the registration process is often an unstructured[3] point set as overlapping areas disrupt the pattern in the data. This data is incompatible in algorithms that require structured data. In some cases, the data has to be structuralised.

Data compression

Even though point cloud simplification reduces the point set size, data compression can also be done on the point set for storage and manipulation tasks. This process reduces the storage space required. Data is encoded into a format which reduces the

[2] A structured point cloud is a one that has data points arranged in a regular manner or grid (Series of lines in identifiable rows or columns).
[3] No identifiable patterns in the arrangement of data points

storage size required. Compression techniques have been presented by various authors with typical examples coming from (Merry et al. 2006; Schnabel et al. 2006; Vieira et al. 2003).

3.2.4 Segmentation

Industrial piping installations are composed of different types of piping elements. For a faithful reconstruction of these elements, their presence in a point set has to be established. This is achieved by identifying points representing each piping element in a point set. The process of identifying points representing the same surfaces together with regions occupied is referred to as segmentation. All points representing a single surface are given the same label. Points are grouped according to the surface they represent. Segmentation is usually carried out before detection or fitting. Segmentation has two distinct advantages when it comes to detecting piping elements. The first is that segmentation eliminates the need for continuously searching the point cloud for piping elements as with RANSAC or Hough based detection methods. Detection is carried out directly to the required set of points. Secondly, segmentation eliminates the task of point by point classification. Points are classified as clusters. This reduces the overall time required for detection.

In segmentation, points must be correctly labelled[4] or the detection might fail. This is because some detection algorithms fit surfaces to the identified surface segments (Lukacs, Marshall and Martin, 1997). If incorrect segments are defined, then the surface fitting will yield incorrect results. Some detection methods do not require a prior segmentation of but process the raw point cloud so as to identify the required surfaces (Chaperon et al. 2001; Rabbanni et al., 2005; Pottmann et al. 2003). These algorithms avoid problems associated with incorrect point labelling (over and under segmentation). Some algorithms have been proposed for dealing with issues of over and under segmentation. An example is Rabbanni et al. (2006) where constraints are used to obtain the right degree[5] of segmentation. Various segmentation approaches exist and these are discussed below.

[4] Incorrect point labelling results in under and over segmentation. Under segmentation identifies fewer surfaces than required and over segmentation identifies more surfaces than required.
[5] Right degree of segmentation refers to a correct segmentation (i.e. points are labelled correctly)

University of Cape Town

Segmentation by region growing

A seed point set or point neighbourhood is selected from the point cloud and measures are established on the point set. The measures are usually geometric properties like curvature or surface normals. These measures are estimated using surface or curve fitting. Neighbouring point sets are then selected from the point cloud and the geometric properties of each point neighbourhood are compared with the seed point set. The point neighbourhoods which exhibit similar geometric properties are merged into segments. This process is referred to as region growing. Region growing techniques depend on how accurately the chosen measure is calculated. Noisy data can cause errors in the estimation of these measures.

A typical example of region growing is presented by Rabbanni et al. (2006) where they segment the point cloud using a smoothness constraint. Normal estimates for each point in a given point neighbourhood are estimated. These neighbourhoods are defined by two different methods, namely

1. K-Nearest Neighbour (KNN) approach where they select the set of points from a point cloud within a minimum distance of each other.
2. Fixed Distance Neighbour approach.

The normals for each point are calculated by fitting a plane surface to the point neighbourhood. This fitting is based on minimising the orthogonal distance of each point from the approximate planar surface. Point normals and residuals based on the fit are calculated. Points are then grouped based on the normals and residuals. Higher residuals are considered as areas of high curvature regions (Rabbanni et al. 2006). Other algorithms which employ the region growing technique are (Jagannathan, 2007; Luckas, Martin and Marshall, 1998).

Scan Line based segmentation.

Scan line based segmentation requires structured data. Structured data is usually in a series of scan lines. Unstructured point cloud data has to be converted to a structured format. By grouping scan lines which exhibit the same geometric properties, segments are identified. This is usually done through fitting a curve to points in a scan line, and

University of Cape Town

then comparing curve properties, for example curvature. Points from curves which exhibit similar surface measures are given the same label. Typical examples are presented by Jiang et al, (1994) and (Khalifa, Moussa and Mohamed, 2003). A major drawback to scan line based segmentation is that points have to be structured. After registration, however, scan data loses the 2.5D nature and results in an unstructured 3D point set. This presents problems as scan line information is lost. A variation to scan line based segmentation to cater for unstructured 3D point clouds is presented by (Sithole, 2005), were scan planes are recreated as profiles in many different directions. Points are then connected in each profile according to surfaces they represent. Finally profiles are overlaid to define the surface segments

Connected Components / Proximity based Segmentation

The concept of point connectivity is used for defining segments. Points from the same surface are connected based on proximity. By defining a threshold measure on points from the same surface, segments can be defined. Segments are generally defined by first establishing a Graph $G(V, E_i)$ on a point set V. A proximity measure based on the edges E_i is established and edges which do not meet the proximity measures are removed. The result is a disconnected graph, where each sub graphs[6] represents a segment. An example of a proximity measure is the Euclidean distance. Proximity is also employed region growing techniques, were points are merged with a seed point set based on the distance between them.

University of Cape Town

3.2.5 Fitting / Detection

After establishing the different segments in a point set, the next step is to determine the surface types represented by the points in each segment. The points in these segments are used in the determination of the underlying surfaces. This is achieved through a fitting or detection procedure. Various fitting /detection techniques have been proposed for detecting piping elements. A brief discussion of the most common fitting/detection methods is given below.

[6] Each sub graph forms a connected component.

The Hough Transform

The Hough Transform (HT) is a technique used to identify shapes like lines, circles and ellipses in n dimension where $n = \{2,3 \dots n\}$. The number of parameters being sought defines the Hough dimension. The HT maps every point from a parameterized primitive to a Hough space, where a voting by the points is done for the best fitting parameters vector (Schnabel et al, 2006: p. 215). Primitives are then extracted using the parameter vector with the most votes. The HT is reliable in the presence of noise. The HT is efficient for primitives with three or less parameters. An increase in the Hough dimension and resolution results in an increase in memory requirements. The HT has been implemented in various algorithms with variations to improve efficiency.

Rabbanni et al. (2005) detect cylinders and planes using the HT but improve the efficiency by breaking it down into a two stage detection procedure. The originally required 5D[7] HT is broken into a 2D and 3D HT stages respectively. This method employs the Gaussian sphere of the input points. The first stage establishes the most probable cylinder direction or orientation using the Gaussian sphere[8] and point normals. A 2D HT is employed since two parameters are used in representing the cylinder direction. Finally the position, which is described by two parameters, and radius is estimated from a 3D HT. Points are projected onto a Hough space with the established cylinder axis as one of the axis. A voting is then done by the projected points for the best fitting parameters.

Random Sample Consensus (RANSAC) based fitting

RANSAC is an algorithm used for parameter estimation of mathematical models from a set of observations. RANSAC works well in the presence of noise and this makes it suitable for laser scanned data. RANSAC works on the assumption that for any set of given point set; a parameterized model can be fit using an established mathematical relationship between the point data and the geometric model. RANSAC's implementation is described below.

[7] Cylinder is described using 5 parameters.
[8] The Gaussian sphere can be regarded as a unit sphere or accumulator space.

University of Cape Town

1. From a given input point set P of size N select a subset p_i of size n_i where $i = \{1,2,3 \ldots . n\}$. n is the number of iterations required in 6
2. Assume the subset p_i consists of inliers and fit the data to the assumed model to get an initial set of parameters
3. Fit the remaining points p_i' to the model using parameters obtained in 2
4. Add those points with the least residuals or those with a residual which fall within the defined threshold to point set p_i
5. Run a confirmation test with the new point set p_i and see the level of fit with parameters from 2. (Parameters are kept for comparison later in the algorithm).
6. Repeat process 1 to 5 starting with a different point set p_{i+1}
7. Compare all set of parameters obtained from 6 and select the parameters that give the best fit

The main advantage of RANSAC is its ability to estimate model parameters in the presence of noise. The major disadvantage of RANSAC is that it can only fit one model at a time thus the presence of multiple models in an observation set results in neither being detected. RANSAC continuously searches for the best model hence it has no defined run time. Defining one can cause termination before achieving a satisfactory fit.

RANSAC is employed differently in some algorithms that deal with the detection of piping elements. An example is presented by (Chaperon and Goulette, 2001). RANSAC is employed on the Gaussian image of the cylinder to estimate the direction, position and size of a cylinder. The Gaussian Image is the result obtained from the Gaussian mapping of the entire point set. The Gauss map refers to the mapped point's normal to its corresponding surface normal (Chaperon and Goulette, 2001: p 37). The method is a two stage procedure, and RANSAC is employed in both steps. The first step is the estimation of the plane normal to the cylinder axis by using the Gaussian Image of the cylinder. This allows for the definition of the cylinder direction. The cylinder direction is given by the normal to this plane. RANSAC is used in extracting this plane. The second stage is to estimate the radius and position of

University of Cape Town

the cylinder. RANSAC is again employed in finding the best possible position and radius. This method only detects cylinders.

Schnabel et al, (2007) presents a method which also employs RANSAC. The method detects various kinds of primitives in the point cloud. The detection of primitives is treated as an optimization problem in this method. The procedure is RANSAC based but an additional score function is employed. The score function is responsible for selecting the best candidate primitive for a set of points from all possible primitives. This avoids the need to test all primitives on a point set since there is no prior segmentation in this method. The score function also verifies the correctness of a selected model by comparing point and surface normals.

Images and Constructive Solid Geometry (CSG) based fitting

CSG is a technique used in solid modelling. This technique allows the creation of different types of complex shapes by performing Boolean operations on basic shapes like cylinders, spheres and tori. An example is the union of two cylinders to form a T-junction (Figure 3-3). Successive unions and intersections of these basic shapes result in different complex models.

As previously stated, Photogrammetry is one of the long established methods in 3D modelling. It is still being employed at present but is now being integrated with other techniques like CSG and point clouds to improve accuracy in reconstruction. Even with other improved reconstruction algorithms, the use of images in detection is still very useful.

University of Cape Town

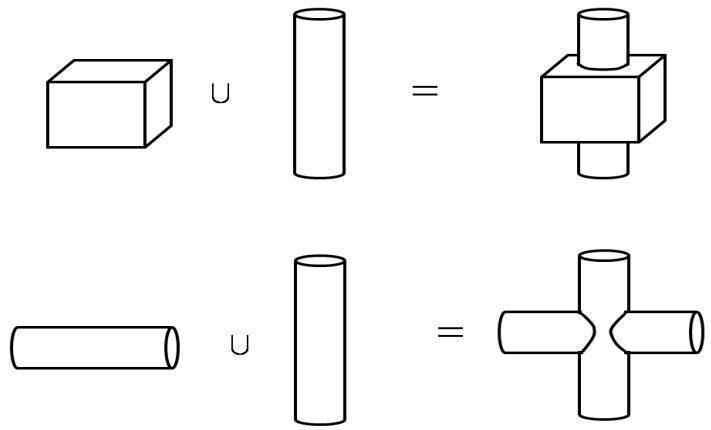

Figure 3-3 CSG Example, Union of basic shapes to form complex piping elements

Three different combinations exist for the fitting/detection using CSG, images and point clouds in the reconstruction of piping installations.

A. The use of CSG models and images only
B. The use of CSG models and point clouds only
C. The use of CSG models, images and point clouds

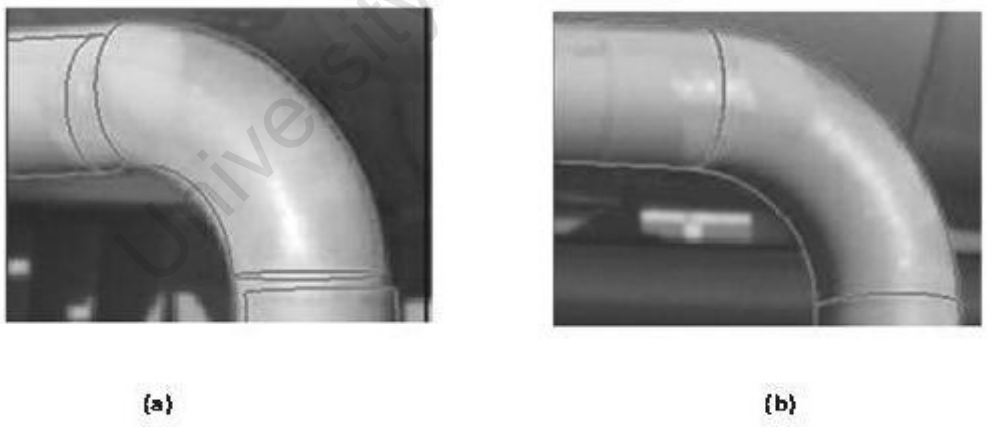

Figure 3-4 Matching CSG models to images (Tangelder et al, 2000: p. 137) (a) wire frame of model matched to image b) wire frame aligned to image

The concept in A is to first select a matching wire frame of a CSG model from a library and aligning it to corresponding primitive on an image as illustrated in figure 3-4 (a). After alignment, the wire frame is fit to the edges of its corresponding

University of Cape Town

primitive on the image to get the proper shape and orientation of the required model (figure 3-4 b). Edge matching techniques are employed in fitting the wire frames. The CSG wire frames have known parameters. Finally, the matched wire frames are combined to form the complete model. The wire frames are then substituted by their corresponding solid CSG models. Examples of this technique are presented by Tangelder et al, (2000), Ermes, van den Heuvel and Vosselman, (1999) and Tangelder et al., (1999).

In B, CSG models are used with point clouds. The CSG models are fit to points after segmentation. An appropriate CSG model is fit to points in a given segment. The fit is based on minimising the orthogonal distance between the points and the CSG model surface as illustrated in figure 3-5.

University of Cape Town

Figure 3-5 Fitting CSG model to point (Rabbani and van den Heuvel, 2004) (a) before fitting (CSG model and point cloud) (b) after fitting

Rabbanni et al, 2004, present three different methods for fitting CSG models to point clouds:

1. Iterative Closest Surface point (ICS)
2. Iterative Closest Triangle Point(ICT)

3. Iterative Closest Point cloud Point (ICP)

The difference between the methods is the distance that is minimised. The first method minimises the distance from the CSG model surface to a point. The second minimises the distance between a point and the corresponding CSG mesh (CSG model is approximated by a mesh). The third method converts the CSG model into a point cloud and minimises the distance of the closest point to the CSG point cloud from the input point set. A more detailed discussion is presented by Rabbani et al., (2004).

In C, the same concept in A is used but in this case the CSG models are also fit to point clouds. This combines step A and B. The best fitting parameters obtained after this integrated fitting is adopted. A typical example is presented by Rabbani et al, (2004). The first step in this method is segmenting the point cloud for the purpose of recognizing certain surfaces or objects in point clouds i.e. planar or curved. A Hough transform is then used to detect the primitives after segmentation. The next stage is to fit CSG models to segments obtained. After fitting CSG models to points, a second fitting of the models to images of the scanned object is performed in a similar manner as the method by Tangelder et al, (2000). An advantage of this approach is that any missing point data from the point set due to occlusions can now be approximated using the images and CSG models. Finally, all data sources are combined and the final parameters are estimated (Rabbani et al, 2004).

University of Cape Town

Surface or Curve Fitting

Surface or curve fitting generally involves the fitting of geometric surfaces or curves to point sets. This usually requires a prior segmentation of the point set. Higher order polynomials (Pratt, 1987), parametric curves (Wang et al, 2004), parametric surfaces or a geometric definition of the relationship between the points and the real world geometric object are used. This definition is usually in the form of a minimising distance function. As with any non-linear problem, good initial estimates of the parameters are needed. Estimating the parameters is a challenge because apart from the point set, no other additional information is available is some cases. Geometric properties like surface normals are usually used in estimating the parameters. The presence of outliers affects the reliable estimation of the parameters (Mitra and

Nguyen, 2003). A comparison of methods for estimating normals is found in (Dey, Li and Sun, 2005).

Least squares' fitting of algebraic surfaces is presented by Pratt (1987). The method employs least squares fitting through the use of polynomials. The level of fit for the detected primitive is then tested by minimising the point to surface distance. The method can detect various types of primitives. Other examples can be found in (Lukacs, Marshall and Martin, 1997; Liu et al, 2005; Zhou et al, 2005 Werghi et al, 1999). Before discussing representation, the next section provides an analysis of the detection techniques that have been discussed

3.2.6 Analysis of Detection/Fitting methods

The detection/fitting algorithms have been discussed in the succeeding sections. This section summarises these method focusing on the advantages and disadvantages. The aim is to identify areas that require improvements in detecting piping elements.

Fitting can be accomplished using traditional photogrammetric techniques. However, because images do not contain explicit 3D object information, user intervention is required to extract 3D point positions. This poses problems in automating the reconstruction process. However, images are useful when used to complement other fitting methods.

Hough based methods detect mostly planes and cylinders. These primitives cannot be used to represent all the piping elements found in installations[9]. The method is thus limited in genericity. Besides good performance of the HT in the presence of noise, the memory requirement of the HT and the space and time complexity also remains a major drawback. According to Rabbanni et al, (2005) the time and space complexity in fitting using the HT can be approximated by $O(s^p)$ and $O(s^{p-1} * n)$ respectively where p is the number of parameters, n is the number of points and s is the sample along one Hough dimension. Considering the point size from laser scanning the application of the HT to fitting is time consuming, even if the resolution is reduced.

[9] Planes and cylinders represent a small fraction of all piping elements.

University of Cape Town

RANSAC has the ability to detect primitives in the presence of noise. However, RANSAC based algorithms usually detect one primitive at a time and the presence of multiple objects in the scene usually results in the detection failing (Rabbanni et al, 2005: p. 60). RANSAC is an iterative process and thus has no defined time limit and introducing one may result in the optimum fit not being attained. RANSAC also depends on a good sampling criterion for the selection of seed point sets, as it assumes that the seed point set to consist of inliers. A desirable property is the fact that it requires a minimal subset of points for primitive detection (Chaperon et al, 2001).

General Surface fitting methods require the provision of good initial estimates. The result of the fit is dependent upon these estimates. A reliable estimation technique is thus required. Chaperon et al, (2001) use the Gaussian sphere to get the initial estimates of the cylinder direction which are then used in a least squares fitting using RANSAC. Some methods use normal and curvature estimates to estimate initial parameters but the estimates become unreliable with high noise levels. In point clouds, partial scans of some piping elements are acquired as a result of occlusions. Most of the fitting is then done to patches of data and the rest of the model is estimated from the fitting results. In the presence of heavy noise, the accuracy of the fitting is reduced and this results in unfaithful reconstruction. Most least squares techniques detect a single primitive at a time and require different representation of each primitive whether parametrically, as an algebraic surface or as a distance minimising function which leads to a high number of different parameters to be estimated (e.g. Pratt, 1987; Lukacs et al, 1997). Werghi et al. (1999) deal with this issue by fitting all the primitives in a single step taking into consideration the geometric relationships of various primitives.

The detection methods discussed do not accommodate the detection of deformations in piping elements. The majority of the methods assume the piping elements are free of deformations. The detection/ fitting methods assume ideal situations, which is not always the case.

University of Cape Town

3.2.7 Representation

After detection, a representation method is required for the results. The detection/fitting algorithm employed usually determines the representation technique used (e.g. CSG models are used for an algorithm that employs CSG fitting). The representation method must aim to minimise the separation between the final model and the original scanned surface. Common representation methods used for representing piping elements are discussed below.

Surface based representation

This representation method approximates the surface form of the scanned object. An example of surface representation is Bicubic Parametric patches (BPP). Each patch is defined by a mathematical formula which can be used to change the resulting shape of the patch. NURBS (Non-Uniform Rational Basis Spline) surfaces or curves are a good example of BPP. NURBS is a mathematical model that can be used for geometric representations of curves or surfaces. Most algorithms which use NURBS for representation require a least squares fitting of the points to curves or surfaces. NURBS geometric representations can describe shapes from a simple curve to a complex 3D surface.

University of Cape Town

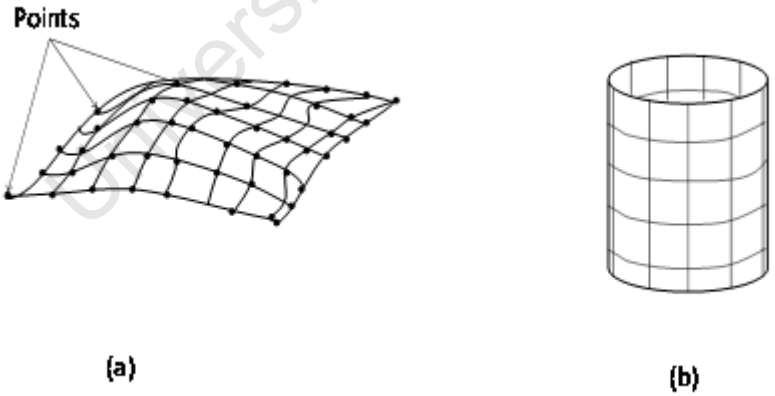

Figure 3-6 NURBS a) NURBS surface fit to points b) cylinder representation using NURBS surface

NURBS curves or surfaces have the advantage of that the shape of the curves or surface patches can easily be changed to follow a desired form. Algorithms

employing NURBS are presented by (Leal et al, 2007; Teutsch et al, 2005; Liu et al, 2005).

Polygonal representations (e.g. triangular meshes, polygons) are another form of surface based representations that are used to approximate the shape of the object. A series of connected polygons are constructed using the points to approximate the surface. Representations methods based on polygons are usually known as Boundary Representations (B-Reps). Polygonal representations are common in mesh based reconstruction techniques. The main disadvantages of B-Reps are that correctness of the resulting surface depends on polygon size (The smaller the polygons the better the surface approximation) and the resulting model is fixed.

Volume based representation

Volume based methods define the object by a combination of 3D solid shapes. An example of volume based representation that has been used for piping elements are CSG models. Detection methods based on CSG fitting employ this type of representation. The data is substituted by the corresponding CSG model after fitting (Tangelder, Vosselman and van den Heuvel, 2000; Rabbani and van den Heuvel, 2004). Other examples of volume based representations are voxels (volume elements). However, voxels are not usually used for representation of pipe models.

Mathematical representation

The detection results are represented by a mathematical function. The function describes the relationship between the point data and a mathematical model. Various primitives that can be described with an explicit mathematical function use this representation (e.g. cylinders, cones, spheres). Points are fit to surfaces based on the mathematical relationship. Implicit functions are also used to represent objects. These are used to represent surfaces that cannot be described using explicit mathematical equations.

3.3 Discussion

Existing detection methods have been discussed. The fitting method in any algorithm usually affects the choice of representation method. Mesh based techniques use polygonal representations while most surface fitting algorithms employ NURBS.

University of Cape Town

Most B-Reps (meshes) do not give secondary information (i.e. parameters and orientation) about the object but are concerned with surface representation. From data filtering, points are rendered to a polygonal mesh without segmentation or fitting. This usually applies to objects where no secondary information is required (e.g. archaeological objects).

NURBS are considered more accurate in representation as they are flexible (shape can be changed). CSG models can only represent a limited number of rigid shapes obtained from Boolean operations on basic shapes. Some complex elements cannot be obtained from these operations. Polygonal shapes are also fixed in shape which is a disadvantage.

From the analysis of detection/fitting methods in section 3.2.6, the following conclusion can be drawn: Prior segmentation enables fast detection with less computations time. A segmentation strategy is incorporated in the design of the detection algorithm. The next chapter therefore deals with the segmentation of pipe data for subsequent detection.

University of Cape Town

4. Segmentation

4.1 Introduction

The aim of segmentation is to establish the extent of surfaces and the regions they occupy in a point set. Points are grouped according to the surface they represent. These points are then classified with respect to piping elements which make up installations e.g. elbow, t-junction, flange, straight pipes.

This chapter discusses the segmentation of pipe data (point cloud). The segmentation operation must establish piping elements' segments in a point cloud. Firstly, a brief review of graphs is given. This will aid in understanding the algorithm presented. Next, the advantages as well as reasons for segmentation are discussed. A definition of a pipe segment is then given followed by methods of obtaining these segments. Finally, the segmentation algorithm is detailed.

University of Cape Town

4.2 Graph concepts

In order to understand the algorithm presented, some definitions and brief explanations of basic graph concepts are given. These concepts are used in the segmentation approach presented. A brief overview of graphs is therefore, given below.

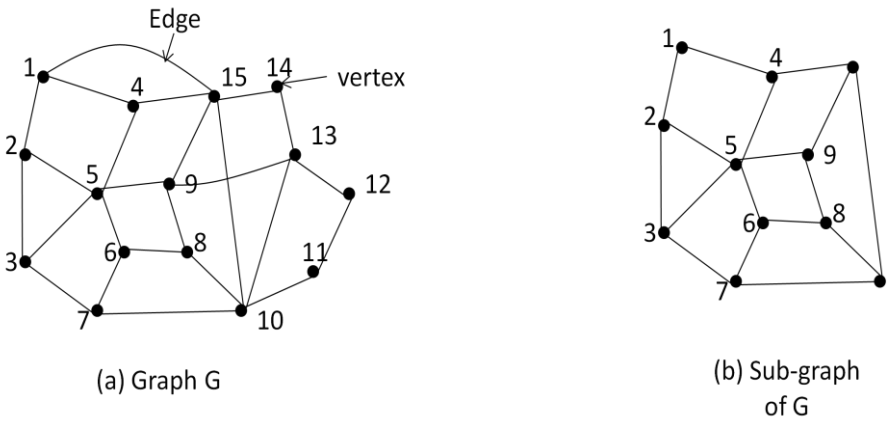

Figure 4-1 A graph ***G***and a sub-graph of ***G***

A graph is a pair $G = (V, E)$ where V is the vertex set (points or nodes) in the graph and E is the edge set, each edge connecting two vertices. A graph is denoted as $G(V, E)$ in this chapter. Figure 4-1 (a) shows an illustration of a graph with 15 vertices and 23 edges. A sub graph $S_G(V_G, E_G)$ of $G(V, E)$ is a graph whose vertex and edge set is a subset of G (i.e.$V_G \subseteq V$), see figure 4-1 (b). If for any given sub graph, if $V_G = V$, then the sub graph is a spanning sub graph. An edgeless graph is one which has no edge set (i.e. it only has vertices, $E = \emptyset$). A graph is connected if for any two vertices, there is a set of edges that connects the two, otherwise the graph is disconnected. Figure 4-1 (a) shows a connected graph

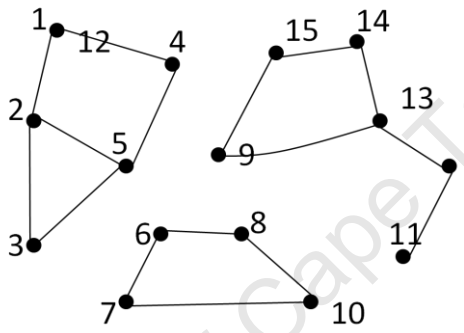

Figure 4-2 Disconnected graph ***G***

Figure 4-2 shows a disconnected graph. However, the connected sub graphs are referred to as connected components. Figure 4-2 shows a graph G with 3 components. Each component can be regarded as a sub-graph. A more detailed explanation on graph theory is found in Diestel (2005).

4.3 Pipe segmentation

The aim of pipe segmentation is to identify the different piping elements in a point cloud. Points are grouped with respect to the piping element they represent. This has some distinct advantages when it comes to detecting piping elements. Pipe segmentation eliminates the need for continuously searching the entire point set for the detection of piping elements. This is common in RANSAC based techniques which do not require a prior segmentation (Chaperon et al, 2001). RANSAC algorithms iteratively searches for points that best fit a given model using a minimal

University of Cape Town

subset of points (Schnabel et al, 2007). The downside to this approach is that no time limit is defined for the search. A user defined limit might result in an unsatisfactory fit. Conversely, with a prior segmentation, fitting or detection is done directly to the required set of points. Another advantage is that segmentation eliminates the task of point by point classification. Points are classified as a cluster. This reduces the overall time required for detection. However, the right degree of segmentation must be attained.

4.3.1 Definition of pipe segments

Piping installations are composed of connected piping elements. Each of these piping elements must be encompassed entirely by a single segment. Figure 4-3 shows a point cloud for a section of an installation (an elbow and two straight pipes). Each piping element must be in a different segment. Three segments must be identified in figure 4-3.

University of Cape Town

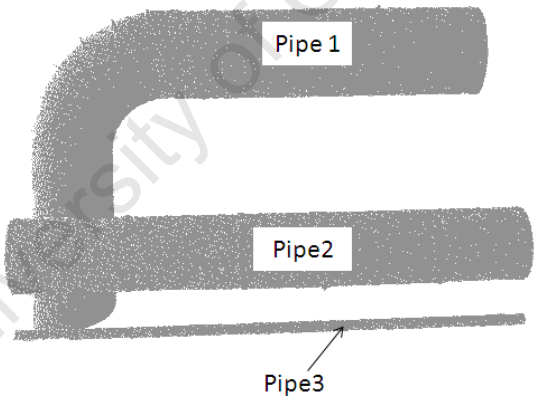

Figure 4-3 Point cloud of three piping elements

Figure 4-4 shows two samples of segmented pipe data. The piping elements are in different segments which is the desirable result.

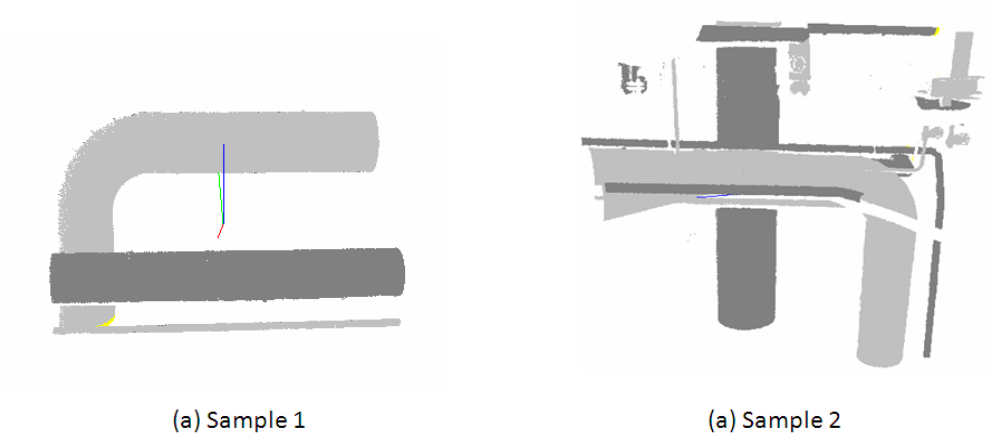

(a) Sample 1 (a) Sample 2

Figure 4-4 Segmented pipe point cloud

The main challenge with the segmentation of pipe data is separating connected piping elements into individual segments. This requires identifying areas where the elements are connected. By treating these areas as segment boundaries, the point data can be separated into different segments. The boundaries are usually marked by flanges, as they introduce discontinuity along pipe surfaces, figure 4-5 (a). Discontinuity also results from different objects connected to pipe elements as shown in figure 4-5 (b). Identifying these discontinuities in point data will form the basis of the segmentation algorithm proposed in this research.

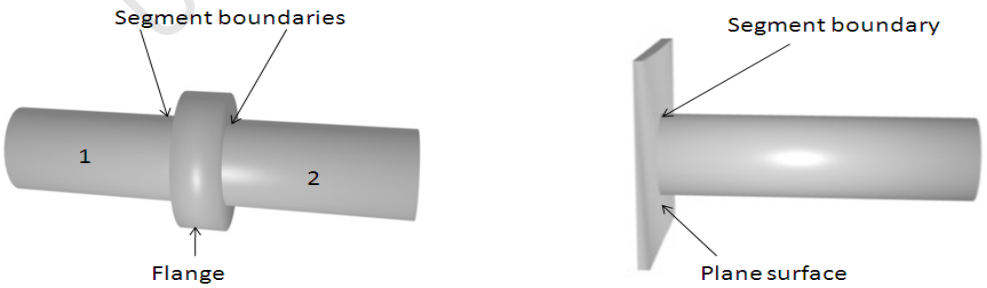

(a) Discontinuity due to change in radius (b)Discontinuity due to different objects

Figure 4-5 Defining pipe segments using discontinuities on surfaces. Discontinuities regarded as segment boundaries.

University of Cape Town

4.4 Methods of segmentation

Various segmentation techniques can be employed in defining surface segments. Some of these techniques have been discussed in Chapter 3, section 3.2.4. The techniques were classified as follows:

- Proximity based techniques
- Scan line based techniques
- Region growing techniques

Not all these techniques are used for the segmentation approach presented in this chapter. In the proposed algorithm, the techniques employed are proximity based and a variation of scan line based techniques. These are selected based on the discussion given below:

Proximity based techniques are based on the assumption that points representing the same surface are closer to each other than any other points. By defining a threshold distance between points from the same surface, segments can be identified. Proximity based segmentation algorithms begin by establishing a graph $G(V, E_d)$. The edges E_d are based on a proximity measure (distance in this case). The edges that do meet a defined distance threshold are removed from the graph. The result is a reduced graph where the connected components of the graph are the required segments. Proximity segmentation is illustrated in figure 4-6.

University of Cape Town

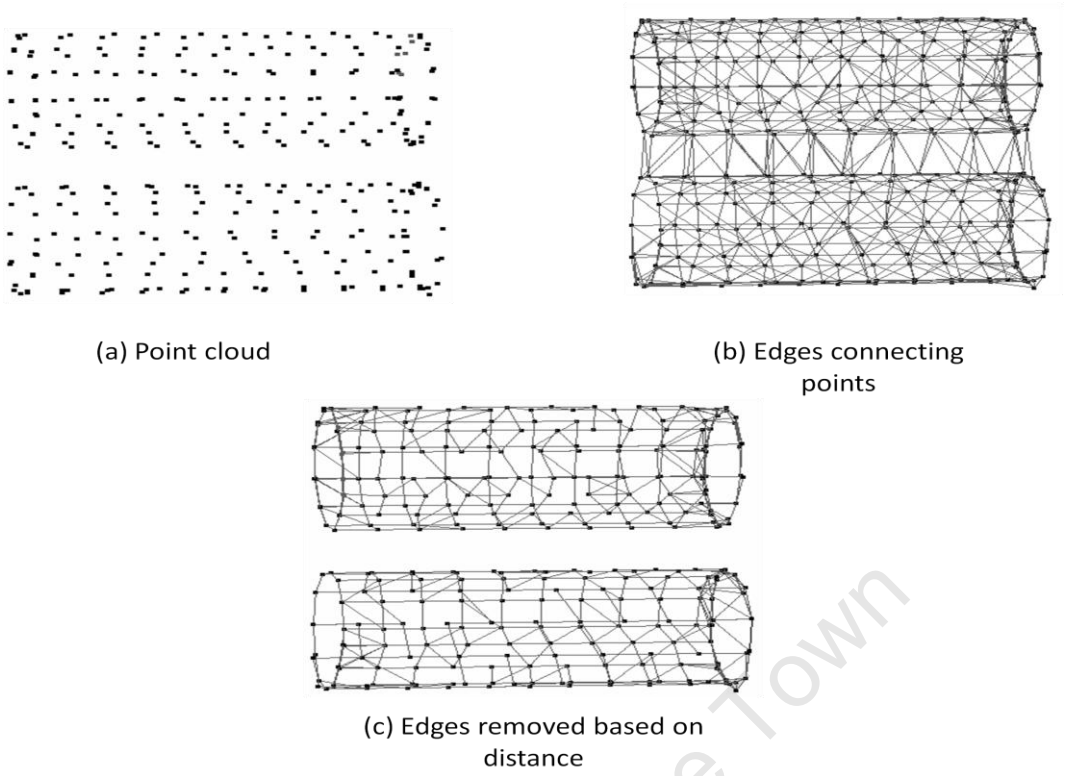

Figure 4-6 Proximity segmentation a) Pipe point cloud before segmentation b) points connected by edges and c) Edges are removed based on a defined proximity measure (distance)

University of Cape Town

Figure 4-6 (a) shows a point set of two disconnected pipes. Figure 4-6 (b) shows the edges connecting the point in the graph. In figure 4-6 (c), edges which do not meet the threshold distance are removed. The result is points connected according to the pipe they represent.

Proximity segmentation can be used in defining piping elements' segments. Proximity segmentation assumes that point spacing is fairly constant. Therefore, varying point spacing usually results in over segmentation. Another disadvantage is segmentation by proximity defines segments of disconnected pipes, see figure 4-7 (a). Therefore, connected piping elements, figure 4-7 (b), cannot be segmented. The two straight pipes and elbow will be merged into a single segment since the points are close together as a result of the connection.

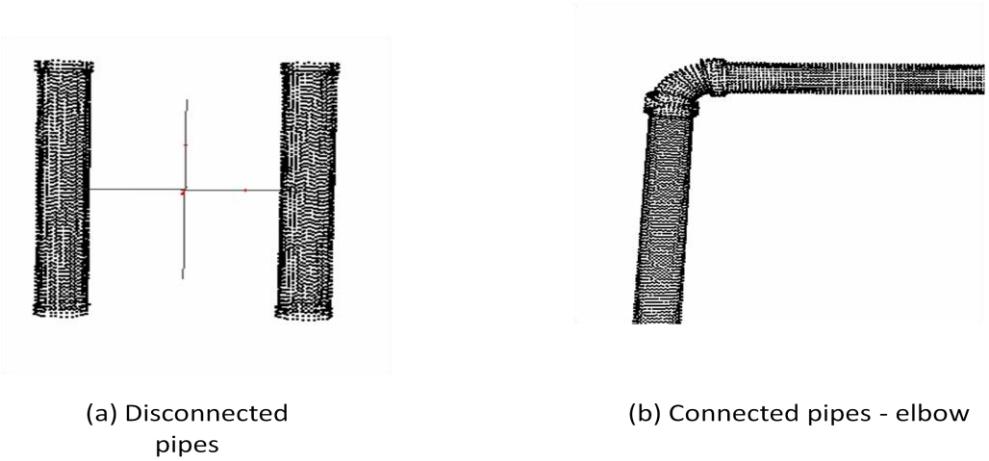

Figure 4-7 Limitation of proximity segmentation a) Proximity segmentation defines segments of disconnected pipes. Segments in b) cannot be identified.

Consequently, proximity segmentation is not sufficient in detecting all the required segments. An additional segmentation technique that enables the segmentation of connected piping elements must be incorporated.

As mentioned in section 4.3.1, connected piping elements can be separated into constituent segments by treating discontinuities along the pipe surface as segment boundaries. These discontinuities can be detected by detecting curvature changes along pipe surfaces. Sharp curvature changes are encountered along the pipe as a result of these discontinuities. This is illustrated in figure 4-8.

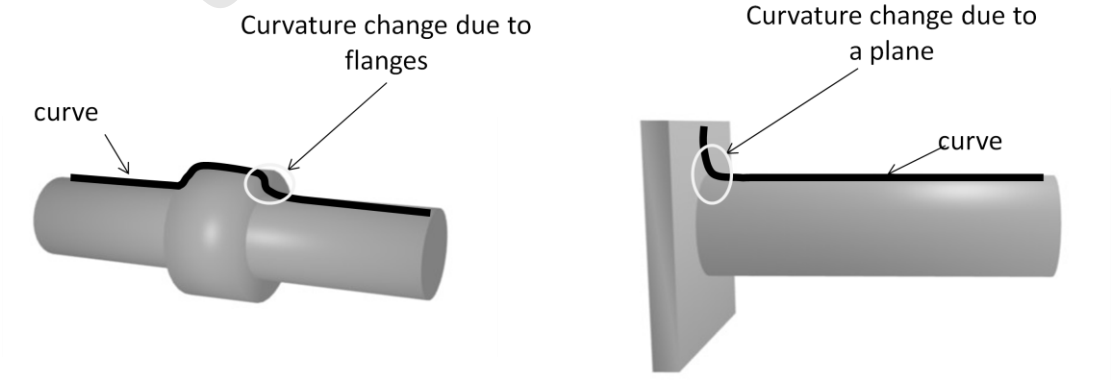

Figure 4-8 Curvature changes caused by discontinuity in surfaces

University of Cape Town

Curvature changes along pipe surfaces can be detected using curves. This is achieved by fitting a curve to points along the pipe surface. The assumption being points are arranged in a regular pattern along the pipe surface. This idea leads to scan line based segmentation techniques.

Scan line based segmentation is based upon the grouping of scan lines that exhibit the same geometric characteristics. This is usually done by fitting curves along scan lines and grouping curves based on geometric properties like curvature and curve normals. All points on a set of curves exhibiting the same geometric properties are assigned to the same segment. Scan line based segmentation are usually employed in the segmentation of range images. Examples of scan line based techniques are presented by (Jiang et al, 1994; Khalifa et al, 2003).

One disadvantage with scan line based segmentation is that scan line information is lost in the case of registered point clouds. In order to utilise the strengths of scan line based segmentation, scan planes have to be recreated on the point set. An example of segmentation based on recreating scan lines is presented by Sithole (2005). In this technique, scan lines are recreated in many different directions as opposed to fixed scan line directions. The recreated scan lines are referred to as profiles. Firstly, points from the same surface in a given profile are identified. Next, points from the same surface are identified across profiles. This is achieved by intersecting the profiles. This is the main technique that is used in the proposed algorithm. Before discussing this segmentation algorithm in section 4.4.2, definitions of terms used in the technique are given in the next section.

University of Cape Town

4.4.1 Profiles and Stacks

The term profile refers to a recreated scan plane on a given point set. The profile is described by a width w and a direction θ. Figure 4-9 (a) shows a profile running in a set direction. The scan lines are not recreated as single profiles. For a given direction θ, the entire point cloud is partitioned into a series of thin profiles of the same width w. This is shown in figure 4-9 (b). A set of profiles in the same direction are referred to as a stack. The stack normal is perpendicular to the profile direction (stack direction). Various stacks can be defined on the same point set each with a different direction.

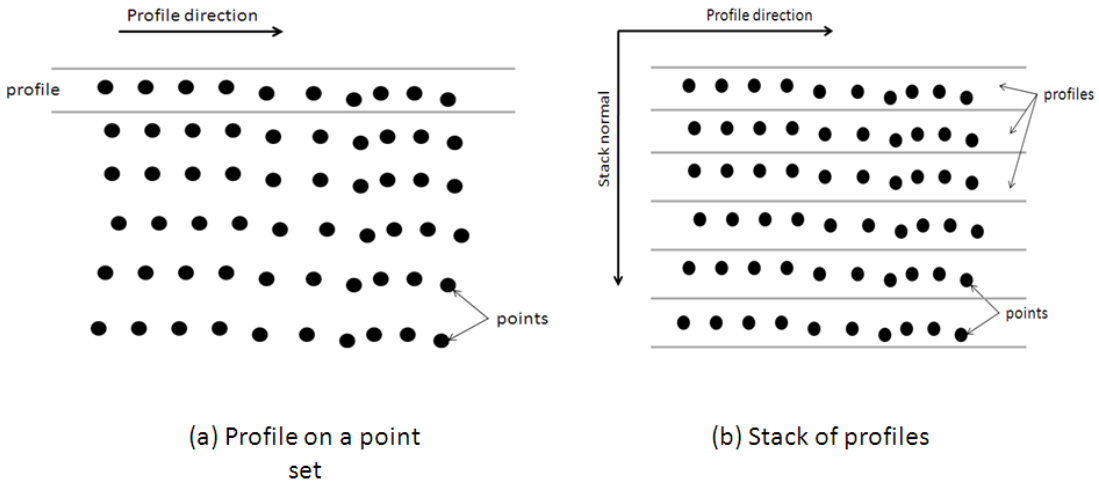

Figure 4-9 A Profile and Stack a) Single profile on point cloud b) Profiles with the same orientation referred to as a Stack

4.4.2 Segmentation by profile intersection

Concept – A surface can be approximated by a network of planar curves all passing through the same points in different directions. This is illustrated in figure 4-10.

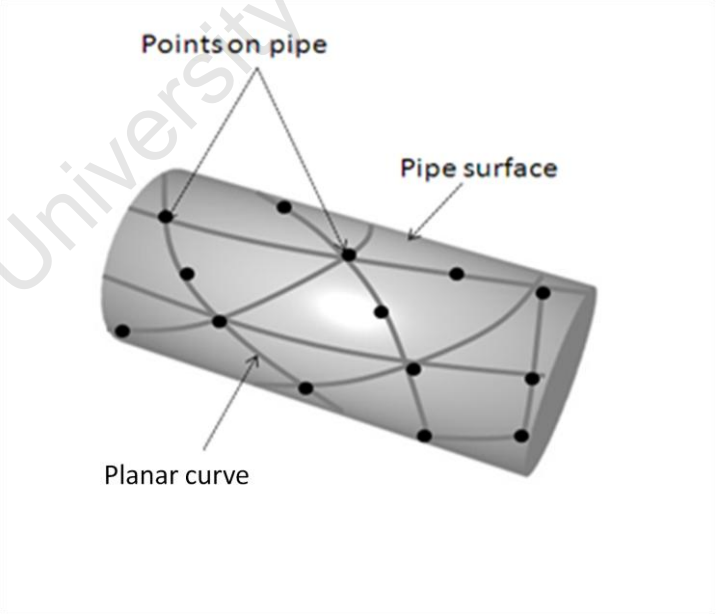

Figure 4-10 Network of planar curves representing pipe surface

University of Cape Town

By recreating such curves on a point set and intersecting the curves, the surface can be reconstructed (Sithole, 2005). Substituting the curves with profiles in many different directions, connecting the points in a profile (e.g. by curve fitting or proximity) and intersecting the profiles, the surface can be reconstructed. This is illustrated in figure 4-11. Figure 4-12 shows an inset of the connected points.

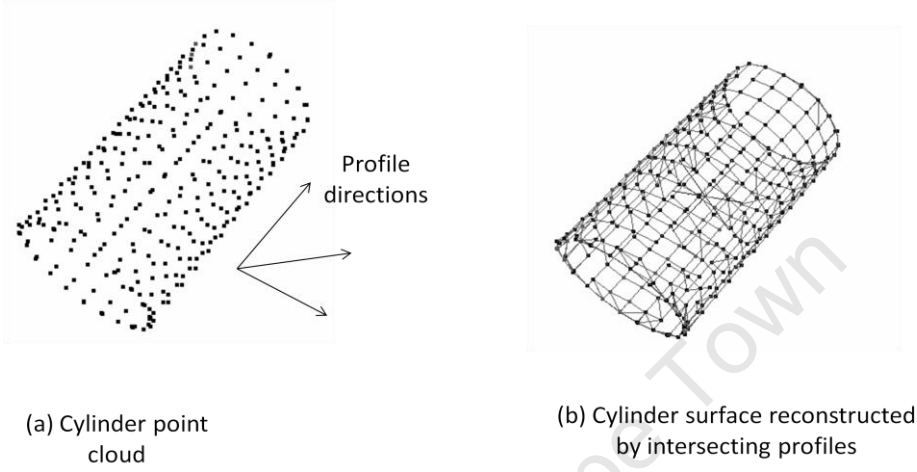

Figure 4-11 Surface reconstruction by profile intersection a) Point cloud of pipe before reconstruction and b) after reconstruction

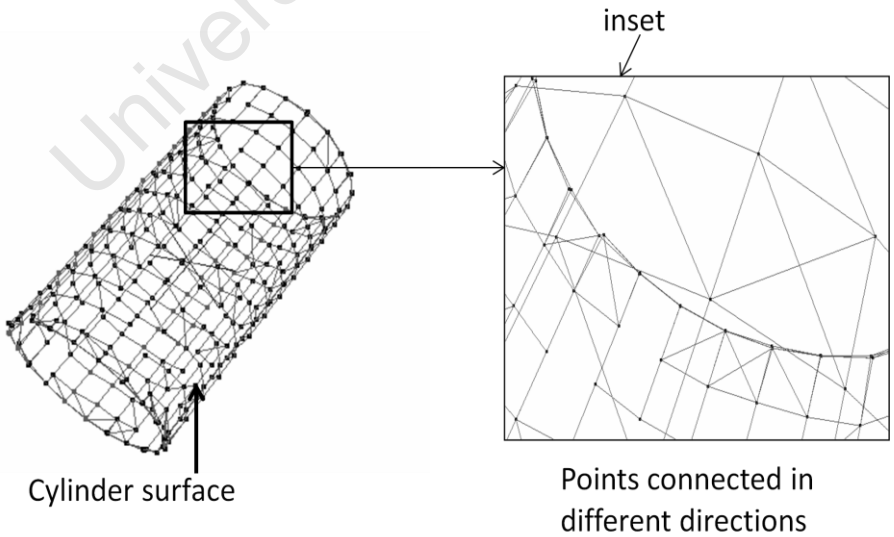

Figure 4-12 Reconstructed surface (inset)

University of Cape Town

For segments to be defined by profile intersection, points in each profile must be connected according to the surface they represent before profile intersection. Each set of connected points in a profile is referred to as a line segment. Multiple stacks are be added to allow for profile intersection. This is illustrated in figure 4-13.

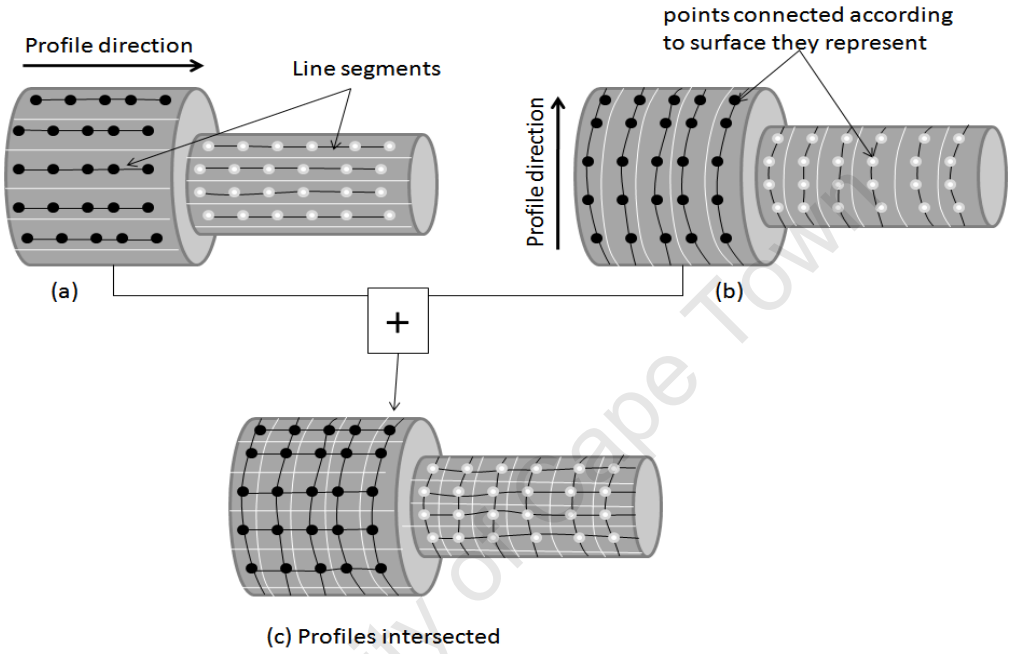

Figure 4-13 Segmentation by profile intersection a) and b) show two different profile directions and the line segments c) Profiles intersected to define segments.

Figure 4-13 (a) and (b) show two different profile directions (stack directions). Points are connected according to the surface they represent along the set profile direction. Figure 4-13 (c) shows the result of the intersection. Points from each surface are connected separately. The two different segments are shown on the diagram (c) (Black points and white points are connected separately).

Figure 4-14 shows sample results on test data. Three profile directions are used as shown in Figure 4-14 (a). Points are connected along each direction. Points in each

University of Cape Town

segment are interconnected. Two different segments are acquired which is the desired result.

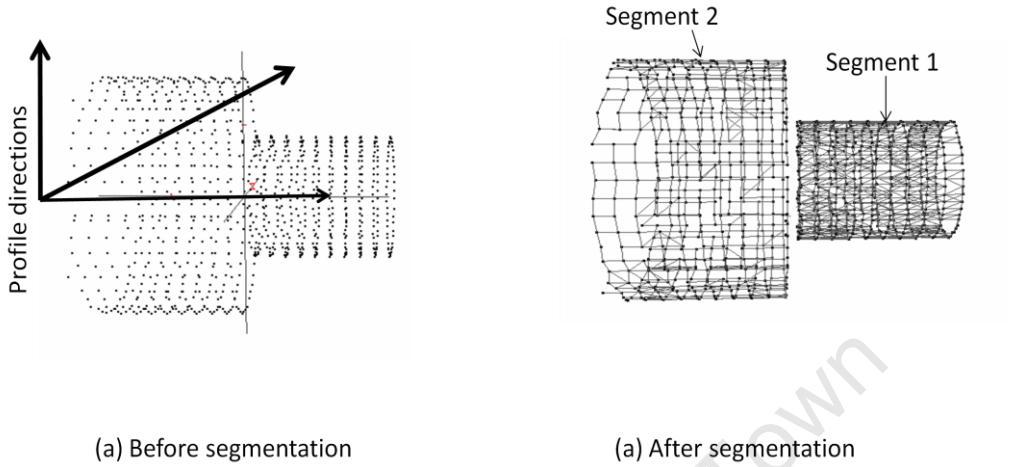

Figure 4-14 Segmentation by profile intersection (test data) a) three profile directions defined on pipe points b) the resulting segments after profile intersection

Segmentation by profile intersection has some distinct advantages which are:

- The form of any given surface can be recreated in any direction thus simplifying the detection process.
- It can be used with 3D data, whereas most scan line based methods use 2.5D data
- Computationally inexpensive

The major disadvantages of the method are that it is memory intensive and if profile width is not selected carefully then the algorithm can fail. This is explained in section 4.5.2.

Segmentation by profile intersection is summarised as follows:

University of Cape Town

1. Partitioning the point cloud into a series of profiles running in different directions (i.e. adding stacks). At least two stacks must be added to allow for intersection of the profiles.
2. Points in each profile are connected based on the surface they represent (profile segmentation) to yield line segments.
3. Profiles are intersected. Intersecting line segments represent the same surface segment.

4.4.3 Representing pipe segments

Segmentation can be explained in terms of connectivity where each segment consists of connected points. By imposing a graph $G(V)$ on the entire point set and connecting points representing the same surface, segments can be defined. The required surface segments are the connected components of the graph. The segmentation task in section 4.3.1 can be equated to finding connected points in a graph $G(V)$. The points are connected based on profile intersection. The next section details the segmentation algorithm.

4.5 The segmentation algorithm

The segmentation algorithm can be summarised as follows:

1. Create a graph $G(V)$ on the point set where V is the entire point set
2. Connect points from similar surface.
3. Find connected components of $G(V, E_g)$. E_g is the set of edges connecting points in the graph. Each component represents a segment

Each of the stages is explained in the sub sections below:

4.5.1 Creating a graph

The first step in the segmentation algorithm is to impose a graph $G(V)$ on the point set. The vertex count V is equal to the number of points in the point cloud. Initially, the graph is edgeless. The graph is later filled with edges connecting points from similar surfaces. The process of establishing the connected points is detailed in the next section.

University of Cape Town

4.5.2 Connecting points from similar surfaces

Profile intersection is used in connecting points. The algorithm for segmentation by profile intersection has been explained in section 4.4.2. Each of the stages involved in the algorithm is explained in relation to pipe data.

1. Partitioning the point cloud

Firstly, stacks are added to the point set each in a different orientation. Each stack is represented by a spanning sub graph $G_s(V)$ of the main graph $G(V)$. The profiles in each stack are represented as sub graphs of $G_s(V)$. The vertex count for each profile graph equals the number of points in the respective profile. The structure of these graphs is explained below:

a) **Main graph $\boldsymbol{G(V)}$:** This is initially an edgeless graph. V is the number of points in the point cloud
b) **Stack graphs $\boldsymbol{G_s(V)}$:** These are sub graphs of the main graph $G(V)$ where $s = \{0, 1, 2 \ldots . . n\}$. n is the number of stacks. All stack graphs are edgeless. V is the number of points in the point cloud
c) **Profile graphs $\boldsymbol{G_{sp}(V_p)}$:** These are sub graphs of stack graphs $G_s(V)$ where $s = \{0,1,2 \ldots n\}$ and $p = \{0,1,2 \ldots . m\}$. n is stack count and m is the profile count in each stack. This implies that every stack has its own profiles. $\cup V_p = V$ for all profiles in a given stack. Points are connected in their respective profiles and the edges are later added up to the main graph.

The profile count in any given stack depends on the width w of each profile and extent of the points in the set direction. At least three stacks were found to work well for a good segmentation.

A profile can be defined by

$$P = p(w, \emptyset)$$

Where $\emptyset \in \mathbb{R}$ and $w \in \mathbb{R}$. P denotes a profile with a width w and orientation $\emptyset$.

A stack is therefore defined as

University of Cape Town

$$S = \{P \mid P \subset V\}$$

Where V is the point cloud

The stacks have the following properties.

- A single stack is made up of the entire point set. Each profile is of the same width in all stacks.
- In a single stack, no two profiles share common points. Points are only shared in different profiles.

The process of partitioning a point cloud is illustrated in figure 4-15. Three profile directions (3 stacks) are defined on the point set (profiles width defined in figure 4-15 is larger for clarity. Setting the correct profile width is explained in the next section).

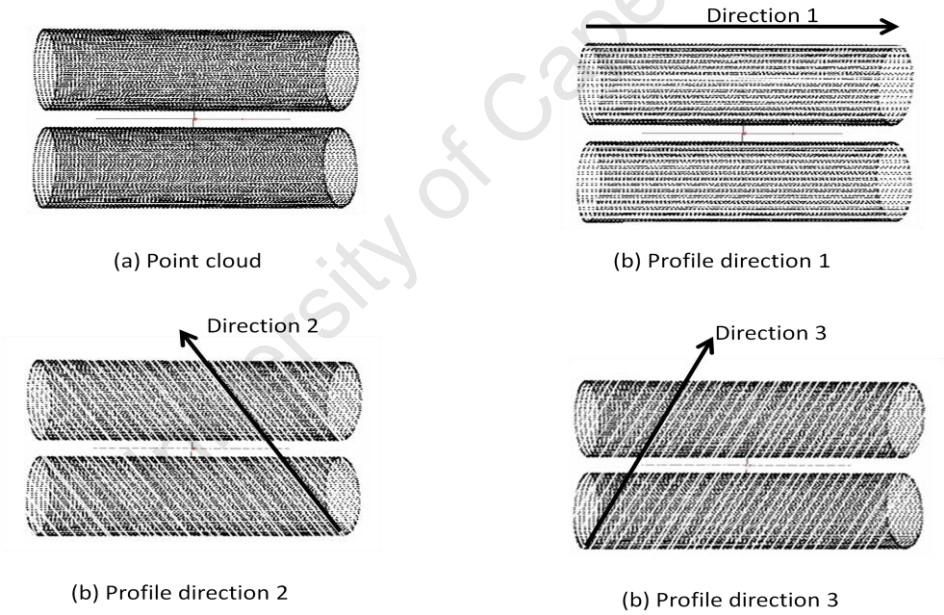

Figure 4-15 Point cloud partitioning a) point cloud before partitioning, b, c, d show three different profile directions

Profile width vs. resolution

Selection of profile width depends on point cloud resolution. The minimum acceptable profile width is the average point spacing. This allows each profile to

University of Cape Town

capture sufficient points in any given profile direction. The form of a surface can then be recreated correctly in any profile.

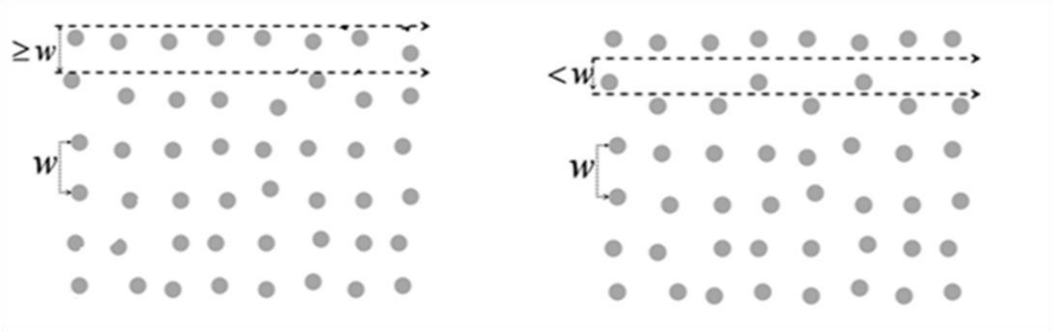

Figure 4-16 The effect of profile width a) sufficient points will be captured and segments identified correctly b) sparse profile which results in incorrect segmentation

University of Cape Town

Figure 4-16 shows a point set with point spacing w. Figure 4-16 (a) shows a profile width greater or equal to the average point spacing. This ensures that sufficient points are captured in each profile. Figure 4-16 (b) shows a width smaller than the average point spacing. The result is a sparse profile. If points in the profile are to be connected based on the average point spacing, not any of the points will be connected to each other since the distance between them is greater than the average point spacing. The concept of proximity segmentation based on distance between points will fail if the threshold distance is approximately equal to average point spacing. Successful segmentation of any point set therefore depends on profile width.

2. Segmenting the profiles

After partitioning the point set, the next step is the segmentation of the profiles. The profile segmentation operation yields connected line segments in each profile. Firstly, points are connected based on proximity. If the piping elements are connected, then the line segments are split where sharp curvature changes are encountered. This stage has the greatest impact on the final segmentation. Retrieving connected line segments (profile segmentation) is discussed in section 4.6. An illustration of line segments in a profile is given in figure 4-17.

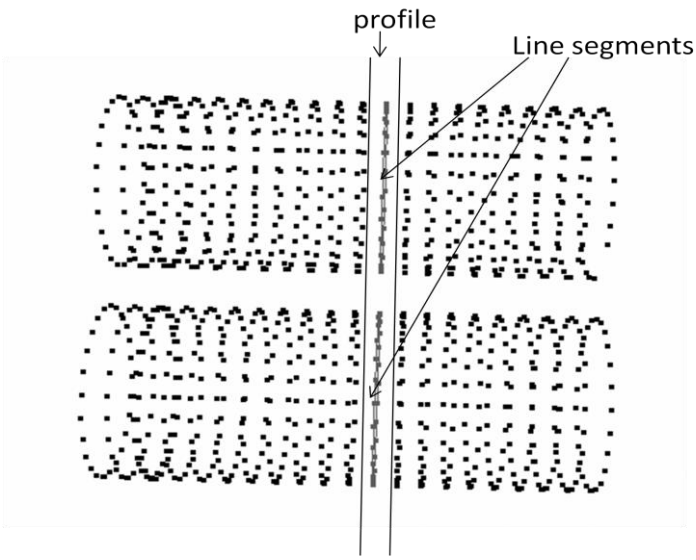

Figure 4-17 Sample line segments from a profile defined on straight pipes

The line segments have the following properties

1. Each line segment is made up of points from the point cloud i.e. $L = \{l \mid l \subset V\}$. Where L is the set of line segments and l is any given line segment. The line segments are connected components of the profile graphs.
2. No two line segments from profiles of the same stack share common points.
3. Two separate line segments from the same profile do not share common points.

The order of points in each profile is not considered in the profile segmentation operations. The edges connecting the line segments in each profile are later added to the main graph to establish connected points. This is explained in the next section.

3. Surface segmentation

In order to get the surface segments, the resulting line segments are intersected. This is achieved by adding all edges connecting line segments to the main graph. Since the profiles are oriented differently, line segments from different profiles will share common points. Adding all the edges to the graph will result in interconnected points. This is illustrated in figure 4-18.

University of Cape Town

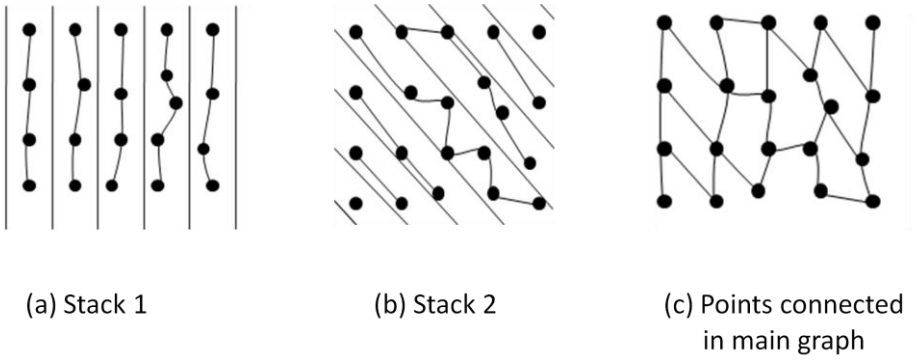

Figure 4-18 Surface segmentation a) and b) show points connected in profiles c) Edges connecting points in different stacks added to the main graph

Figure 4-18 shows points connected in profiles from different stacks. The edges connecting the points are added to the main graph. The result is a disconnected graph, G, in which the connected sub-graphs are the required segments. The interconnected points form connected components in the main graph (connected components have been discussed in section 4-2). Each segment is represented by a component.

4.5.3 Connected components

After adding edges to the main graph, the connected components are identified. Each component represents a pipe segment. Figure 4-19 shows an example of two connected components where each component represents a pipe segment.

University of Cape Town

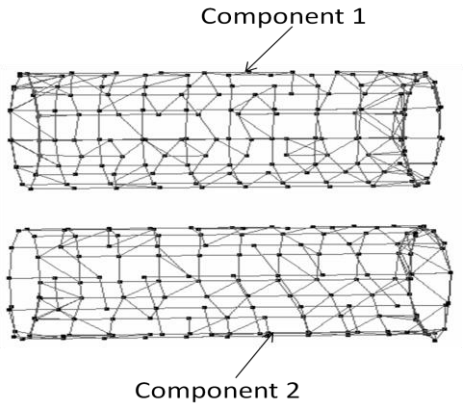

Figure 4-19 Connected components of segmented pipes

4.6 Profile segmentation

Retrieving correct connected line segments from profiles is the basis of a successful segmentation operation. The profile segmentation operation involves identifying the points that belong to the same surface and then connecting these points (using edges). Two methods are outlined for the identification of connected line segments. Before the profile segmentation operation, points in each profile are transformed to a 2D frame in the profile to simplify the process.

4.6.1 Profile Segmentation by proximity

The purpose of proximity segmentation is to establish segments of disconnected piping elements. The distance between the elements must be greater than the threshold distance used in proximity segmentation or the elements are merged into a single segment. The profile segmentation operation can be described as follows:

1. Perform a Delaunay Triangulation on points from each profile P. $G_{sp}(V_p, E_d)$. Edges E_d are based on a distance measure.
2. Establish a threshold distance measure based on average point spacing
3. Eliminate all edges that do not meet the defined distance measure.

The result is a set of line segments, each connecting points from the same surface, refer to figure 4-20.

University of Cape Town

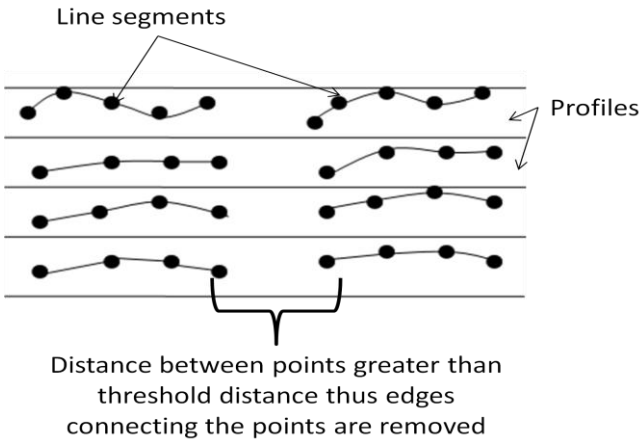

Figure 4-20 Line segments formed in proximity segmentation

4.6.2 Profile Segmentation by Curve Fitting

The Purpose of profile segmentation by curve fitting is to separate connected piping elements. This is carried out after proximity segmentation to establish whether any of the line segments retrieved from proximity segmentation is from a single element or connected elements[1]. The line segments are split so as to separate the elements if any connection is established. The points of connection are marked by changes in curvature. This is illustrated in figure 4-21 (a) and (b).

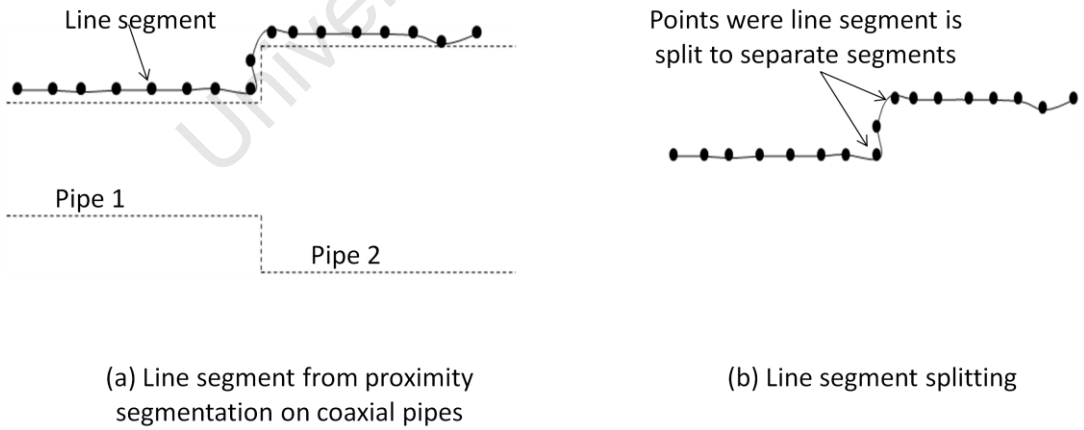

Figure 4-21 Detecting curvature changes using curves

[1] Proximity segmentation cannot establish segments of connected piping elements

University of Cape Town

Points from the same surface form a continuous curve. By fitting a curve to points in a line segment, smoothly connected curves are established. Sharp curvature changes along the curve are identified and the line segments are separated at these points. Profile segmentation by curve fitting is performed after proximity segmentation. The algorithm is described below:

1. Select a curve[2] function *C*
2. Fit a curve *C* to points in a given line segment (from proximity segmentation).
3. Identify points on the curve where sharp changes in curvature occurs and split the curves at these points
4. Perform a Delaunay Triangulation on points on each continuous curve
5. Remove edges that do not meet the defined distance measure (this is the distance measure from proximity segmentation. The aim is to establish a new edge set connecting the points on each continuous curve and remove redundant edges.

The success of segmentation by curve fitting depends on the curve function used. An illustration of the curve fitting and splitting process is shown in figure 4-22 and Figure 4-23.

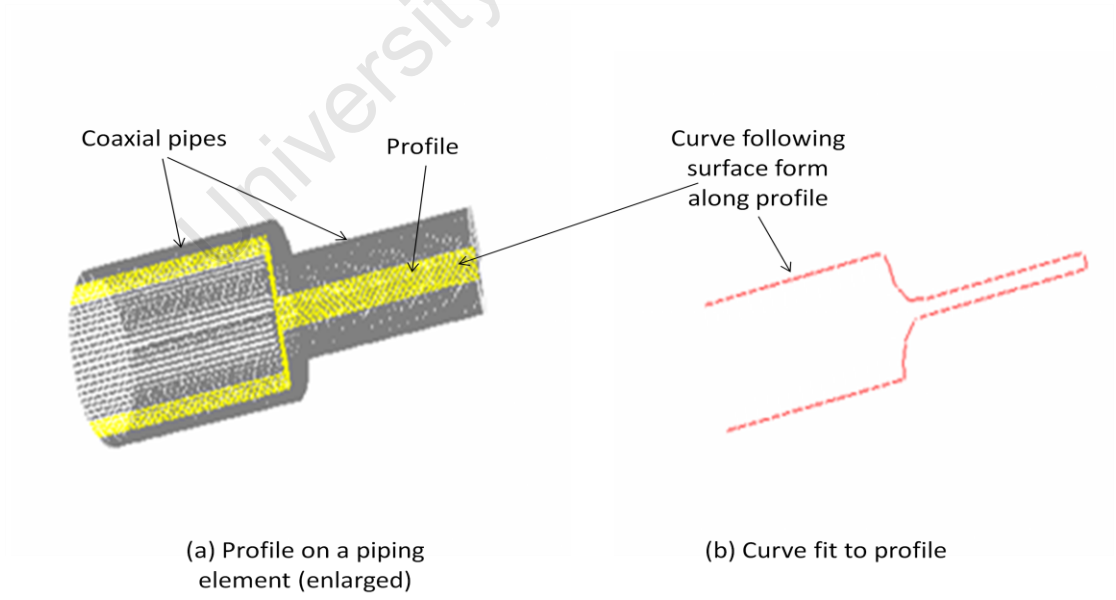

Figure 4-22 a) Sample profile on coaxial pipes b) sample curve fit to points in profile

[2] NURBS are used in the algorithm proposed

University of Cape Town

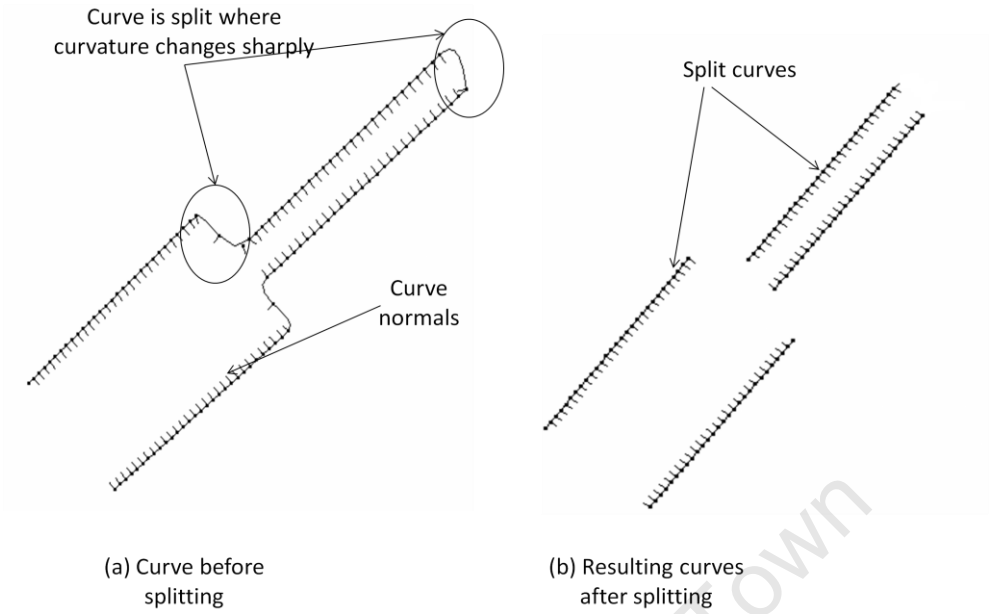

Figure 4-23 Segmentation by curve fitting a) curve fit to points in profile b) curve is split where sharp curvature changes occur

Figure 4-22 (a) shows a sample profile on coaxial pipes. The curve required is one that will trace the outline of the pipe surface as shown in Figure 4-22 (b). Figure 4-23 (a) shows the same curve and the corresponding curve normals. Changes in curvature are computed along the curve and the curve is split at these points (Figure 4-23 (a)). The resulting curves are shown in Figure 4-23 (b). Each curve connects points from the same surface.

One major disadvantage of curve fitting is the presence of noise. A curve will follow the form of a pipe if there are adequate numbers of points in a profile from the surface. The presence of noise will attract the curve away from the actual surface. If there are high levels of noise, sharp changes in curvature are encountered where the curve is attracted away from the surface. This will lead to over-splitting of the curve and will result in over-segmentation.

University of Cape Town

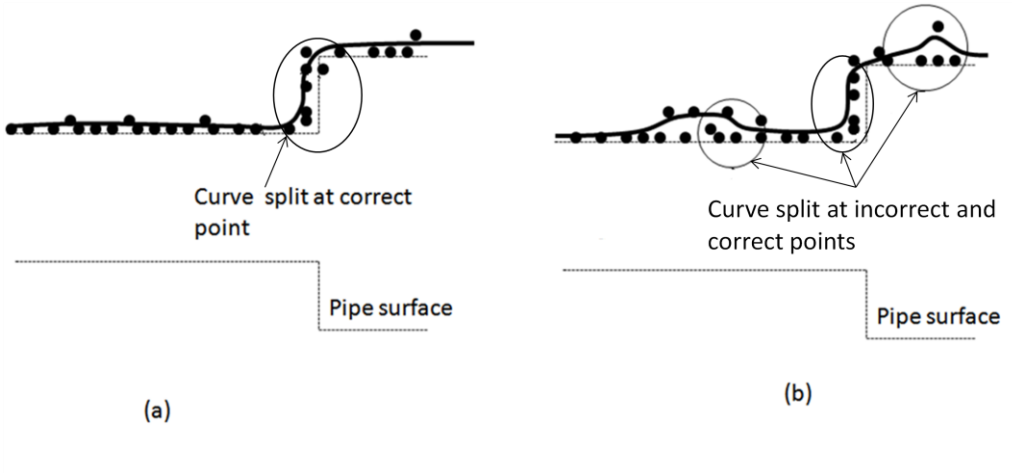

Figure 4-24 Effects of noise on curve fitting a) curve is split correctly since there are no outliers b) curve is incorrectly split as a result of noise

Figure 4-24 shows the effects of noise on curve fitting. The curve in (a) will follow the correct form of the pipe surface and the segmentation is correct as the curve is split at the correct points. The curve in (b) is split at correct and incorrect points as a result of noise. Sharp changes in curvature are encountered at incorrect points on the curve due to noise.

The segmentation algorithm was tested on pipe data and the results are given in the next section.

4.7 Segmentation Examples

Real and simulated data was used in testing the segmentation algorithm. Simulated data was used to model various scenarios encountered in pipe data. Examples of segmentation using the test data is given below.

Example 1: Disconnected piping elements

University of Cape Town

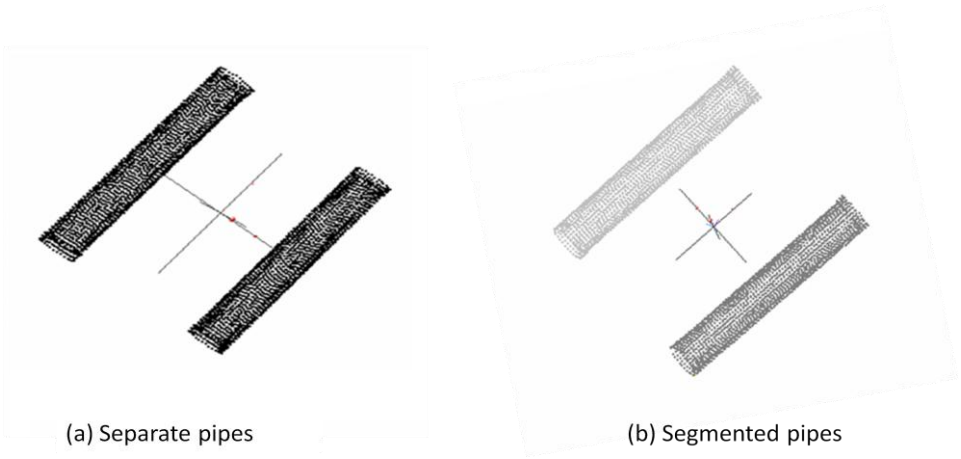

Figure 4-25 Segmentation of separate piping elements (point spacing = 0.002m)

The segmentation parameters used for the example are given and explained below:

- Method of profile segmentation = Proximity segmentation using Euclidean distance
- Distance threshold = 0.003 m
- Stack count = 3
- Profile width = 0.004 m

Figure 4-15 shows the segmentation of piping elements that are disconnected (separate). This was simulated using two straight pipes shown in figure 4-25 (a). Since the elements are not connected proximity segmentation is used.

Method of segmentation is selected based on the fact that the piping elements are separate. Profile segmentation by proximity is thus selected for the example 1 (refer to section 4.6.1). This requires defining a threshold distance used in connecting points to form line segments. The distance used is the Euclidean distance. The threshold distance defined for example 1 is 0.003m. Since the point spacing is approximately 0.002m, a distance threshold of 0.003m ensures points from the same surface are connected. If the distance between the pipes is greater than 0.003, then correct segments are obtained, see figure 4-25 (b).

University of Cape Town

The profile width has to be greater than the point spacing to ensure sufficient sampling of points in a given profile. Profile width is set at 0.004, which is twice the point spacing. This avoids a sparse profile (widely spaced points) which usually results in over-segmentation. A stack count of at least 3 was found to work well for profile segmentation by proximity thus 3 stacks were defined on the points.

Example 2: Coaxial pipes

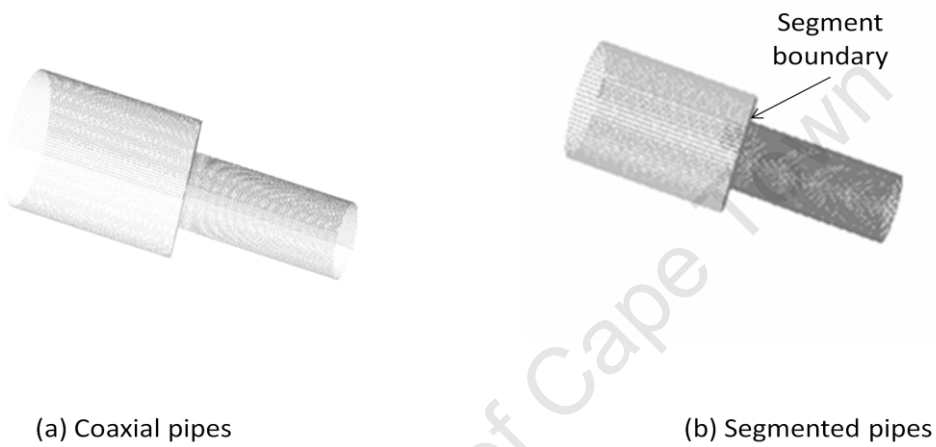

Figure 4-26 Segmentation of coaxial pipes **(**Point spacing = 0.002m) a) point cloud before segmentation b) after segmentation, two separate segments identified

University of Cape Town

Segmentation parameters

- Method of profile segmentation = Profile segmentation by proximity and curve fitting
- Distance threshold = 0.004m
- Profile width = 0.009m
- Curvature threshold = 10
- Stack count = 4.

Figure 4-16 shows the segmentation of coaxial pipes. Since the pipes are connected, profile segmentation by proximity will not detect the required line segments. This requires profile segmentation by curve fitting thus it is employed in example 2. As

mentioned in section 4.6.2, profile segmentation by proximity is first carried out. This ensures that a curve is fit to points in a line segment since a profile might have more than one line segment.

Since curves are to fit to points in line segments, each line segment must have sufficient points on the pipe surface to attract the curve to the surface and counter the effect of noise[3]. The profile width is therefore increased to 0.009m compared to 0.004m which is set for example 1. The curvature threshold is set at 10. A value of 10 was found to produce a correct segmentation for this dataset. This is because the curvature avoids over-splitting of the curve as a result of noise but allows for sharp curvature changes to be detected. Four stacks were defined on the points. The segments obtained are shown in 4-26 (b). The change in radius for coaxial pipes must be significant (refer to example 3).

Example 3: Segmenting a pipe elbow

(a) Pipe elbow

(b) Segmented pipe elbow

Figure 4-27 Segmentation of pipe elbow (Point spacing = 0.02m) a) point cloud before segmentation b) after segmentation, 5 separate segments identified

[3] if there are more points on the pipe surface the effect of erroneous points pulling the curve away from the surface is reduced

University of Cape Town

Segmentation parameters:

- Method of profile segmentation = Profile segmentation by proximity and curve fitting
- Distance threshold = 0.03m
- Profile width = 0.06m
- Curvature threshold = 10
- Stack count = 4.

Figure 4-27 (a) shows an elbow composed of five different elements (i.e. 2 straight pipes, 2 flanges and a pipe bend). Profile segmentation by proximity and curve fitting are both employed since the elements are connected. The threshold distance set is 0.03m which is one and a half times larger than the point spacing. The profile width is set at 0.06m which is three times larger than point spacing. This is to ensure the curve is attracted to the pipe surface and counter the effect of noise. The stack count is 4.

Figure 4-27 (b) shows the 5 different segments obtained. The flanges are in different segments. However, the flange edges were not demarcated correctly in figure 4-27 (b). This is because the change in radius was fairly small. A significant change in radius allows for the demarcation of correct flange boundaries as the discontinuity is discernible. This is illustrated in figure 4-28.

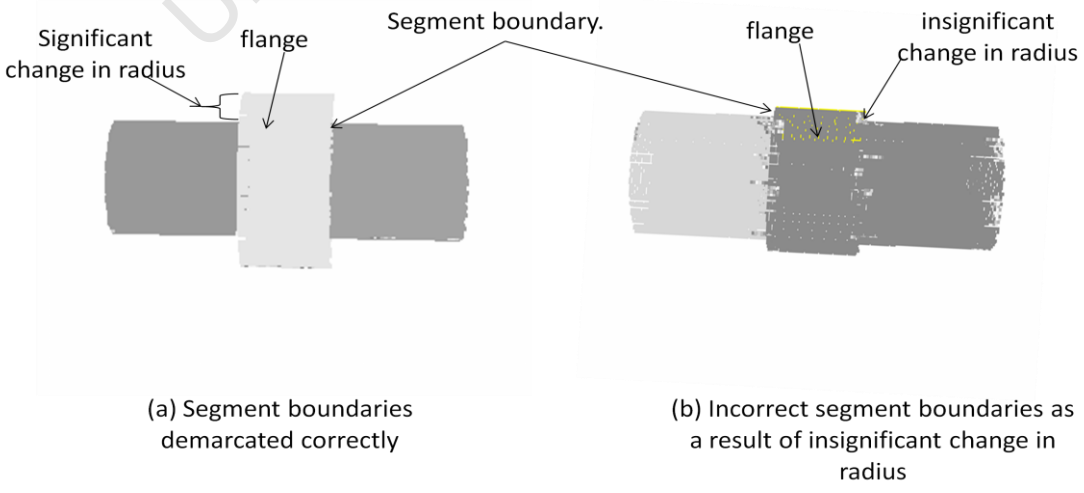

Figure 4-28 Boundary detection in segmentation

University of Cape Town

Figure 4-28 (a) shows the result of the segmentation where the flange has a significantly large radius. The segments are not correctly demarcated in figure 4-28 (b). This is because the change in radius is smaller compared to the figure 4-28 (a).

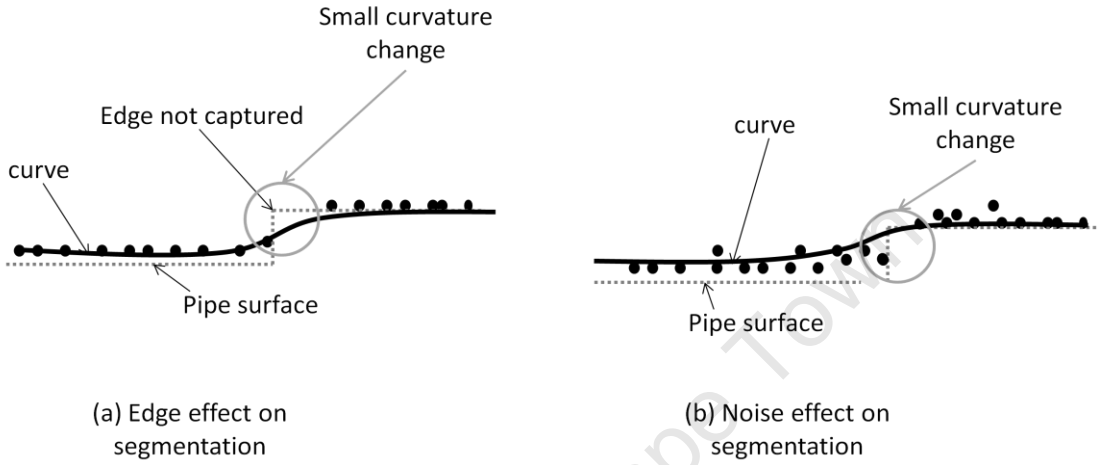

Figure 4-29 Edge and noise effect on curve splitting a) sharp curvature changes are not identified since the edge is not captured b) noise attracts the curve away from surface hence curvature changes are along the surface

University of Cape Town

Another factor that causes incorrect discrimination of segment boundaries is that when scanning, the edges are not captured accurately. This has been discussed in chapter 2, section 2.3. The result is that sudden changes in curvature will not be detected along the curve as illustrated in figure 4-29 (a). In such cases, the discontinuity is not discernible. Noise also affects the segmentation in a similar manner as illustrated in figure 4-29 (b). The curve will not follow the exact form of the surface. Discontinuities will not be detected in some cases, figure 4-29 (b).

Not only is curvature change encountered with a change in radius. Curvature changes are also encountered when pipes are connected to other surfaces that are not associated with a radius (e.g. plane). This is illustrated by the example in figure 4-30.

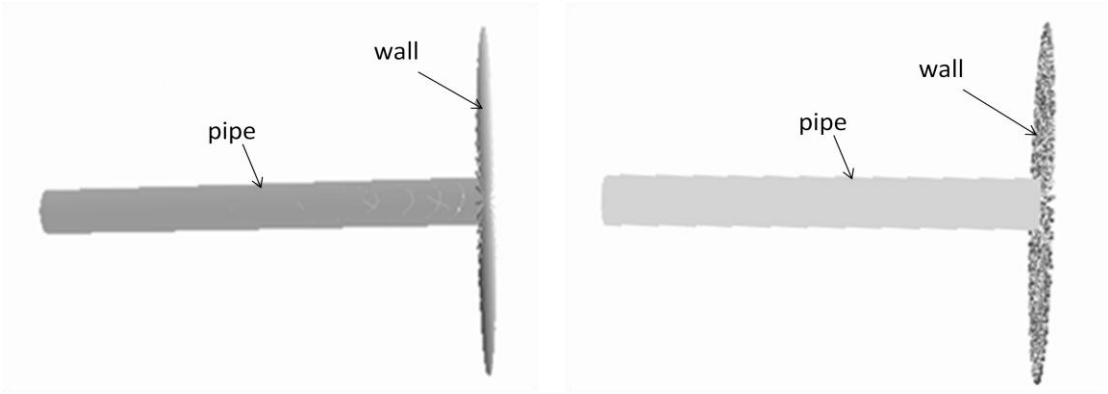

Figure 4-30 Segmentation of pipe segment connected to plane surface a) point cloud before segmentation b) point cloud after segmentation, pipe points separated from wall points

Figure 4-30 (a) shows a pipe running into a plane surface. Figure 4-30 (b) shows the detected pipe segment. Profile segmentation by proximity is used in obtaining the straight pipe segment.

Example 4 Segmenting real data

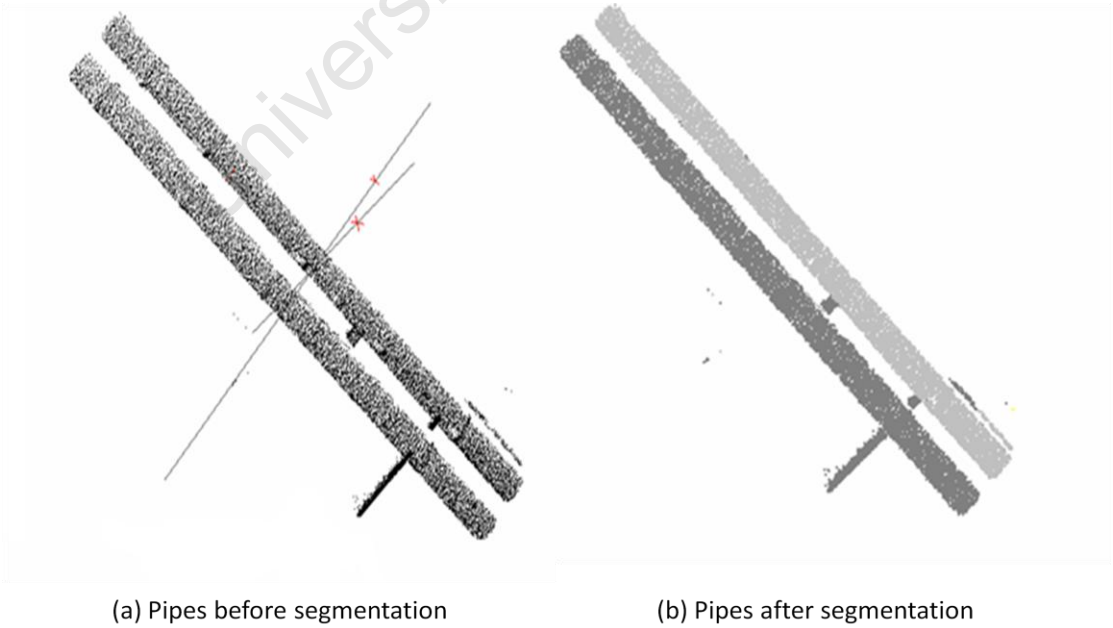

Figure 4-31 Segmentation of real data sample (point spacing < 0.006) a) point cloud before segmentation b) identified segments

University of Cape Town

Segmentation parameters:

- Method of profile segmentation = Profile segmentation by proximity and curve fitting
- Distance threshold = 0.01 m
- Point spacing < 0.006m
- Profile width = 0.02 m
- Curvature threshold = 10
- Stack count = 4.

Figure 4-31 shows the segmentation of real pipe data. Both profile segmentation by curve fitting and proximity were used in segmenting the data. Four stacks were used in the segmentation. The different segments obtained are shown in figure 4-31 (b).

The distance threshold used in the example above is 0.01m which is almost two times greater than the point spacing. This is because more variations in point spacing are encountered in real data as a result of occlusions, range of object from scanner and outliers (this is discussed in chapter 2). Consequently, the profile width set is even larger, which is 0.02m. The profile width ensures sufficient point sampling in each profile. A stack count of 4 is also used.

University of Cape Town

4.8 Discussion

Profile segmentation by proximity has the advantage of identifying most outliers in a point set. All points which do not meet the proximity measure (this includes outliers) are regarded as separate segments hence outliers are identified. The effect of outliers in detection is therefore reduced.

Correct segmentation results using this algorithm depend mainly on profile width and point density. Uneven distribution of points results in over segmentation. With profile segmentation by proximity, a threshold distance is difficult to set due to varying point spacing. As a result, points are not connected correctly in some cases. Increasing the threshold distance can result in under segmentation as neighbouring surfaces are

merged into segments. Uneven point distribution also affects curve fitting in profile segmentation by curve fitting. Sufficient point densities are required on the pipe surface to attract the curve to the surface and counter the effects of noise. Noise results in the curve being attracted away from the surface if the point set has a high percentage of outliers and fewer samples on the pipe surface.

It is imperative to carry out profile segmentation by proximity before segmentation by curve fitting. This ensures a single curve is fit to a single line segment. Profile segmentation by curve fitting then ensures that a line segments is made up of points from the same pipe surface.

Profile segmentation by curve fitting depends on detecting geometric discontinuities introduced by abrupt changes in surface characteristics. Change in radius of a pipe or pipes running into walls are good examples. If pipes are smoothly connected without noticeable discontinuities, figure 4-32 (a), one segment is detected.

University of Cape Town

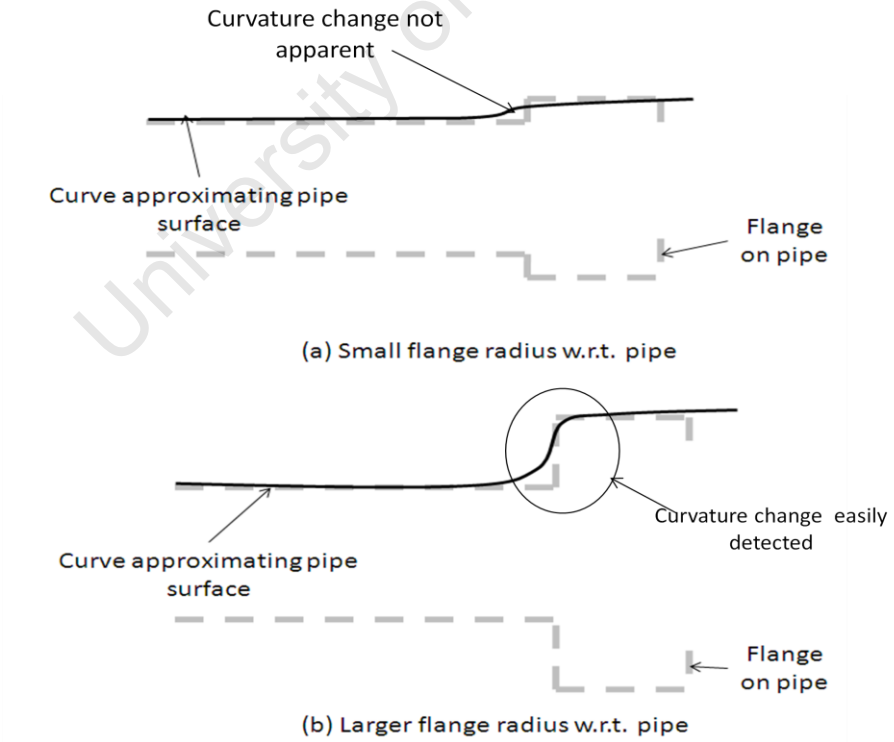

Figure 4-32 Segmentation by curve fitting (effect of flange radius on segmentation. The larger the radius of the flange w.r.t pipe, the more accurate the segmentation)

Figure 4-32 (a) shows a flange that has a radius slightly larger than the pipe and (b) shows a larger flange radius. The boundary of the pipe is more likely to be detected in (b) as the change in curvature introduced by the change in radius is more evident than in (a). The algorithm requires a higher point density for the surface form to be recreated correctly.

The product of the segmentation is various segments representing different piping elements. The next step is to detect the actual element represented by these segments (i.e. straight pipe, elbow or pipe bend, sphere). The detection of these elements is detailed in the next chapter.

University of Cape Town

5. Pipe Detection

5.1 Introduction

A segmentation approach for piping elements was proposed in the previous chapter. Each segment consists of points representing a piping element. A detection procedure must be carried out to establish the type of piping element represented by each segment.

This chapter details the algorithm designed for detecting piping elements after segmentation. Firstly, a description of what constitutes a piping element is given. Next, the concept used in the detection is detailed and finally, the detection algorithm is presented.

5.2 Piping elements

Most piping elements (elbows, t-junctions, flanges, straight pipes etc) can be represented by four geometric primitives namely cylinder, sphere, cone section and torus (i.e. they can be constructed by performing boolean operations on the primitives). Figure 5-1 shows examples of some boolean operations on the above mentioned primitives. Some complex elements cannot be described explicitly by mathematical equations but can be described using equations of primitives used in constructing the element.

Detecting piping elements can therefore be considered as detecting the individual geometric primitives which constitute that element. The algorithm will thus be detailed in terms of detecting the four geometric primitives. The concept used in the detection of these primitives is outlined in section 5.3. Before explaining the detection a definition of the axis of each primitive is required for explaining the detection concept. This definition is given in the next section.

University of Cape Town

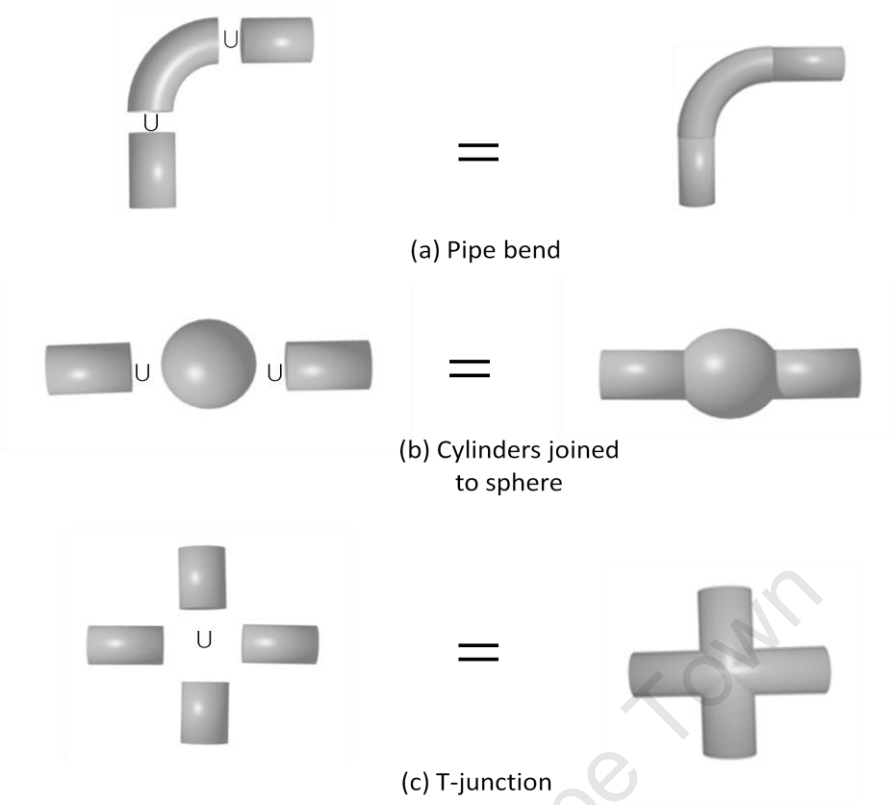

Figure 5-1 Constructing piping elements using Boolean operations on geometric primitives

University of Cape Town

5.2.1 Axis of geometric primitives

Each of the primitives mentioned in the previous section are associated with an axis. A definition of this axis for each primitive in this context is given in figure 5-2. A cylinder axis is the line formed by connecting the centres of the cylinder bases. The axis of a cone is the line which passes through the apex and centre of the base. The torus axis in this context is the circle formed by rotating the major radius of the torus about the centre of the torus.

A sphere has an infinite number of axes that can be defined. Any line which passes through the centre of the sphere will be referred to as the axis.

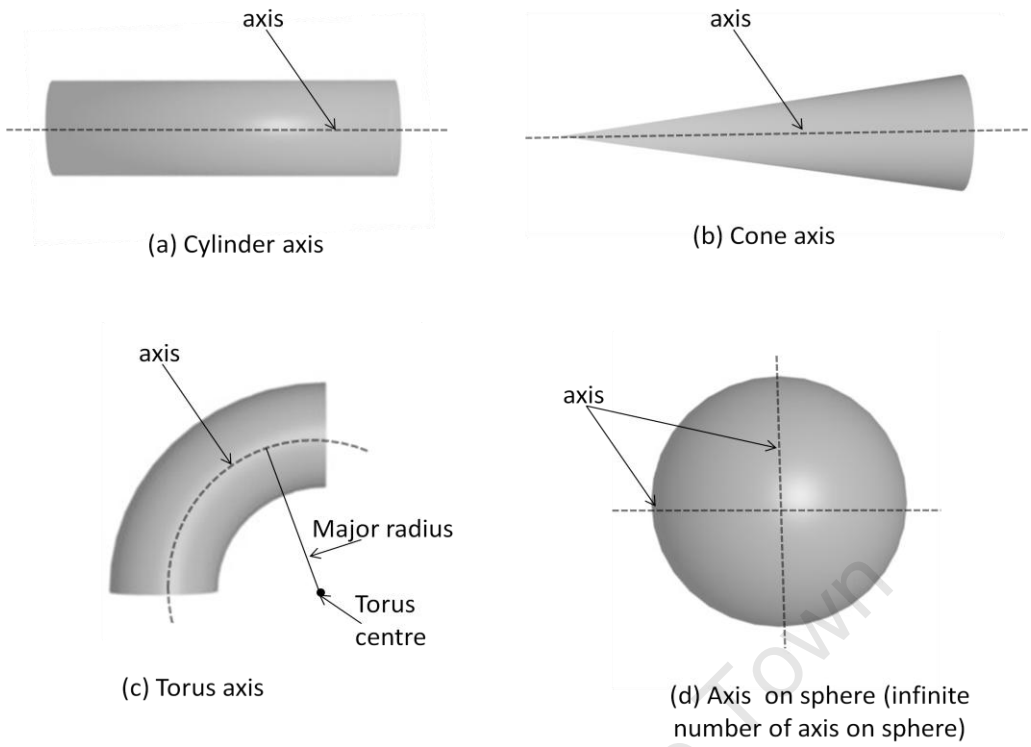

Figure 5-2 Axes of geometric primitives

University of Cape Town

5.3 Detecting geometric primitives

The four geometric primitives (cylinder, sphere, torus and cone) can be described using a radius and an axis, refer to figure 5-2. The intersection of these primitives with a plane provides a shape cue that can be used in detecting piping elements.

The intersection of any of the four primitives with a plane surface forms an ellipse on the plane if the plane cuts the axis of the primitive. This is shown in figure 5-2.

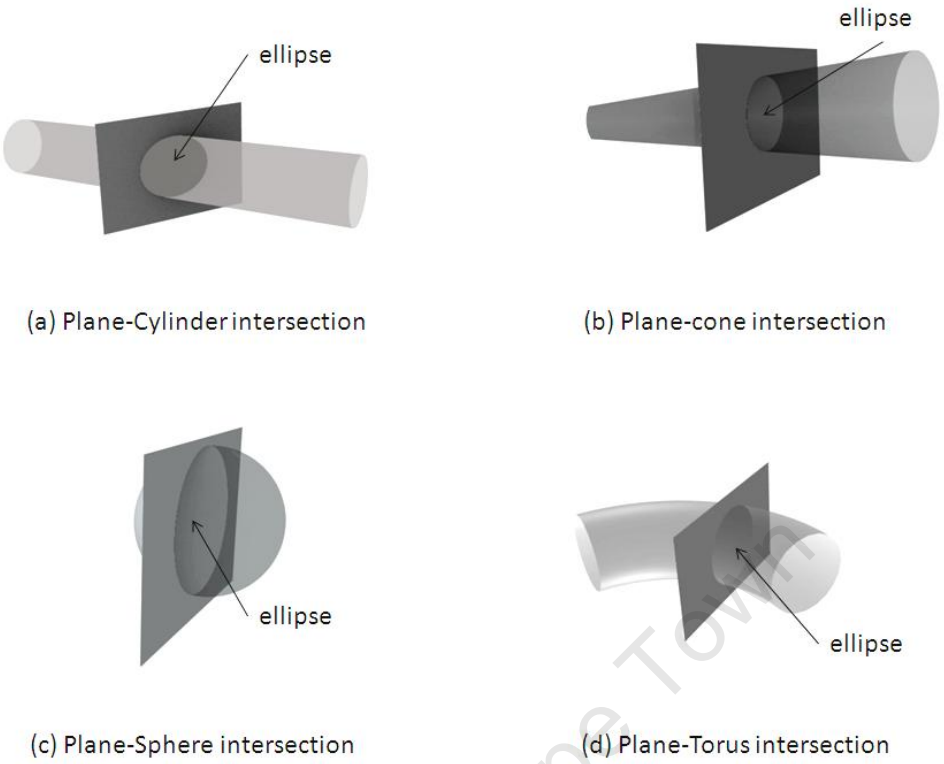

Figure 5-3 Intersection of planes and geometric primitives

University of Cape Town

The ellipses formed have the following properties:

1. The minor axis of the ellipse is equivalent to the diameter of the primitive. The semi-minor axis therefore gives the radius of the pipe. This applies to cylinders and tori.
2. The ellipse centres lie on the axis of the primitive. This condition is true for cone sections only if the ellipses formed are circles (i.e. major and minor axis equal). This occurs when the plane is perpendicular to the axis of the cone section.
3. The axis direction is traced out by the centres for all primitives.
4. A circle is always produced from the intersection of spheres[1] with planes.

[1] A sphere is an ellipsoid. Other ellipsoids (e.g. prolate or oblate spheroid) exists but their intersection with planes does not always produce ellipses

5. The radius of a sphere is equivalent to the semi minor axis of the ellipse whose centre coincides with the centre of the sphere.

These properties are based on the assumption that the primitives are free of deformations. This implies the piping elements are also free of deformations.

In a given point cloud, piping elements are represented by points. This means the primitives which constitute the element are represented as points. Intersecting a plane with these points will result in an ellipse traced out by points on the plane. This is illustrated using a straight pipe (cylinder) in figure 5-4.

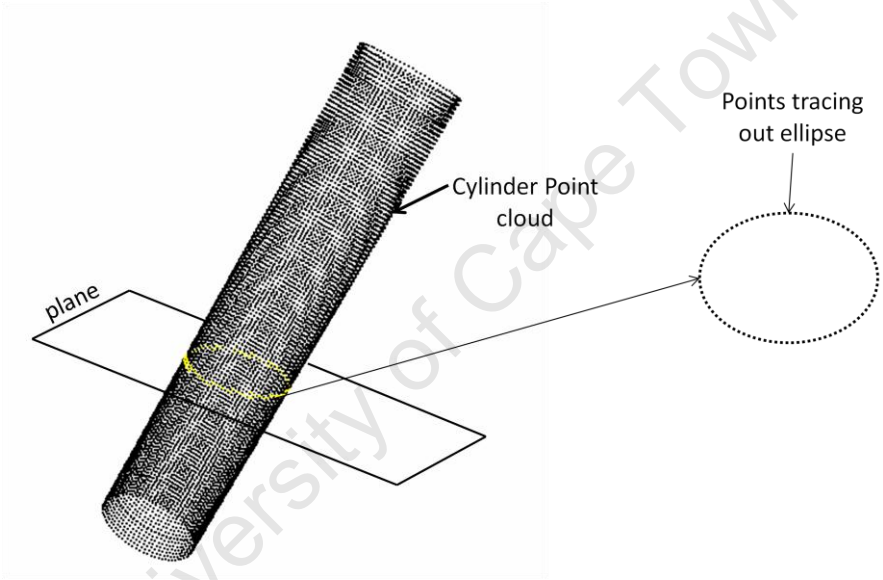

University of Cape Town

Figure 5-4 Intersection of a cylinder point cloud and plane or profile. An ellipse is traced out at the points of intersection

Figure 5-4 shows the intersection of a cylinder point cloud and a plane. Points on the plane will trace out an elliptical path as shown in figure 5-4. By substituting the plane with a thin profile, the points in the profile will trace out an elliptical path[2]. This is illustrated in figure 5-5. The points are then transformed to a 2D frame. This is the

[2] The profile width is larger for illustration. The width is usually smaller

X’Y’ plane (profile plane) shown in figure 5-5. The result is a set of 2D points tracing out an ellipse.

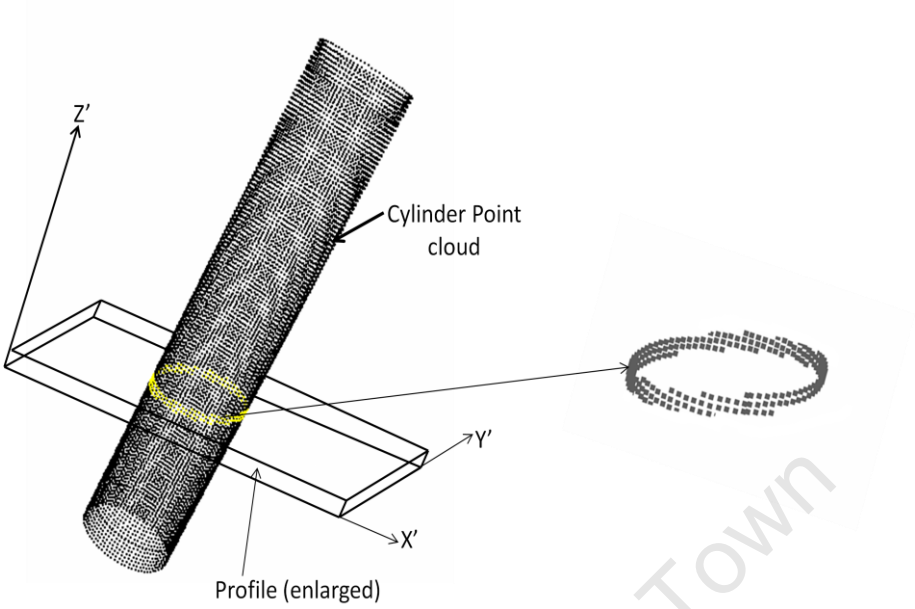

Figure 5-5 Profile intersection with cylinder point cloud, points follow an elliptical shape

From property 1 in section 5.3, by fitting an ellipse to the transformed points, the cylinder radius can be approximated using the semi-minor axis of the ellipse. The centre of the ellipse will be on the axis of the cylinder. If multiple ellipses are fit to different sections of the cylinder, then the axis of the cylinder will lie on the centres of the ellipses.

By detecting ellipses in profiles, the centres of the ellipses and the minor axis lengths of the ellipses, geometric primitives can be identified. The detection task can now be described in terms of finding ellipse centres and ellipse minor axis for primitives in a point cloud. The axis of each primitive is then represented by the centres and the radius is deduced from the ellipse minor axis. This detection concept is outlined in the next section.

University of Cape Town

5.3.1 Detection concept

By stacking profiles in such a way that they are contiguous, points in any given profile after transformation, will trace out an ellipse if the profile cuts the axis of the primitive. This is illustrated using a cylinder in figure 5-6.

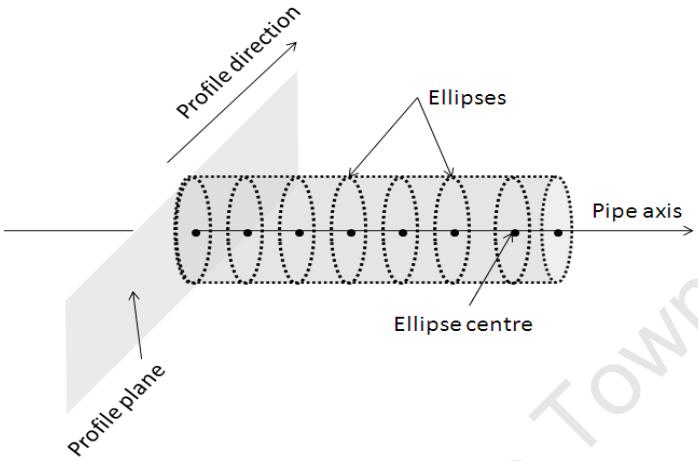

Figure 5-6 Detecting a cylinder in a point cloud using ellipses. The cylinder axis lies on the centres of the ellipses

If ellipses are fit to points in each profile then for a cylinder:

- The axis of the cylinder lies on the ellipse centres (Figure 5-6)
- The radius of the cylinder is ideally equal to the semi-minor axis of any ellipse.

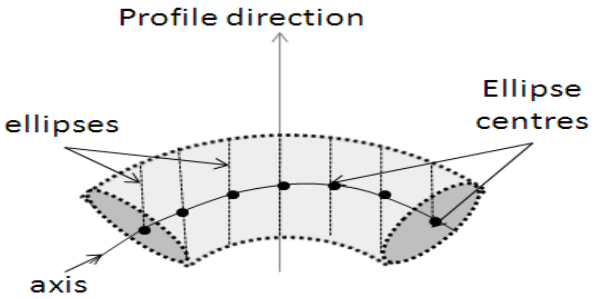

Figure 5-7 Detecting a torus in a point cloud using ellipses. The axis of the torus lies on the ellipse centres.

University of Cape Town

For a 90˚ torus:

- Ideally, the axis of the torus lies on the set of centres (Figure 5-7)
- The minor radius of the torus is ideally equal to the semi-minor axis length of any ellipse.

For a sphere:

- The ellipse centres will trace out an axis that passes through the centre of the sphere
- The radius for the sphere is given by the ellipse whose centre coincides with the centre of the sphere. Circles are always obtained from intersecting spheres and planes
- The ratio a/b is always one for any ellipse formed from the intersection. If all ellipses from differently oriented profiles have a ratio of one then the primitive is a sphere (a is minor axis and b is the major axis).

For a cone:

- The axis of the cone will lie on the ellipse centres if the stack normal is parallel to the cone's axis i.e. the ellipses formed are circles
- The base radius of the cone is obtained from the ellipse formed in the profile at the base of the cone i.e. last profile at the opposite end of the apex.

The scenarios described above are for ideal situations. However as a result of outliers and profile orientation the results will slightly differ from the cases presented here. The effects of outliers and profile orientation on detecting the ellipses are discussed in the next chapter.

5.4 Line segment shapes

Geometric primitives that constitute piping elements are usually oriented differently. As a result, a single profile direction will not cut the axis of all the geometric

University of Cape Town

primitives of some elements. Consequently, not all points in profiles trace out ellipse. Other line segment shapes are traced out by points in profiles at certain orientations. This section discusses the line segment shapes that are traced out by points in profiles at certain orientation.

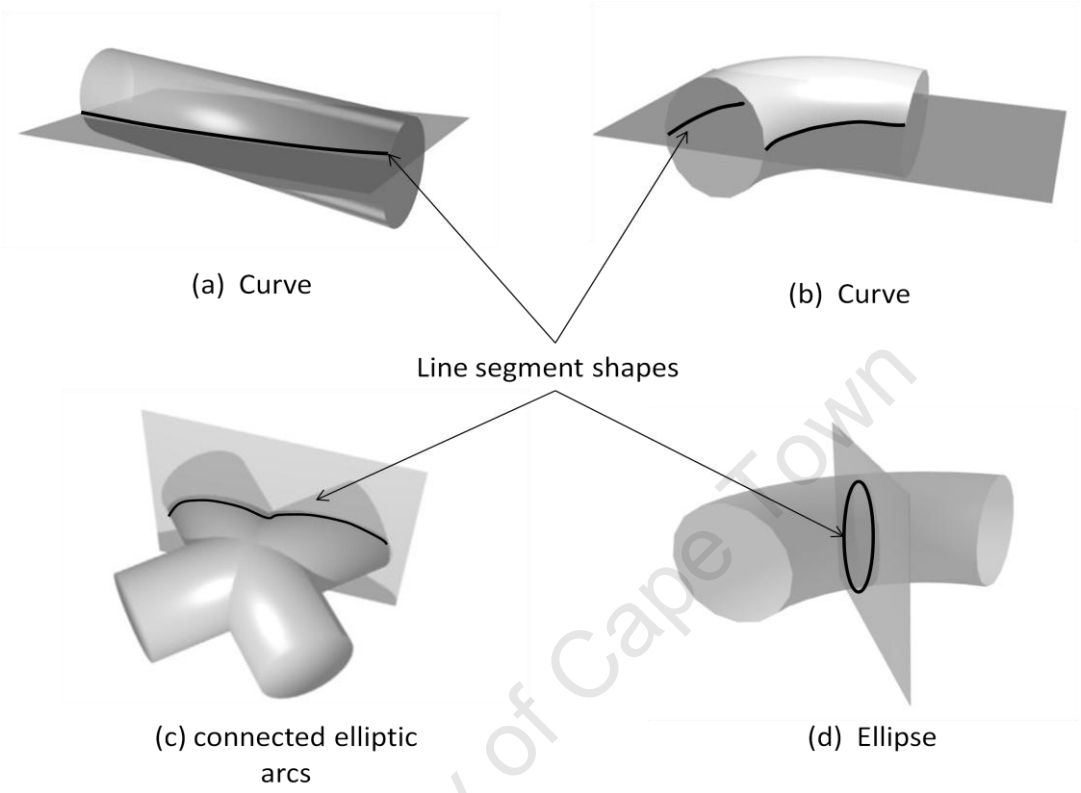

Figure 5-8 Line segment shapes formed from intersecting planes with various piping elements

University of Cape Town

Figure 5-8 shows the possible line segment shapes that can be produced at various profile orientations with some piping elements. Depending on profile orientation and surface area of the piping element captured by the scanner, points in a given profile will trace out 5 basic line segment shapes namely:

1. Line (if stack normal is perpendicular to cylinder axis).
2. Connected elliptic arcs (figure 5-8 (c)).
3. Curve or Parabola (figure 5-8 (a)).
4. Ellipse or elliptic arc.

In instances were partial scans of the primitives are captured points will not trace out the entire ellipse. Elliptic arcs are traced out in such cases, figure 5-9 (a).

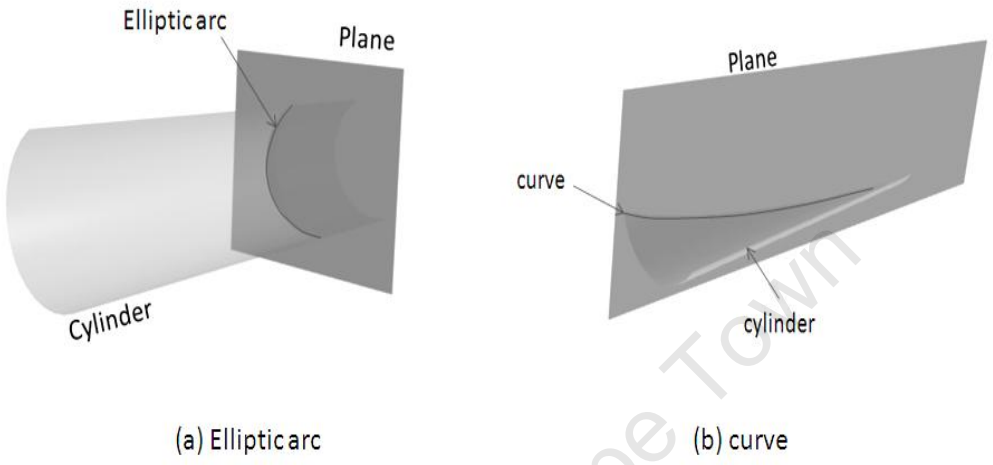

Figure 5-9 Elliptic arc and curve resulting from partial scans of piping primitives

University of Cape Town

The only useful line segment shape is the ellipse or elliptic arc as this indicates explicitly the presence of a geometric primitive. The ellipses or elliptic arcs are then used in calculating the primitive parameters. Lines and curves can be obtained from intersecting other geometric primitives (e.g. cubes) with planes. Therefore, they will provide explicit information regarding the presence of the four geometric primitives mentioned in section 5.2.

Multiple profile orientations have to be defined on piping elements composed of more than one geometric primitive. This will ensure all the primitives constituting the pipe element have at least a profile direction that cuts through the axis. The detection algorithm is based on detecting the ellipses and elliptic arcs. The algorithm is outlined in the next section.

5.5 The detection algorithm

The pipe detection algorithm can be summarised as follows (A successful segmentation is assumed):

- For each line segment in a profile from a given segment, detect ellipses (ellipse fitting). Select ellipses with the required ratio a/b. These ellipses selected are from suitably oriented profiles
- Validate fit (model selection)
- Store the semi minor axis and centre of each ellipse
- Segment the centres (Proximity Segmentation)
- Classify detected pipe elements.

5.5.1 Detecting ellipses

Various profile directions are defined on the entire point set. The directions are set during segmentation. The same profiles are then used in detecting ellipses. Not all profiles defined in segmentation have ellipses or elliptic line segment shapes traced out by points. In order to determine the appropriate ellipses to use for each segment, a selection criterion is placed on the ellipse that is fit to points in a given line segment. The selection is based on the ratio a/b where a is the minor axis and b is the major axis of the ellipse.

The most ideal profile direction is one perpendicular to the primitive axis as shown in figure 5-10. The ratio a/b is approximately one, since the intersection produces a circle. Conversely, it is not possible to define directions that will have ellipses with this ratio in all profiles. A deviation of the stack normal from the primitive axis must be allowed. A deviation of 45˚ was found to be acceptable by experimentation. Any profile direction set in the segmentation that has a deviation angle of 45° in relation to any of the primitives' axis is used.

University of Cape Town

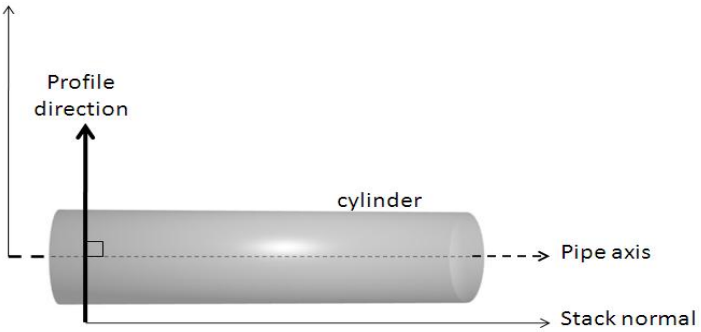

Figure 5-10 Ideal profile orientation for detection

For cylinders and tori[3], a deviation angle of 45˚ will increase the major axis to 1.414a. The ratio a/b will be reduced to 1/√2. The ratio for any ellipse that is fit must therefore be greater than 1/√2. Ellipses with a ratio less than 1/√2 are not considered. The same ratio is applied to cone sections. However, the base radius of cone sections can only be obtained when the ratio is approximately one. Deducing radii values for cone sections is outlined in the next chapter. The ratio for sphere and plane intersection is approximately one.

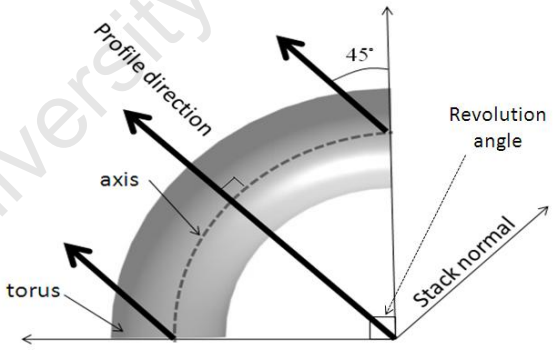

Figure 5-11 Profile direction required for detecting a 90˚ torus

A 45˚ deviation angle allows for the detection of a 90˚ torus; refer to figure 5-11. This is because the torus' axis is circular. The deviation angle will increase along the stack

[3] For tori, the deviation angle is measured from the tangent to the axis

University of Cape Town

normal. After a 90˚ revolution angle the ratio becomes less than 1/√2. Different orientations must be introduced to allow for the detection of torus with a revolution angle greater than 90˚. For a sphere, any profile direction is appropriate. The detection is achieved through ellipse fitting. Ellipse fitting methods used in the algorithm are discussed below.

Ellipse fitting

An ellipse is fit to each line segment in a profile. Firstly, ellipses with a ratio less than 1/√2 are not considered. For the selected ellipses, model selection is carried out so as to select point which best describe an ellipse. Model selection is discussed in section 5.5.2. The ellipse fitting methods employed in the algorithm use two different concepts:

Method 1: Minimising the sum of the squares of the algebraic distance, $F(a, x)$ of a point from the surface of the ellipse subject to the constraint $4ac - b^2$. This algebraic distance, $F(a, x)$ is given by

$$F(a, x) = a.x = ax^2 + bxy + cy^2 + dx + ey + f = 0 \qquad (5.1)$$

Where a is the parameter vector $[a\ b\ c\ d\ e\ f]^T$ and x =$[x^2\ xy\ y^2\ x\ y\ 1]$.

This method is presented by Fitzgibbon et al, (1999). The equations can be solved using a generalised eigensystem (Fitzgibbon, Maurizio and Fisher, 1999). The method requires no parameters estimation for the ellipse. An ellipse fit is always produced even with a high percentage of outliers (i.e. allows elliptical regression). However, ellipse fitting uncertainty remains a problem (i.e. does not return the required ellipse as the distribution of points around the ellipse decreases). Ellipse fitting uncertainty is discussed in section 5.5.4.

Method 2: This method uses non linear regression to fit an ellipse to data points. The method minimises the squares of the distance v of a point from the ellipse surface: The distance v is given by:

University of Cape Town

$$v = d - r \tag{5.2}$$

Where d is the distance from the centre to the data point[4] given by:

$$d = \sqrt{(X - Xc)^2 + (Y - Yc)^2} \tag{5.3}$$

r is given by:

$$r = \sqrt{(0.5a^2 * 0.5b^2) / ((b * \sin(\theta))^2 + (a * \cos(\theta))^2)} \tag{5.4}$$

Where r is the radius value associated with the point from the centre to the surface of the ellipse. Xc and Yc are centre coordinates of the ellipse. X and Y are coordinates of the data point. b = major axis length, a = minor axis length and θ is the angle of the ellipse orientation with respect to the x axis (Nonlinear Regression, 2009).The problem of fitting uncertainty also affects the results. As a consequence, the radius will be difficult to approximate. Examples of other ellipse fitting methods are presented by Gander et al, (1994) and Bookstein (1976).

A point set might fit an ellipse well but produce a better line fit as shown in figure 5-12. In order to validate the fit, model selection is carried out on each point set to find the data which best describes an ellipse. The other line segments are not considered because fitting ellipses to this point data generally yields a ratio less than 1/√2.

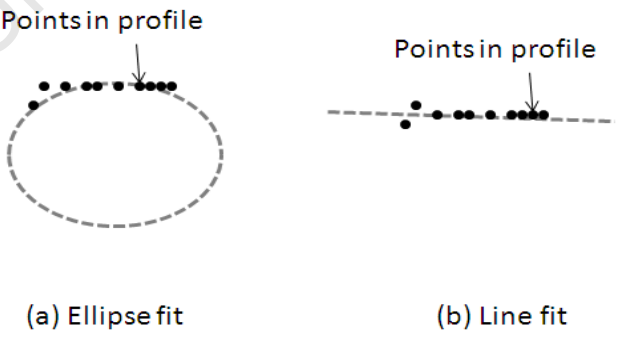

Figure 5-12 Models that can fit line segments a) an ellipse fit to points b) a line fit to the same points as in (a)

[4] Data point refers to the scan point

University of Cape Town

5.5.2 Model selection

Model selection is the task of selecting a statistical model from a set of potential models, given a set of data. A statistical model refers to a set of mathematical equations than can be used to describe the data. The set of data refers to points in a given line segment.

The line segments shapes that are traced out in any profile have been discussed. The detection algorithm requires only an ellipse. In order to establish which model the points in each profile fit better, model selection is carried out. The statistical models are a line and an ellipse. Both models are single-equation models[5]. The selection is carried out on these two models because points tracing out short straight line segment shapes can produce a good ellipse fit, figure 5-12.

If the points fit a line model better, the ellipse parameters obtained from the point set are not considered as this can cause uncertainty as to the kind of underlying surface (Planes can also produce lines when they intersect with cubes or other planes).

The Akaike information criterion (AIC) is used in the algorithm. The AIC only selects the best model between competing models. The requirement is that the models be established prior to the selection. (In this case it is a line and ellipse).

The equation for the AIC is given below:

$$AIC = 2k + n\left[\ln\left(\frac{2\pi RSS}{n}\right)\right] \tag{5.7}$$

Where n = number of data points. RSS = sum of the squares of the residuals from the fit. k = number of parameters in statistical model. The model which produces the least AIC value is selected. If the line model is selected then the fit is rejected but accepted if the ellipse model is selected. Literature on AIC is presented by Burnham et al. (2004).

[5] A single equation is used to describe the data.

University of Cape Town

5.5.3 Segmentation of centres and classification of primitives

The result of the detection algorithm is a set of centres from many different ellipses detected in profiles. An ellipse centre is stored with its corresponding minor axis. Centres of ellipses that represent primitives which constitute a given piping element have to be identified. Since the primitives are connected, the centres representing the axis of each primitive are closer together than any other centres. Therefore, a proximity segmentation of the entire set of centres identifies the sub sets which form the combined[6] axis representing the piping element.

Proximity segmentation of a set of centres is illustrated in figure 5-13. Despite the fact that primitives are detected separately, the centres of primitives which constitute a piping element are connected. Each segment is a set of connected centres representing a single piping element. Proximity segmentation has been discussed in section 4.4.

University of Cape Town

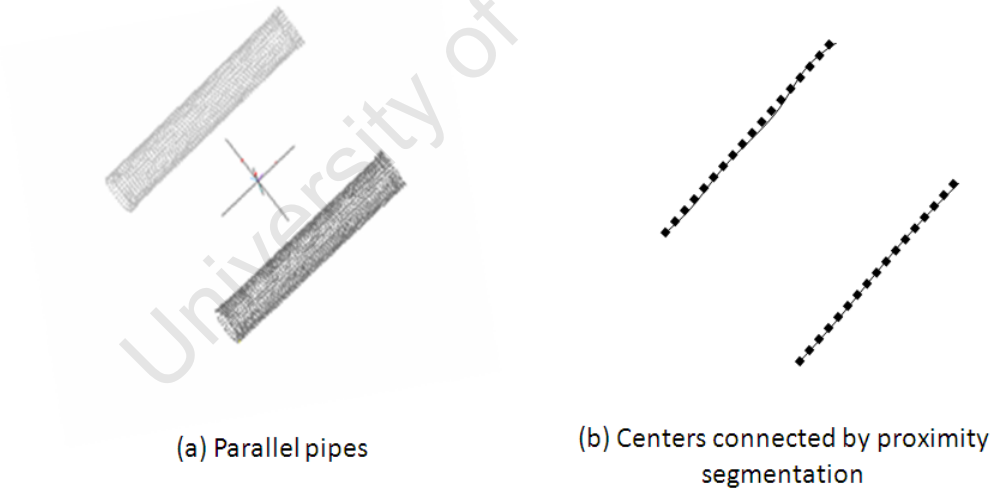

Figure 5-13 Proximity segmentation on centres. Centres representing the axis of a primitive are connected as shown in (b)

[6] Combined because the axes of primitives which are connected are detected as one axis.

Classification

The connected centres do not provide information about the kind of piping element represented by the points. The centres provide information about the orientation and extent of the axis. The only kind of primitive that can be detected from the centres is the torus because the centres will form a circular arc.

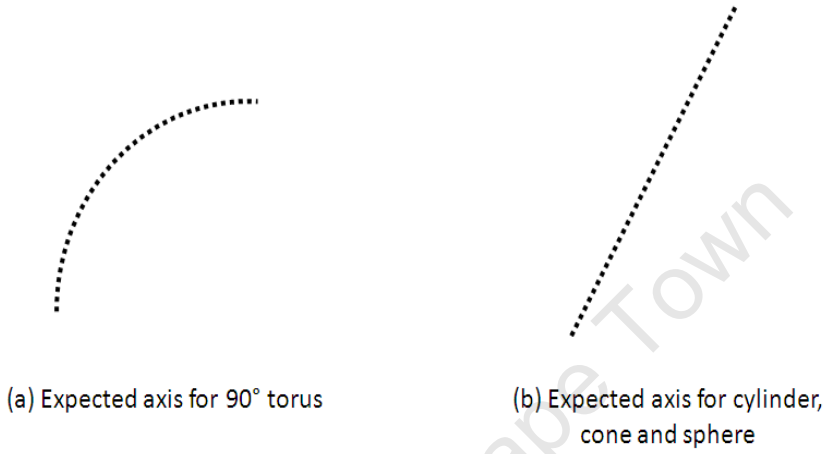

Figure 5-14 Expected axis patterns a) centres from ellipses on tori will follow a circular shape b) centres from ellipses on cylinders, cones and spheres will follow a straight line

Figure 5-14 (a) shows a torus axis represented using ellipse centre. The axis of a cylinder, cone section and sphere will all form a line as in 5-14 (b). A further classification by radius is required to identify the three primitives separately. A plot of the semi- minor axis, which represents the radius, from each ellipse on a given segment, follows different patterns for the primitives. This is shown in figure 5-15. The shape of each graph will help in determining the underlying primitive. Piping elements' segments that consist of composite primitives can also be classified. An example is figure 5-15 (d), where a cylinder is connected to a sphere. The result is a combination of the pattern of the individual primitives. If the pipe element consists of more than one primitive, this will be shown by the shape of the graph.

University of Cape Town

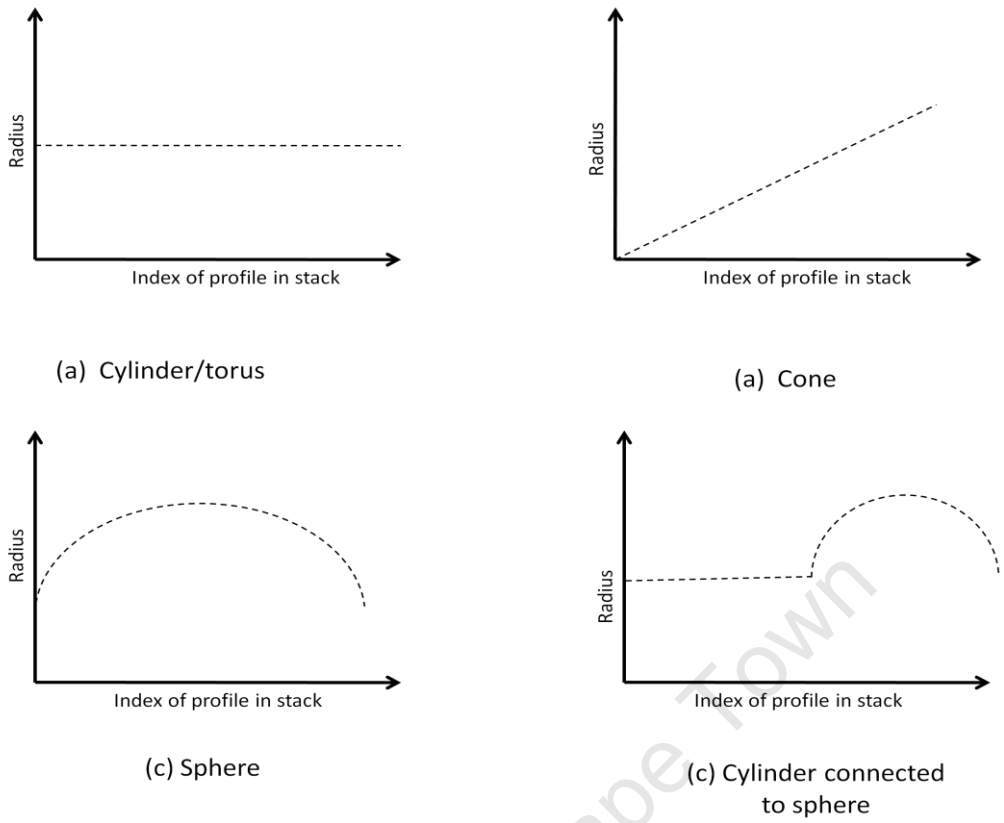

Figure 5-15 Radii value patterns formed by different geometric primitives

University of Cape Town

5.6 Detecting pipe deformations

The detection criteria explained in section 5.3.1 assumes primitives that are free of deformations. For a pipe free of deformations, the primitives' axes will lie on the set of centres obtained from ellipses formed on the primitives. However, if there is a deformation in the primitives, the centres deviate from the axis. The magnitude of the deformation determines the amount by which the centres deviate. This is illustrated in figure 5-16. The ellipses that are fit become smaller[7] (e.g. ellipse 2 smaller than ellipse 1) and the centres are shifted at the points were the pipe is deformed. The result is ellipse centres that deviate from the axis position. This deviation is used for identifying deformations in piping elements. Modelling of these deformations is discussed in the chapter 6.

[7] The ellipses can become larger (e.g. in the case of expansion due to heat)

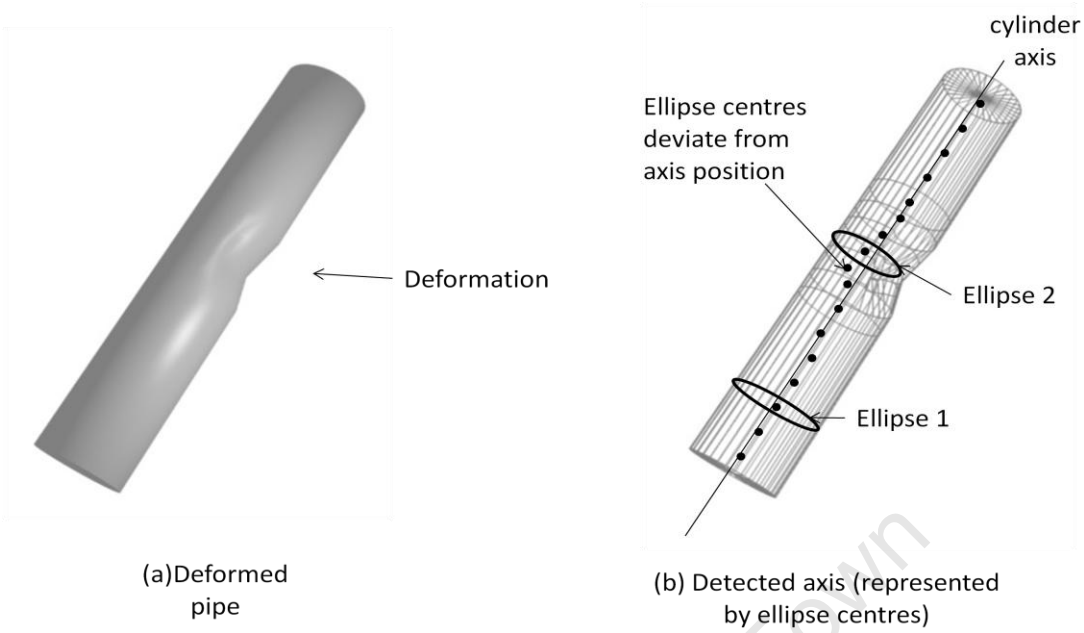

Figure 5-16 Detecting deformations in piping elements a) deformed pipe section will result in the centres deviating from the axis as shown in (b)

University of Cape Town

The semi minor axis of ellipses at the deformed sections can be used as a measure of the magnitude of deformation. This can be achieved by comparing the semi minor axis of ellipses around the deformed area and the rest of the pipe. Not only is the deviation of the centres from the axis is encountered. The same deviation is encountered in the radii values as illustrated in figure 5-17 which is the expected graph for the cylinder in figure 5-16.

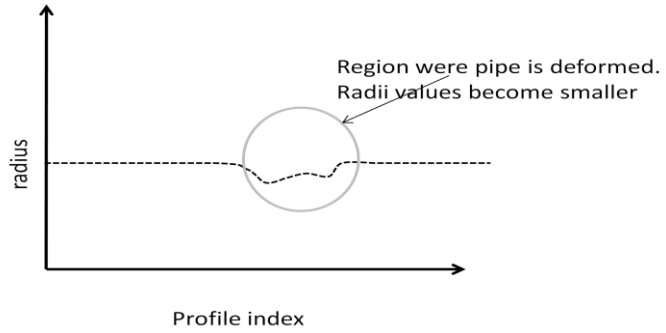

Figure 5-17 Effect of deformations on pipe radii values: variations in the radius values are encountered where a deformation exist

5.7 Errors in ellipse fitting

The ellipse fitting results obtained will differ from the ideal case. This is as a result of outliers in the data, shift in the position of the centre due to the 2D transformation in respective profiles and sampling of points around the ellipse. The sampling of points has the greatest effect on ellipse fitting. Ellipse fitting ambiguity is encountered when the entire ellipse is not sampled. This and errors from transformation are discussed below.

5.7.1 Ellipse fitting ambiguity

Point distribution and density will vary across all profiles for each element. The effect is that ellipses fit to each point set in a profile will have different parameters. Point distribution has the greatest impact on the ellipse fitting. Reduced point samples around ellipses in each profile results in multiple ellipses that can fit points from a given line segment in that profile. This is illustrated in figure 5-18.

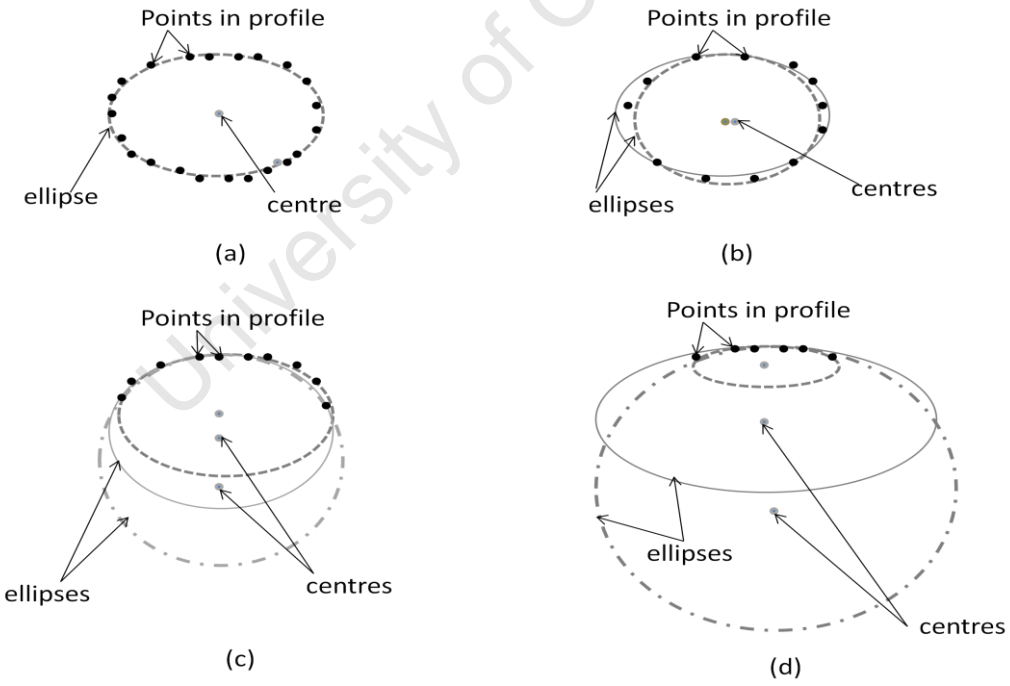

Figure 5-18 Ellipse fitting ambiguity

University of Cape Town

Figure 5-18 (a) shows an even distribution of points around an ellipse. A single ellipse can be defined for the points. Figure 5-18 (b) shows a different distribution in the same profile. Another ellipse can be defined that can fit the same point set. Figure 5-18 (c) and (d) shows an increased number of ellipses that can be fit to a set of points as point samples around the ellipse decreases. The result is a displaced centre from the true position and varying minor axis. This is referred to as ellipse fitting ambiguity. Another factor that causes ellipse fitting ambiguity is outliers. Noise is usually reduced in the segmentation procedure thus the effect is less compared to the distribution of points around the ellipse (i.e. point sampling around the ellipse).

5.7.2 Transformation errors

As previously mentioned in section 5.3, points in profiles are transformed to a 2D frame which is the profile plane. This is illustrated in figure 5-19.

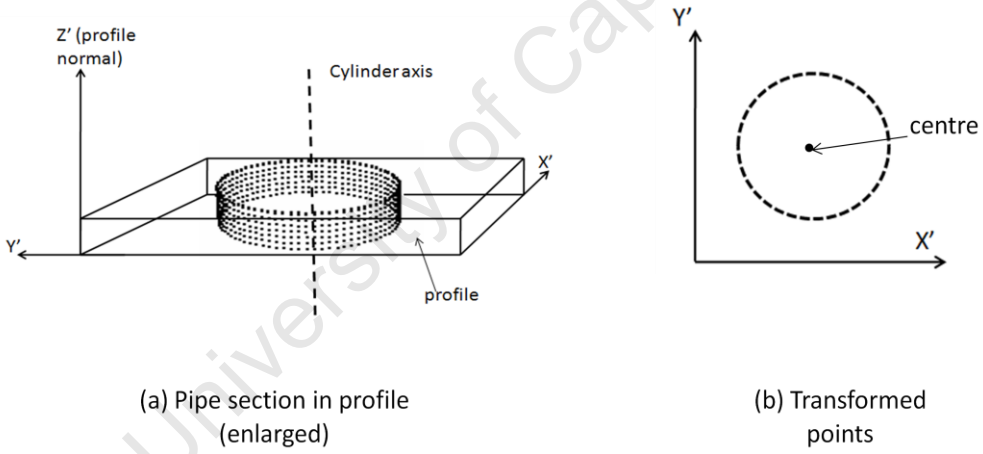

Figure 5-19 Transformation of profile points to a 2D frame a) points in profile in 3d b) points are transformed to a 2D frame

The points are projected to the profile plane (X'Y' plane) along the profile normal (stack normal). If the stack normal and the cylinder axis are parallel, the transformed points form an ellipse (circle) on the profile plane as required. However, if the cylinder axis and stack normal are not parallel (deviation angle is greater than zero), the position of the centre will shift. This is illustrated in figure 5-20. When projected

University of Cape Town

along the profile normal, points closer to the profile plane form an ellipse with boundary 1-2. The furthest points form an ellipse with boundary 3-4. This results in a shift in the position of the centre of the ellipse that are fit. The magnitude of the shift depends on profile width and the deviation angle. The greater the profile width and deviation angle, the greater the shift. This will be referred to as transformation shift/error. This transformation shift is reduced by defining thin profiles. The effect of this shift is encountered if profile segmentation by curve fitting is carried out since it requires the profile width be larger so as to attract the curve to the surface. The centres are slightly shifted from axis position. However, a regression of the centres to find the best fitting axis is performed.

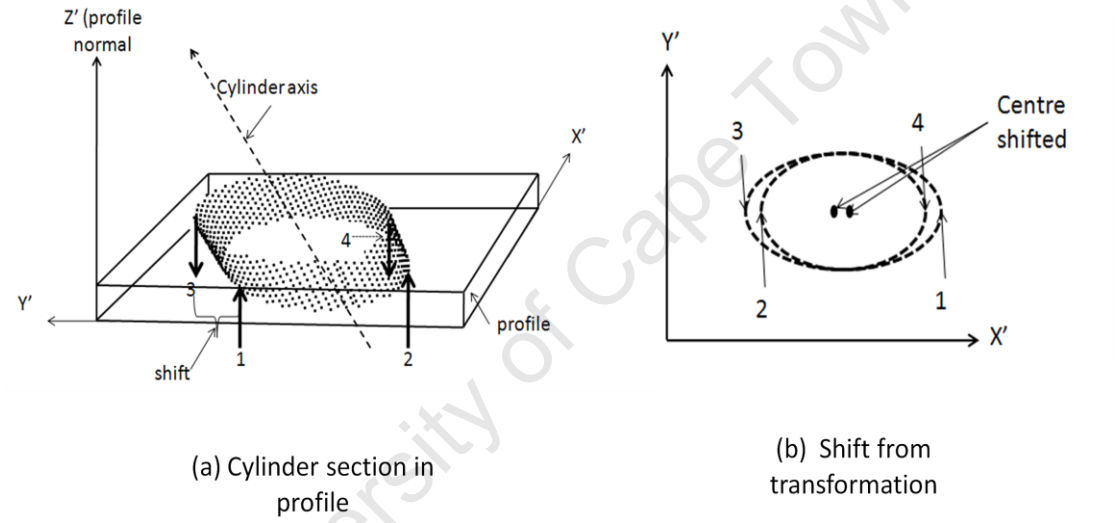

University of Cape Town

Figure 5-20 Shift of ellipse centres due to transformation of points in profiles

If outliers are present around the ellipse, the projected positions of these outliers are outside the bounds of 3-1 in figure 5-20 (b). The effect is that the ellipse is further stretched.

5.8 Discussion

The detection process is generic for most piping elements. Any piping element composed of the four geometric primitives discussed in the chapter is detected. An

essential fact in the detection process is that a single profile direction is inadequate for detecting all primitives. Various profile directions have to be defined on a point set. The orientation and shape of piping elements will dictate the profile directions that are suitable for detecting each piping element.
The success of the algorithm also depends on the ellipse fitting method employed. Ellipse fitting is affected by point distribution and noise. The effect of point distribution and noise on ellipse fitting is discussed in the next chapter.

The true axis position of a cone section is traced out by the centres if the ellipses used have a ratio $a/b \approx$ one. For a ratio less than one, only the direction is traced out but there is a shift in the axis position. However, if multiple ellipses are fit in profiles from many different orientations, a linear regression of the centres will give the best axis position.

The classification of each of the primitives depends on the minor axis lengths of detected ellipses. Tori and cylinders cannot be classified by pattern of the minor axis values because cylinder radii values exhibit the same pattern as tori radii values. The shape of the axis is also used to identify tori. However, the shape of the graph for sphere and cone form unique patterns.

The detection algorithm allows for the detection of deformations in piping elements. These deformations can be detected using either the plot of radii values or the centres representing the axis.

The next chapter presents results of the detection algorithm. The effects of profile orientation, point distribution, deformation and noise on detection are also investigated.

University of Cape Town

6. Results and Quality Analysis

6.1 Introduction

A detection procedure for piping elements was proposed in Chapter 5. The detection algorithm is based on detecting ellipses in a point cloud. These ellipses result from the intersection of profiles with points representing geometric primitives in the point cloud. The first stage of the algorithm is to detect the ellipses in profiles[1]. This is achieved through ellipse fitting after which model selection is carried out to validate the fit. The centre and the semi minor axis of each selected ellipse are stored. The result is a set of centres and semi minor axes of many different ellipses from primitives in the point set. Proximity segmentation is then carried out on the set of centres to establish centres representing axes of individual primitives. Each segment consists of centres representing the axis of a primitive. The radius of each primitive is then approximated from ellipses' centres in each segment. The primitives are then classified based on this radius value after which the elements composed of the detected primitives are determined.

This chapter presents results on the detection algorithm and methods for classifying piping elements. Firstly, test data used the algorithm is described. Next, results of the tests on various elements are presented together with the classification of these elements. Finally, a discussion of the results is presented.

University of Cape Town

6.2 Test data

Data used for testing the algorithm consisted of simulated and real data (point data). The structure of each data set is explained below.

6.2.1 Simulated data

Simulated data was generated with varying point spacings. This data was used in order to:

[1] The profiles are set during segmentation

- Model ideal scenarios of piping elements and establish expected detection results i.e. establish a classification benchmark based on ideal cases/scenarios. Ideal cases refer to detection results of primitives or elements that are free of errors. Ellipses selected in ideal cases have a ratio a/b of approximately one except for tori. This implies the deviation angle is zero hence minimal transformation error. The error resulting from transformation of points in profiles is explained in chapter 5, section 5.7.2.
- Model and investigate the effects of outliers and profile orientation on expected results. Profile orientation is the cause of transformation shifts.
- Use results obtained from simulated data to compare with results from real data in order to classify piping elements detected in real data.

As mentioned in Chapter 5, most piping elements result from performing Boolean operations on four geometric primitives namely cylinders, torus, sphere and cone. These primitives are described using a radius. Each point is associated with this radius value. In order to model errors encountered in scanning, an error is introduced in the radius of each primitive when generating each point. This is explained using the equation of a cylinder below. Introducing an error *e*, see figure 6-1, the position of a point *P* on a cylinder is given by:

$$P = (r'cos\theta, r'sin\theta, h) \qquad 6.1$$

where $r' = r \pm e$ and $h =$ height of point on cylinder.

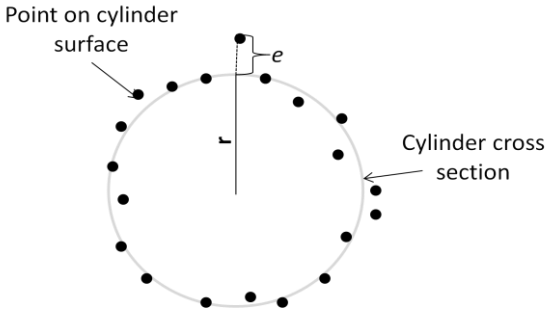

Figure 6-1 Error modelling in data simulation

University of Cape Town

6.2.2 Real data

The real data is a scan of a piping installation. The point spacing is less than 0.006m. Each point has an associated RGB value. The data was split into subsections focusing on individual piping elements to allow for comparison with results from simulated elements.

6.3 Profile orientation vs. ellipse ratio

The concept of profile orientation and ellipse ratios has been discussed in chapter 5, section 5.5.1. This is explained again in this section as it is used in interpreting the results.

As mentioned in chapter 5 section 5.5.1, the most ideal profile direction is one perpendicular to a primitives' axis. This implies that the angle between the stack normal and the axis (deviation angle) is zero. Ellipses formed at this orientation will have a ratio a/b of approximately one.

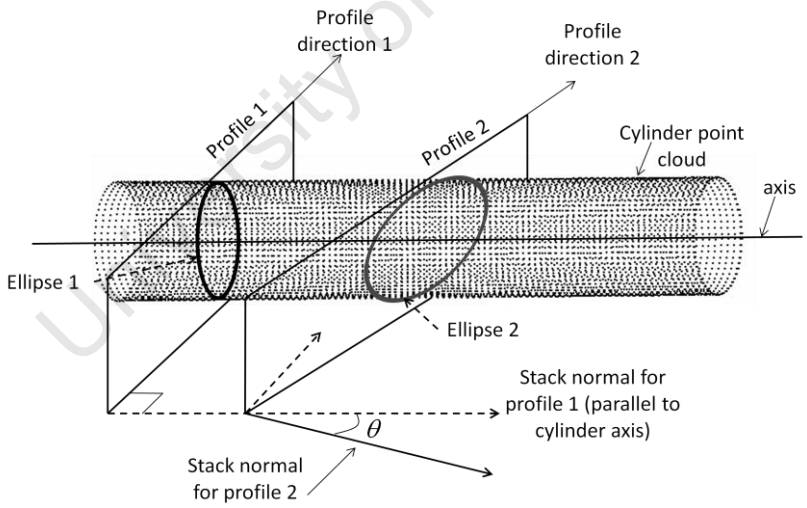

Figure 6-2 Relationship between Profile orientation and ellipse ratio $\boldsymbol{a/b}$**.** Ellipse ratio is given by $\sin(90-\theta)$: Ellipse 1 has a ratio of sin (90) and ellipse 2 has a ratio $\sin(90-\theta)$

This is shown by profile 1 in figure 6-2. Profile 2 has a deviation angle θ from the cylinder axis. An increase in θ will decrease the ratio a/b from approximately one

University of Cape Town

to $\sin(90-\theta)$. Each stack direction is therefore associated with the ratio $\sin(90-\theta)$ which is obtained from ellipses formed in profiles from a stack i.e. a/b. The maximum deviation angle set for the algorithm is 45˚ which corresponds to a ratio of $1/\sqrt{2}$. The effects of selecting ellipses at this ratio are discussed in the sections to follow.

6.3.1 Proximity segmentation of centres

The concept of proximity segmentation was explained in chapter 4, section 4.4. As mentioned in chapter 5, section 5.5.3, proximity segmentation is carried out on the ellipse centres in order to select the points that are closest to each other on the primitives' axes. The result is a set of connected centres. The threshold distance used in connecting the centres is twice the profile width. This will ensure that points are connected since the centres are at least a profile width apart. This profile width is set in the segmentation process. The next section presents the detection results on simulated data.

6.4 Detection results on simulated data

Firstly, the detection results for each of the four primitives in ideal cases are presented, and with each primitive, the effects of outliers and profile orientation on the detection are investigated. The classification procedure for each primitive is discussed based on the results presented. As mentioned in chapter 5, a prior segmentation is required before detection. The segmentation parameters for each primitive are discussed first before the detection results are explained. The segmentation parameters are kept constant for each primitive in all tests.

University of Cape Town

6.4.1 Cylinder detection

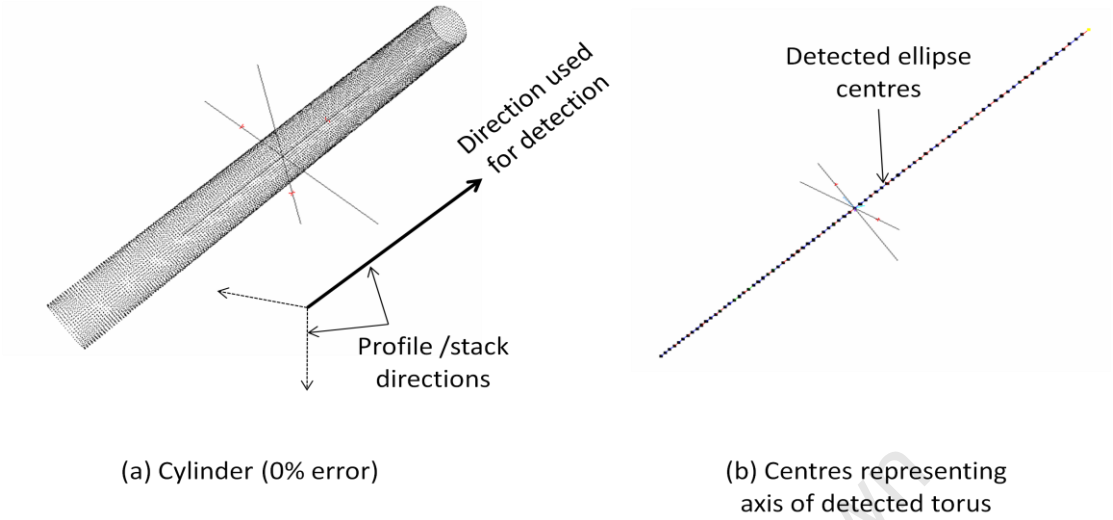

Figure 6-3 Cylinder detection (ideal case) a) simulated cylinder point cloud and the profile direction used b) detected ellipse centres from selected ellipses

Figure 6-3 shows the detection of a cylinder in the ideal case. The cylinder is generated with a 0% error level. The cylinder is shown in figure 6-3 (a). The point spacing is 0.02m. Firstly, segmentation parameters used for the primitive are briefly discussed.

Segmentation

In the segmentation of the cylinder, three stacks are defined. Profile segmentation by proximity is used for the segmentation. A profile width of 0.03m is used. The distance threshold set is 0.025m which is one and a half times greater than the point spacing.

Detection results – Ideal case

Table 6-1 Results of detected cylinder

	Simulated cylinder-radius (m)	Error in cylinder (%)	Detected cylinder radius	Deviation angle (°)	Minimum Ratio (a/b)	Standard deviation (%)
Stack 1	0.2	0	0.2	0	0.95	0

University of Cape Town

In the ideal case for a cylinder, ellipses with a ratio of one are selected. This implies a profile direction with a zero degree deviation angle as shown in figure 6-3 (a). The axis of the cylinder lies on the set of centres shown in figure 6-3 (b). Figure 6-4 (b) shows the set of ellipses that are selected. The ellipses are circles since the ratio is one.

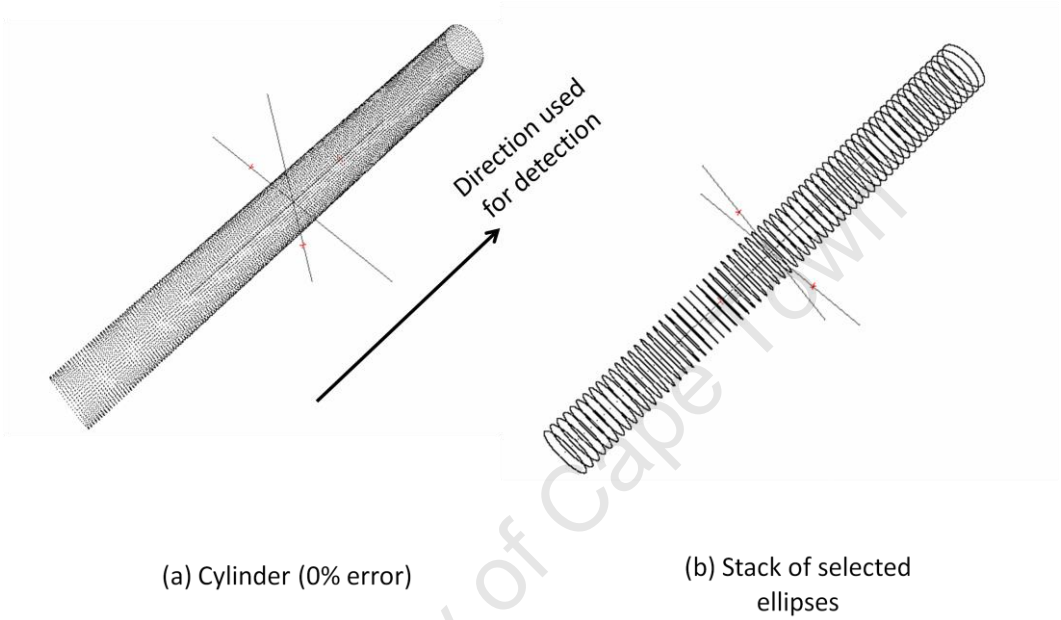

Figure 6-4 Stack of ellipses selected for cylinder detection a) cylinder point cloud and profile direction used b) selected ellipses for detection

University of Cape Town

A plot of the radii values of the selected ellipses[2] is shown in figure 6-5. The radii values from the ellipses are the same across all profiles. The cylinder was generated with a radius of 0.2m which is equal to the value shown in the graph.

Classification of Cylinders (ideal case)

For classification purposes, a cylinder or straight pipe is classified using the shape of the graph in figure 6-5 and the pattern of the centres which form a straight line

[2] Radii values are obtained from semi minor axis of ellipses in each profile from a given primitive segment.

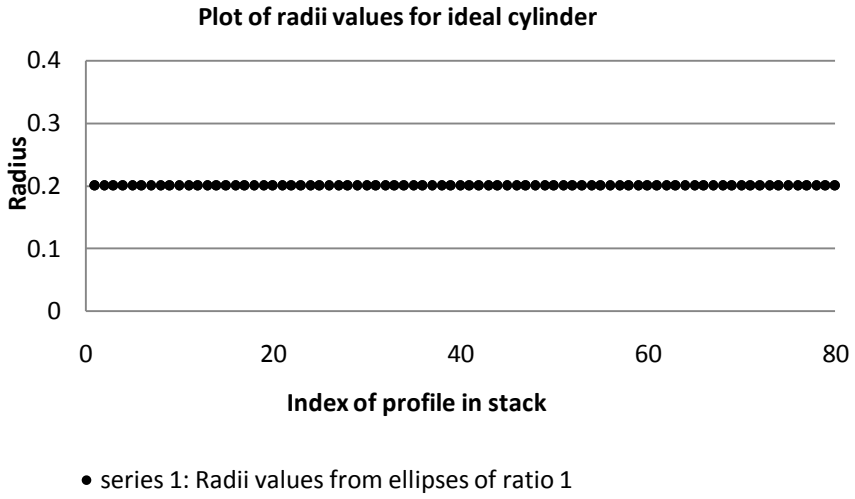

Figure 6-5 Cylinder radii values from selected ellipses: the radii values are semi minor axes lengths of selected ellipses

University of Cape Town

The results obtained from real data will differ from ideal cases as a result of three main reasons namely:

1. Real data contains outliers and partial representation of the primitives as a result of occlusions. This reduces the point samples around the ellipse. As a consequence, different ellipse parameters are obtained in profiles of the same stack for the same primitive. The radii values in the graph will deviate from the true radius values.
2. The algorithm includes ellipses with a ratio of least $1/\sqrt{2}$ (profile orientation of 45˚) in the selection criteria. This results in a shift in the axis position as a result of transformation errors as explained in Chapter 5, section 5.7.2.

Cylinder detection - 5% error

In order to investigate the combined effect of outliers and profile orientation, a second cylinder with an error level of 5% is generated. The ratio for selecting ellipse is reduced to at least $1/\sqrt{2}$. Three profiles directions are set with a deviation of 0˚, 30˚

and 45˚ respectively[3]. This implies the ellipse ratios are approximately one for the profile direction with 0˚ deviation angle, $\sqrt{3}/2$ for a deviation angle of 30˚ and $1/\sqrt{2}$ for a 45˚ deviation angle.

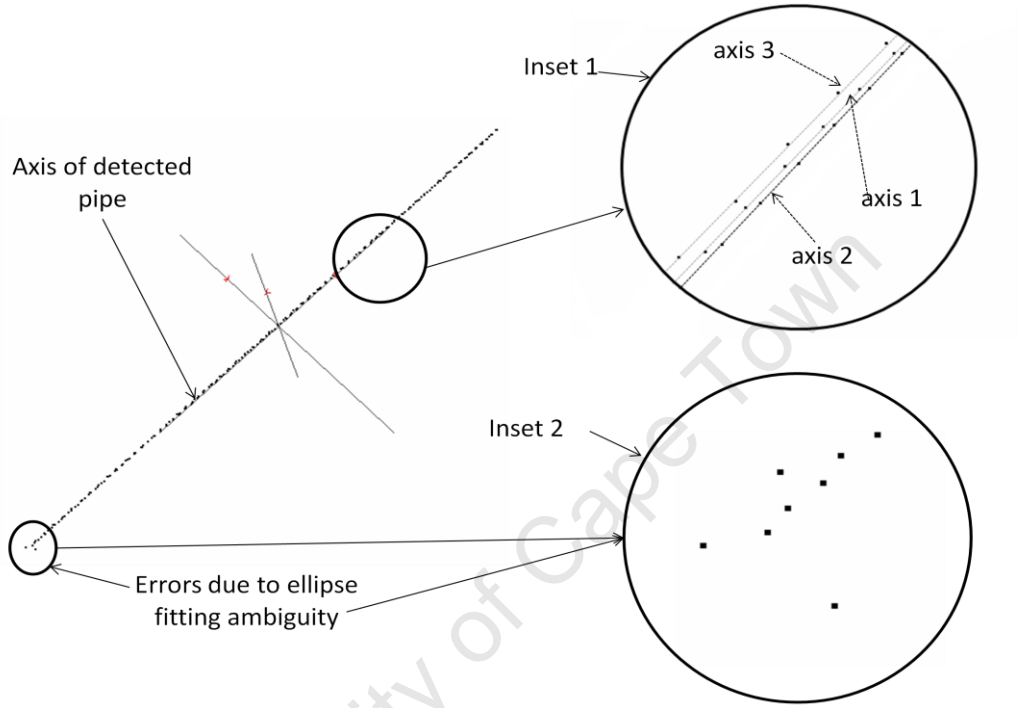

Figure 6-6 Effects of outliers and profile orientation on detected axis for cylinder. Ellipse centres will deviate from the true axis position as the ratio for selection decreases and noise levels increase

University of Cape Town

Figure 6-6 shows the centres of detected ellipses. Inset 1 shows a shift in the axis position as the deviation angle increased. Axis 1 was obtained from a profile direction with a 0˚ deviation angle. Axis 2 was obtained from a profile direction with a 30˚ deviation angle and axis 3 from a 45˚ deviation angle. However, this shift is relatively small compared to the pipe radius and is not easily discernible. A linear regression on the centres however, gives the best approximate axis position.

[3] The stacks that are set for segmentation are the also used in detection. Only profiles with the acceptable orientation are selected. However, for the purposes of testing the algorithm, the directions were explicitly set to the required orientations on the cylinder in the segmentation process.

For a profile direction with a deviation angle of 30˚ and 45˚, the distribution of points around the ellipse decreases towards the ends of the cylinder. This results in ellipse fitting ambiguity (refer to chapter 5, section 5.7.1.). This is illustrated in figure 6-7. Two profiles with the same orientation are shown. Points in profile 1 sample the entire ellipse. Points in profile 2 will only trace out part of the ellipse since only a section of the cylinder intersects with the profile. The distribution of points around the ellipse decreases towards the ends as a result of profile orientation.

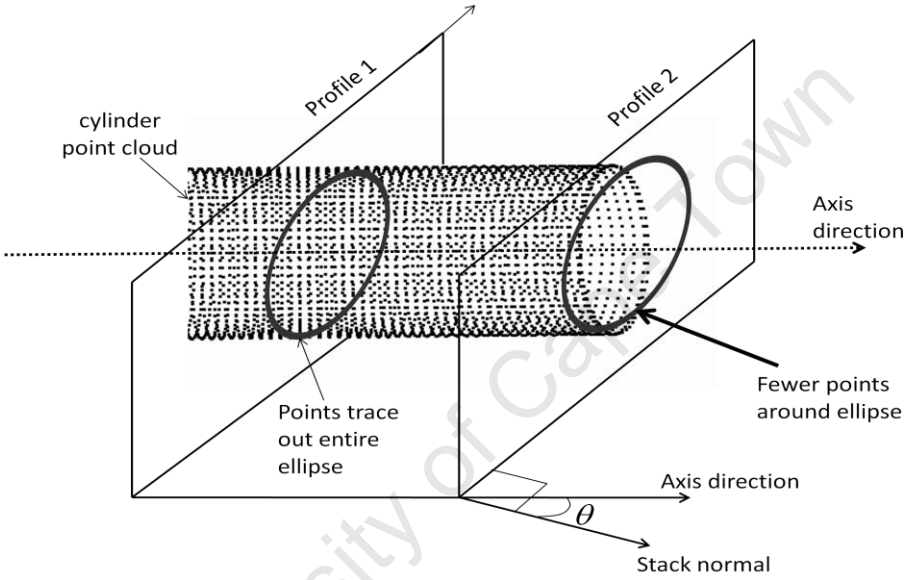

Figure 6-7 Effect of profile orientation on ellipse points sampling: Ellipses at the ends of the pipe will have less point samples around ellipse as illustrated in profile 2

The centres from the ellipse in these profiles will deviate from the true axis position at the ends of the cylinder. This is shown at the end of the axis represented in figure 6-6. The effect of ellipse fitting ambiguity is shown in figure 6-8 (b), which shows ellipse of ratio $\sqrt{3}/2$ i.e. deviation angle of approximately 30°.

University of Cape Town

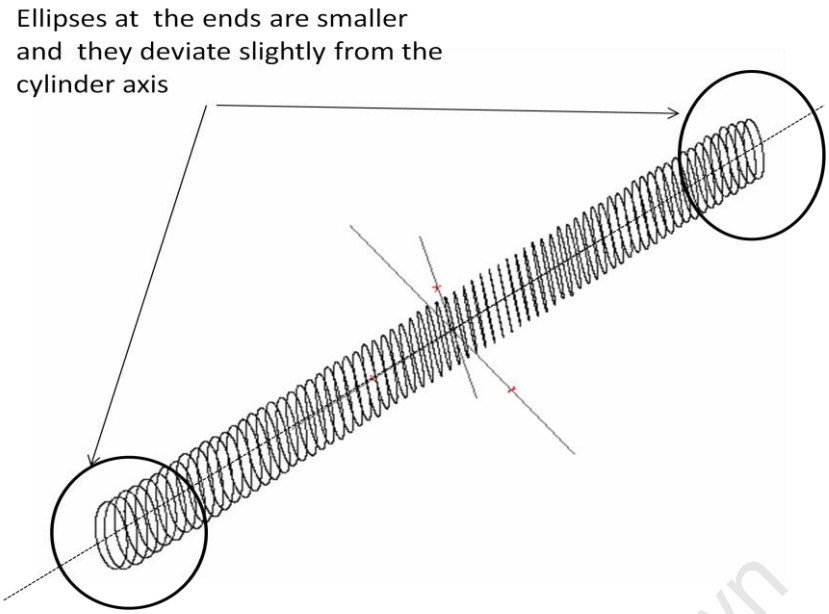

Figure 6-8 Ellipse fitting ambiguity due to profile orientation: Ellipses at the ends are affected by fitting ambiguity as a result of point sampling in profiles and noise

University of Cape Town

The parameters obtained from the detection at different orientation are shown in table 6-2.

Table 6-2 Results for detected cylinder-5% error

	Simulated cylinder-radius(m)	Error in cylinder (%)	Detected cylinder radius (m)	Deviation angle (°)	Minimum selection ratio (a/b)	Standard deviation from true radius (%)
Stack 1	0.2	5	0.197	0	0.95	1.5
Stack 2	0.2	5	0.202	30	$\sqrt{3}/2$	1.5
Stack 3	0.2	5	0.214	45	$1/\sqrt{2}$	7

A plot of the radii values from ellipses in each of the profiles from all stacks is shown in figure 6-9.

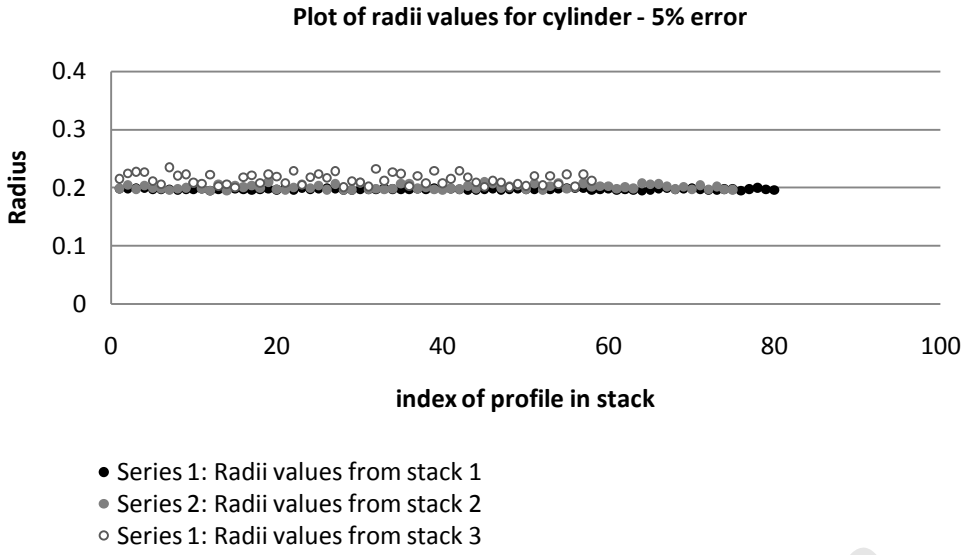

Figure 6-9 Effects of outliers and profile orientation on cylinder radius. Deviation from the true radius value increase as noise and increases and ellipse ration decreases. Series 1, 2 and 3 have ratios 1, $\sqrt{3}/2$, and $1/\sqrt{2}$ respectively

University of Cape Town

Series 1 represents radii values from ellipses with a ratio approximately one from stack 1 since the deviation angle is zero. The average radius of detected cylinder is 0.197m. The standard deviation of this value from the true radius is 1.5%. The profile count for stack 1 is 80.

Series 2 represents radii values from stack 2 which has a 30° deviation angle. The average radius is 0.202m. The standard deviation is 1.5%. The profile count decreases as the deviation angle increases hence the fewer profiles. The profile count is 76. The error in the radius is acceptable.

Series 3 represents radii values from stack 3 with a deviation angle of 45°. The average radius is 0.214m which has a standard deviation of 7%. The profile count is 59. The average radius from stack three has the highest error. This is as a result of transformation errors/shift. As mentioned in chapter 5, transformation shift increases as deviation angle increases. The presence of outliers increases the shift and also stretches the ellipse in both the x and y plane of the ellipse. This accounts for the variations in radii values for stack 3 which are mostly increasing than decreasing. The

minimum value of series 3 do not fall below the values of series 1 and 2. Therefore, minimum radii values for the series 3 give a more accurate radius than the average radius. Profile orientation has less significant effect on the detected axis than on the radii values. This is because the main effect of stretching due to transforming is increasing the minor and major axis of the ellipse. Ellipses with a higher ratio give more accurate results.

Classification

Since ellipses with a ratio $1/\sqrt{2}$ are selected, the combined pattern[4] of the radii values in figure 6-9 is expected from real data. This pattern thus indicates the presence of a cylinder or straight pipe.

Similar test were carried out on the remaining three primitives and the results are presented in the following sections.

University of Cape Town

6.4.2 Torus Detection

A torus of minor radius 0.2 is generated with 0% error. The point spacing of the torus is 0.01m. This torus is shown in figure 6-10 (a).

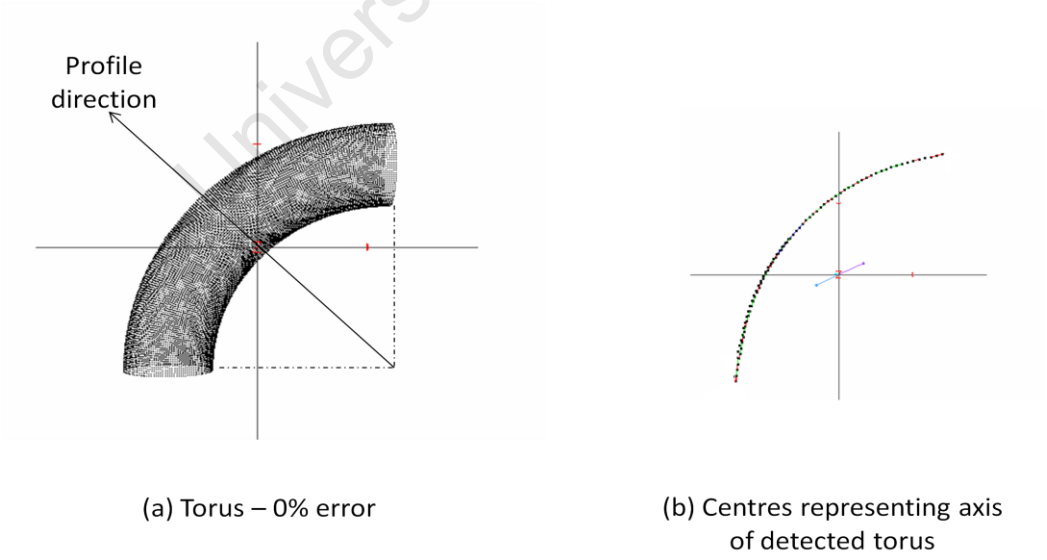

Figure 6-10 Torus detection (ideal case)

[4] Combined pattern refers to all radii values merged into a single series

Segmentation

For segmenting the torus, the profile width is set to 0.03m. Profile segmentation by proximity is used as method of segmentation. A distance threshold of 0.025m is used. Three stacks are defined on the torus for the segmentation. The profile direction shown in figure 6-10 (a) is used in the detection.

Detection – Ideal case

Figure 6-8 shows the detection of a torus in the ideal case. The torus is generated with a 0% error level as shown in figure 6-10 (a), and has a radius of 0.2m. The ratio for selecting ellipses is reduced to $1/\sqrt{2}$ for the ideal case. This is because selecting ellipses with a ratio of one for detecting the torus section requires multiple profile directions. Any stack direction that cuts the circular axis of a 90˚ torus is perpendicular to the torus' axis at a single point. The profile at this point has an ellipse with a ratio of approximately 1. The connected centres after segmentation are shown in figure 6-10 (b). The results for the radius are shown in table 6-3.

Table 6-3 Results for torus detection (ideal case)

	Simulated Torus-minor radius(m)	Error in torus (%)	Detected torus-minor radius (m)	Deviation angle (°)	Minimum selection ratio (a/b)	Standard deviation from true radius (%)
Stack 1	0.2	0	0.206	N/A	$1/\sqrt{2}$	3%

A single stack is used for the detection. The stack direction is shown in figure 6-10 (a). A plot of the radii values obtained from the ellipses is shown in figure 6-11. The average radius for the torus is 0.206m which has an error of 3%.

University of Cape Town

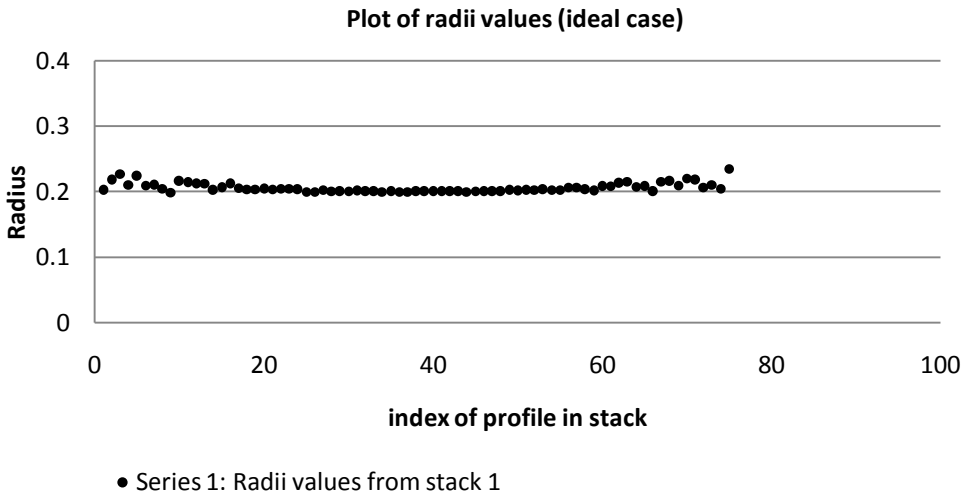

Figure 6-11 Torus radii values from selected ellipses (Ideal case): Ellipse ratio for series one is $1/\sqrt{2}$

The error in the radius is due to the fact that the ellipse is not entirely sampled at the torus ends. The sampling of the points about the ellipse decrease towards the torus ends. This results in fitting ambiguity towards the ends. This is shown by the variations towards the ends of the graph. The ellipses selected for the torus are shown in figure 6-12.

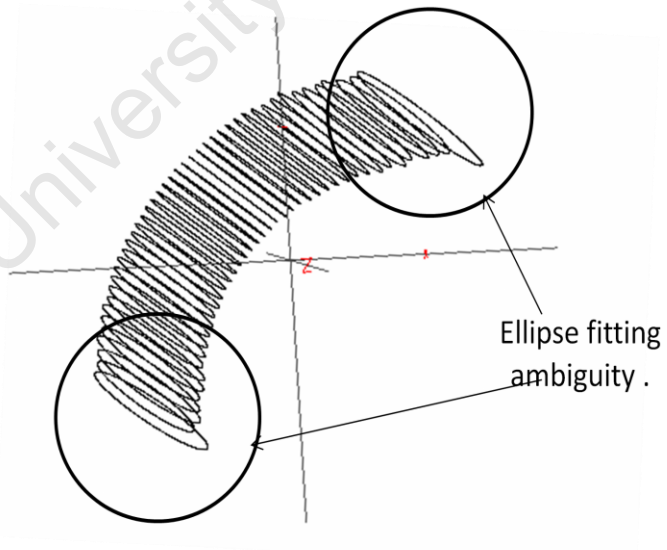

Figure 6-12 Stack of selected ellipse in torus detection: Ellipse at the ends of the torus are larger as a result of fitting ambiguity

University of Cape Town

The ellipses at the ends are larger than expected. These ellipses affect the average value calculated for the torus. In determining the accurate radius of the torus, ellipses which are sampled entirely are used. These ellipses are in the middle of the torus. Therefore, the torus is better modelled in the middle where the values are more precise. The average radius value obtained from using ellipse from profile index 30 to 50 is 0.2m which is the exact radius.

Classification

The shape of the graph is used in classifying the torus. This graph has a similar shape compared to the graph for cylinder radii values. The shape of the axis however, is used in differentiating between a cylinder and a torus.

Torus detection- 5% error

An error of 5% is introduced in generating the torus and the tests are repeated. The results are shown in Figure 6-13, table 6-4 and figure 6-14. The connected centres representing the axis of the torus are shown in Figure 6-13 (b).

The centres deviate from the axis towards the pipe ends. This is as a result of ellipse fitting ambiguity and a slight increase in the shift as a result of transformations. Two stacks in opposite directions are used so as to validate the results.

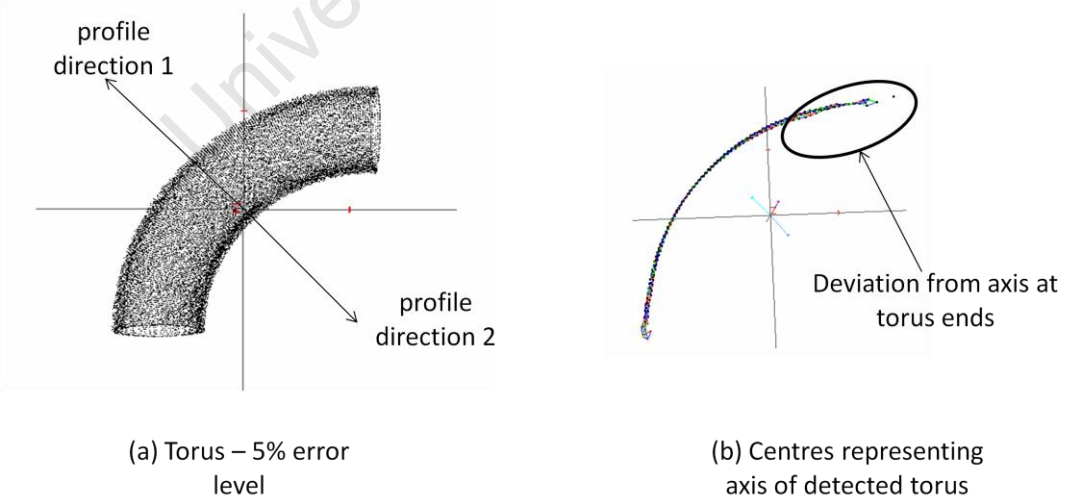

(a) Torus – 5% error level

(b) Centres representing axis of detected torus

Figure 6-13 Torus detection – 5% error: Ellipse centres will deviate from the true axis position as the ratio for selection decreases and noise levels increase

University of Cape Town

The radii values obtained with a 5% error level are shown in Table 6-4. The values are also more precise midway the graph as in the ideal case.

Table 6-4 Torus detection results-5% error

	Simulated Torus minor radius(m)	Error in torus (%)	Detected torus radius (m)	Deviation angle (°)	Minimum selection ratio (a/b)	Standard deviation from true radius (%)
Stack 1	0.2	5	0.206	N/A	$1/\sqrt{2}$	3
Stack 2	0.2	5	0.216	N/A	$1/\sqrt{2}$	8
Profile index 30-50	0.2	5	0.204			2

University of Cape Town

A plot of radii values from ellipses in each profile from the two stacks is shown in figure 6-14. The shape of both graphs is similar to the graph obtained in the ideal case. The increase in the standard deviation is as a result of outliers, fitting ambiguity and transformation shift.

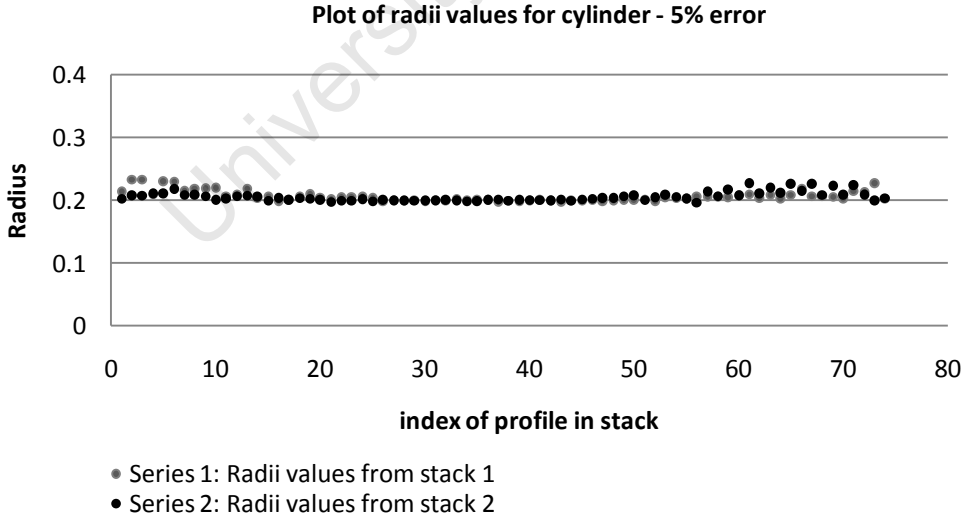

Figure 6-14 Effects of outliers and profile orientation on torus radius: Deviation from the true radius value increase as noise and increases and ellipse ration decreases. Series 1 and 2 have a ratio of $1/\sqrt{2}$

The errors do not affect the classification that is discussed in the ideal case.

6.4.3 Sphere detection

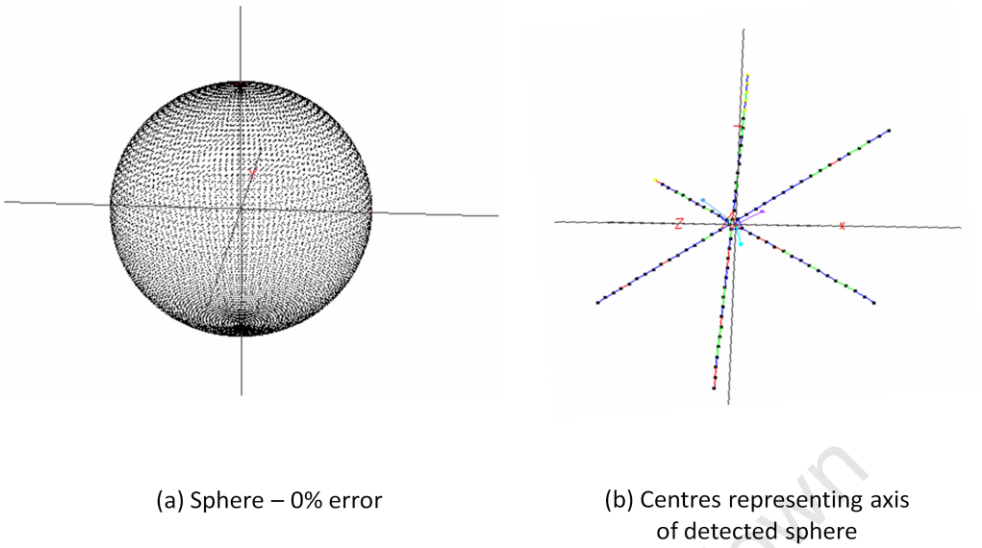

Figure 6-15 Sphere detection (ideal case)

University of Cape Town

Figure 6-15 (a) shows a sphere generated with 0% error. The point spacing is 0.002m. First the segmentation parameters are discussed.

Segmentation

For segmenting the sphere a profile width of 0.004m is used. A stack count of three is used. Profile segmentation by proximity is the method of segmentation used. Distance threshold is set at 0.0035m.

Detection

A sphere has an infinite number of axes that pass through its centre. The axis that is traced depends on the stack direction. When detecting spheres, ellipse centres from profiles of the same stack will trace out an axis direction that is parallel to the stack normal. Figure 6-15 (b) shows the resulting connected centres from the detection. Three profile directions are used in the detection. Therefore, three axes are traced out all passing through the centre. This is one criterion used in classifying spheres. Any stack direction produces similar results on a sphere in the ideal case. This is shown in the graph of radii values from all profiles in figure 6-16. Table 6-5 shows the radius of

the detected sphere from one stack for the ideal case. The ratio of all ellipses for a sphere is approximately one hence no selection ratio is set.

Table 6-5 Sphere detection results (ideal case)

	radius(m) [Simulated sphere]	Error in sphere (%)	radius(m) [Detected sphere]	Deviation angle (°)	Minimum selection ratio (a/b)	Standard deviation from true radius (%)
Stack 1	0.5	0	0.500	N/A	N/A	0

The plot of radii values for a sphere form a circular pattern as shown in figure 6-16. Since all ellipses from a sphere have a ratio of one, the semi minor axis lengths will follow the same pattern for all stacks.

The radius of the sphere is given by the maximum value on the graph. This is deduced from the profile that coincides with the centre of the sphere. For the above example, a sphere of radius 0.5m was generated. The maximum value is approximately 0.5m

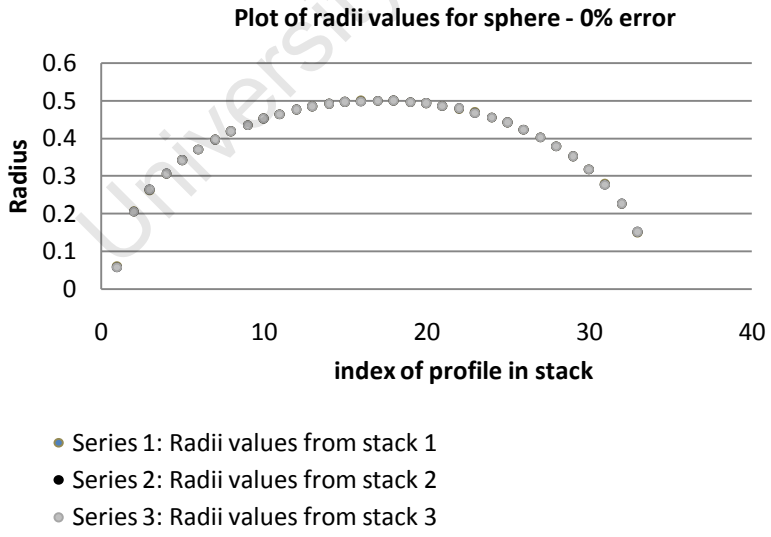

Figure 6-16 Ellipse semi minor axis lengths for sphere: Ellipses from all series have a ratio 1 since the element is a sphere

University of Cape Town

Classification

The shape of the graph obtained from a sphere is shown in figure 6-16. The radii values form circular arc. This is the main classification criteria for a sphere. Depending on how the sphere is sampled, the shape follows a circular arc. Another criterion which can be used is that if more than one profile direction is used in detecting the sphere, crossing axis are encountered. Each axis direction is parallel to a stack normal.

Sphere detection – 10% error

The results for detecting a sphere with a 10% error level are shown in figure 6-17, table 6-6 and figure 6-18.

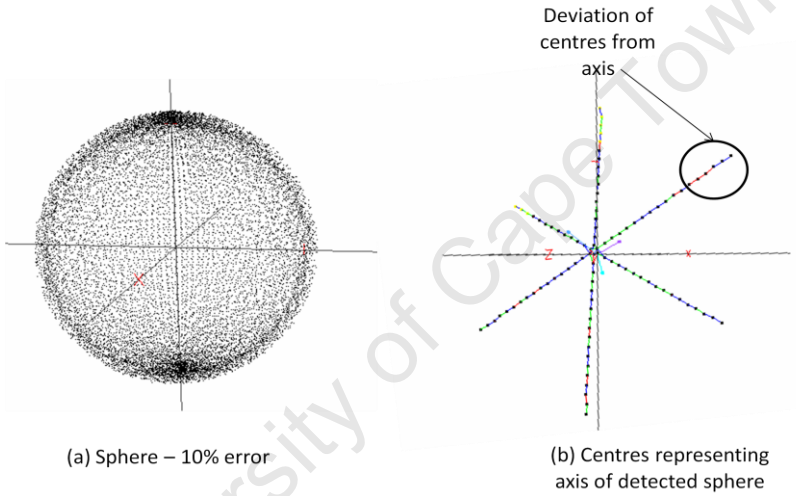

Figure 6-17 Sphere detection – 10% error: Ellipse centres will deviate from the true axis position as noise levels increase

The detected centres for the sphere with 10% error are shown in figure 6-17 (b). Slight deviations are encountered at the ends of the detected axes of the sphere. This is because ellipses at the ends of the sphere will have point samples inside the ellipse since the sphere is closed. The deviations depend on the number of points inside the ellipse. Noise also contributes to this deviation. The radius obtained for the sphere from two stacks is shown in table 6-6

University of Cape Town

Table 6-6 Detection results for sphere - 10% error

	radius(m) [Simulated sphere]	Error in sphere (%)	radius(m) [Detected sphere]	Deviation angle (°)	Minimum selection ratio (a/b)	Standard deviation from true radius (%)
Stack 1	0.5	10	0.525	N/A	N/A	5
Stack 2	0.5	10	0.520	N/A	N/A	4

The radius of the sphere obtained from any stack is the same, see figure 6-18. This is due to the fact that there is only a single ellipse which whose centre coincides with the sphere's centre in each stack. This ellipse will have the same value in all stacks. The classification outlined in the ideal case applies for all spheres. A stack of the ellipses used for detecting a sphere with 10% error is shown in figure 6-19.

University of Cape Town

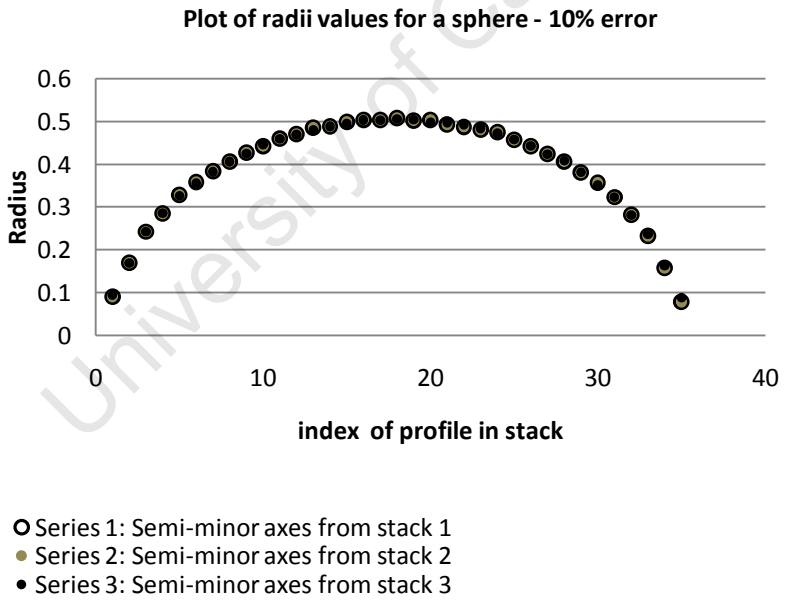

Figure 6-18 Effects of outliers and profile orientation sphere radius: Profile orientation and outliers have a small effect on sphere detection since the ratio used is always 1

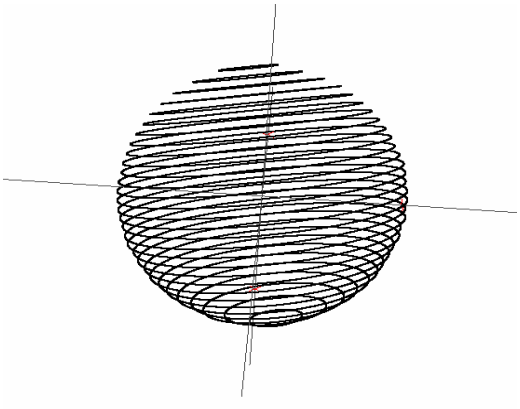

Figure 6-19 Stack of selected ellipses for sphere – 10% error

6.4.4 Cone Detection

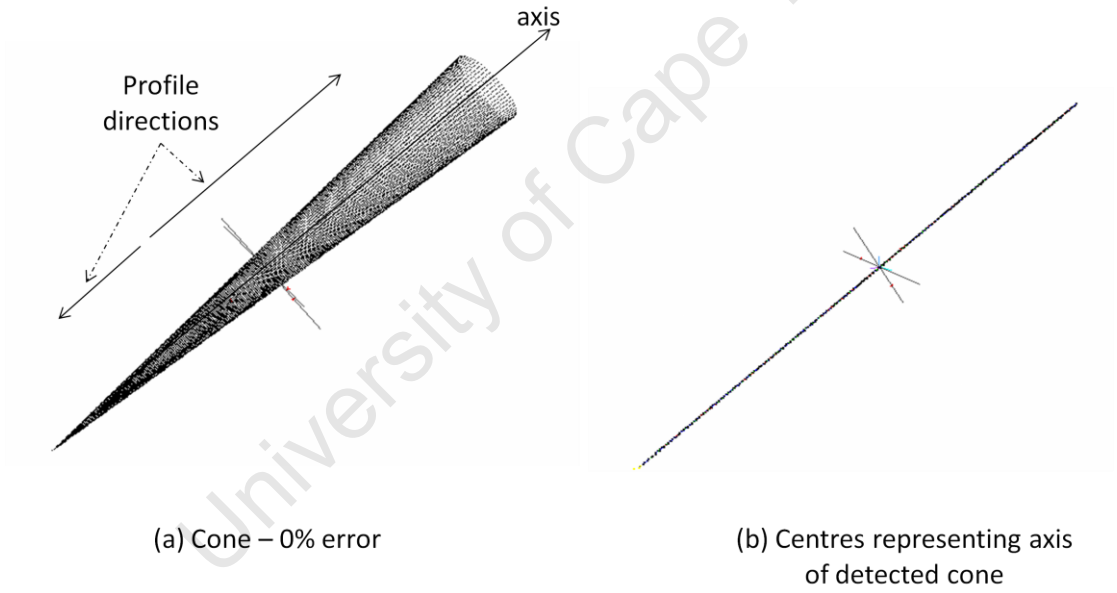

University of Cape Town

Figure 6-20 Detecting cone sections a) cone point cloud b) the detected centres representing axis of cone

A cone of base radius 0.44m is generated with 0% error and point spacing 0.01m. For segmenting the cone, parameters are given below.

Segmentation

A profile width of 0.03m is set for the segmentation. The method of profile segmentation is proximity segmentation. The distance threshold is set at 0.02m. Four stacks are defined for the cone. This allows for the accurate estimation of the position of the axis in the detection stage through regression of centres. The two directions shown in figure 6-20 are used for detecting the cone in the ideal case.

Cone Detection (ideal case)

The detected centres for a cone are shown in figure 6-20 (b). Ideally, the axis of the cylinder lies on the set of centres in figure 6-20 (b) if ellipses with ratios close to one are selected. Therefore, ellipses with a ratio of at least 0.95 are used for the detection in the ideal case. This will give the most accurate axis position. Two stacks are used in the detection. The parameters obtained are shown in table 6-7.

Table 6-7 Detection results for cone (ideal case)

	radius(m) [Simulated cone]	Error in cone (%)	radius(m) [Detected cone]	Deviation angle (°)	Minimum selection ratio (a/b)	Standard deviation from true radius (%)
Stack 1	0.44	0	0.436	N/A	0.95	1
Stack 2	0.44	0	0.435	N/A	0.95	1

The graph of the semi minor axis of each ellipse across the cone is shown in figure 6-21. The base radius for the cone is given by the ellipse with the largest minor axis length with a ratio close to 1. The slight deviation is because the minimum ellipse ratio used is 0.95m since a ratio of one cannot be attained practically.

University of Cape Town

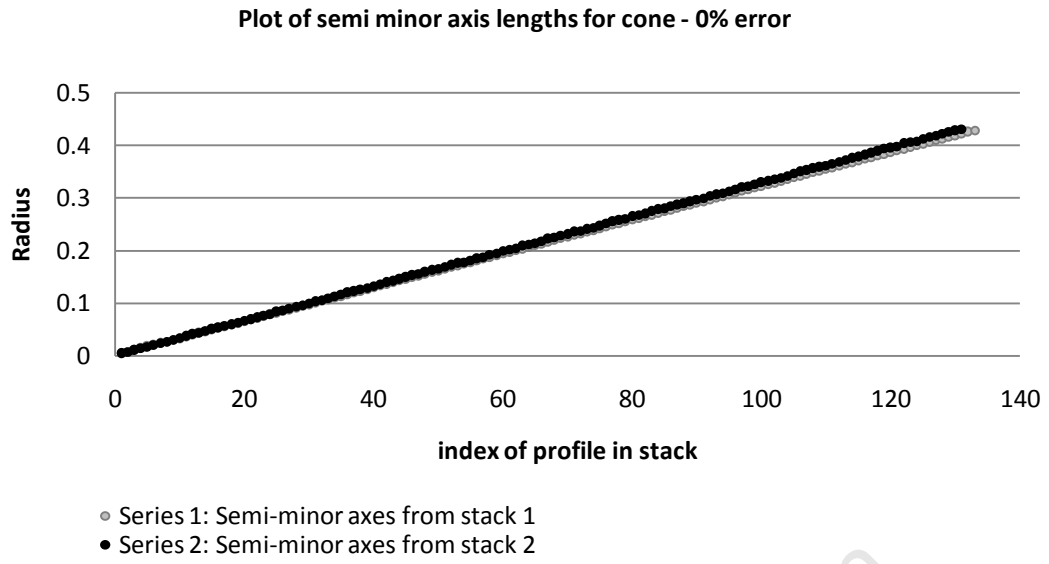

Figure 6-21 Ellipse semi minor axis lengths for cone (ideal case): The semi minor axis length follows a line with gradient l/r where l is the length of the cone and r is the base radius

University of Cape Town

Classification

The shape of the graph is used to classify the cone. The axis shape forms a straight line similar to the axis for a cylinder. Therefore, the axis alone cannot be used in classifying the cone. A graph similar to figure 6-21 indicates the presence of a cone.

Cone Detection – 10% error

An error of 8 % was introduced in generating the cone. The ratio for selecting ellipses was reduced to $1/\sqrt{2}$. Three profile directions were used each with deviation angles of 0°, 30° and 45° respectively. The results are shown in figure 6-22, table 6-8, figure 6-23 and 6-25.

Figure 6-22 (b) shows the axis of the cone with 8% error. For ellipses with a ratio less than one, the centres do not lie on the axis of the cone. The centres shift away from true axis position as the ratio decreases. This is shown in figure 6-22 (b) where the centres deviate from the axis. A linear regression, however, would give the best axis possible if ellipses with a lower ratio are used.

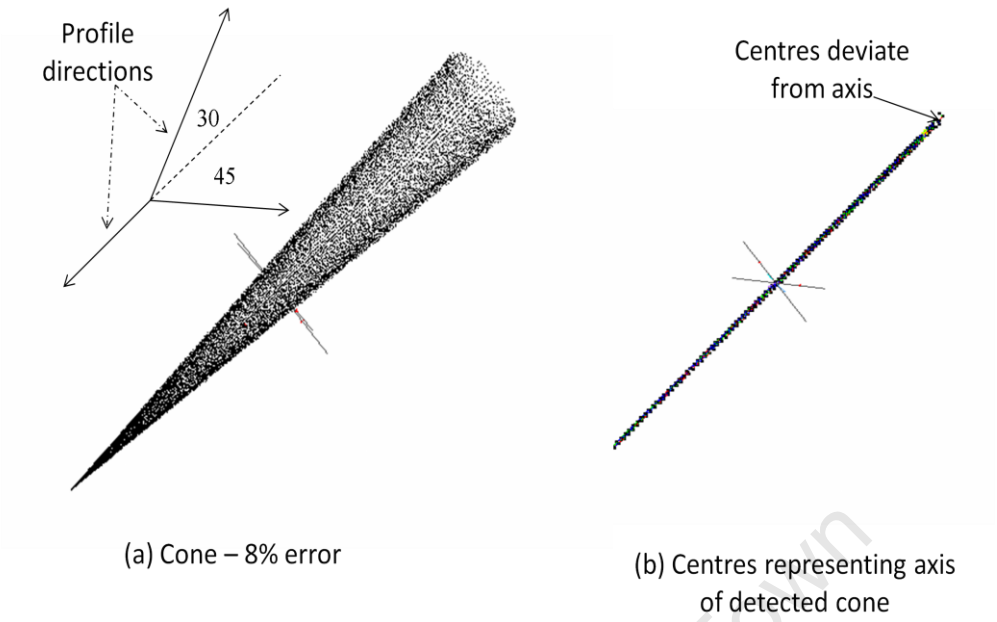

Figure 6-22 Cone detection – 8% error: a) cone point cloud with 8% error b) Deviation from the true radius value increase as noise and increases and ellipse ration decreases

University of Cape Town

Figure 6-23 shows an inset to show the deviation of the centres from the axis. The deviation increases at the base of the torus as a result of ellipse fitting ambiguity. This ambiguity is shown in figure 6-24.

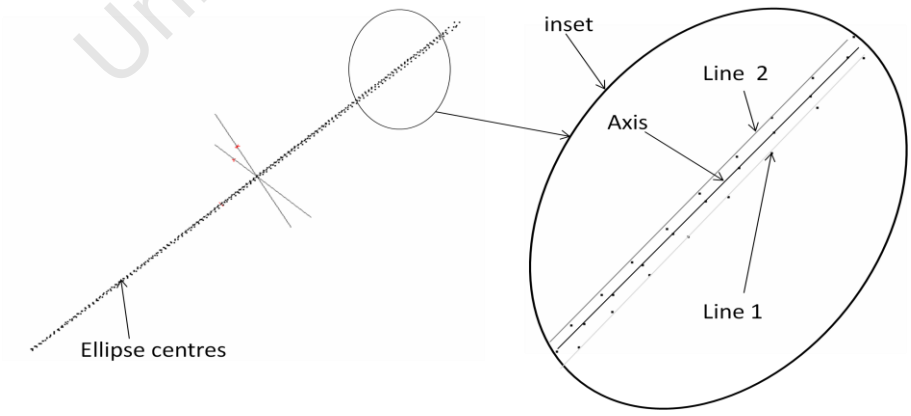

Figure 6-23 Effects of outliers and profile orientation on detected axis (cone): Ellipse centres will deviate from the true axis position as the ratio for selection decreases and noise levels increase

The centres with a ratio of greater than 0.95 are representing the axis of the cone. Line 1 and 2 represent the centres from ellipses with a ratio of at least $\sqrt{3}/2$ and $1/\sqrt{2}$ respectively. A linear regression using centres on line 1 and line 2 gives a line approximately equal to the axis position.

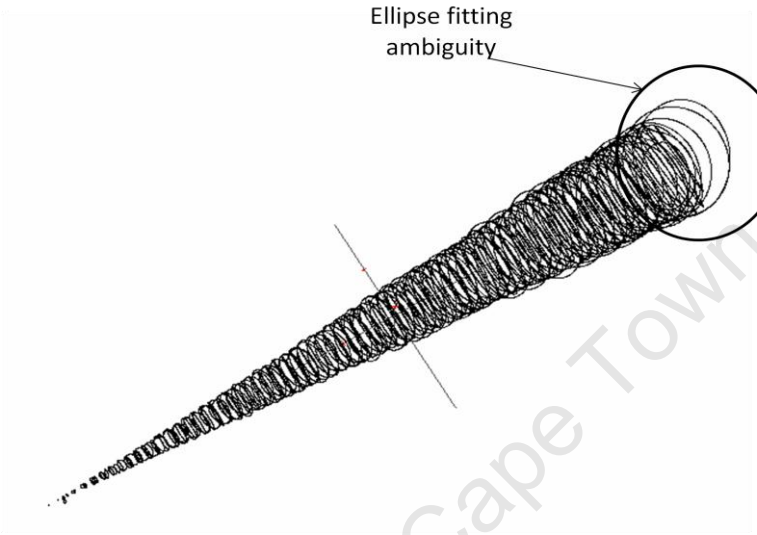

Figure 6-24 Stack of selected ellipses for cone fitting

The ellipses which are not sampled entirely due to profile orientation cause fitting ambiguity at the base of the torus as shown in figure 6-24. The results of the radius value from each stack are shown in table 6-8

Table 6-8 Detection results for cone – 8% error

	radius(m) [Simulated cone]	Error in cone (%)	radius(m) [Detected cone]	Deviation angle (°)	Minimum selection ratio (a/b)	Standard deviation from true radius (%)
Stack 1	0.44	8	0.47	0	0.95	7
Stack 2	0.44	8	N/A	30	$\sqrt{3}/2$	N/A
Stack 3	0.44	8	N/A	45	$1/\sqrt{2}$	N/A

For a cone, an accurate base radius is obtained from the ellipse with the longest minor axis with a ratio approximately one. This is given by stack 1, which is 0.47m. The

University of Cape Town

standard deviation is 7%. A plot of the minor axis lengths from each stack is shown in figure 6-25.

Figure 6-25 Detection of cone – 8% error: Deviation from the line of gradient l/r as noise and increases and ellipse ration decreases. Series 1, 2 and 3 have ratios 1, $\sqrt{3}/2$, and $1/\sqrt{2}$ respectively

Series 1 represents semi minor axis from a stack 1, with deviation angle zero. The ellipses have a ratio approximately one. The standard deviation for the radius value obtained is 7%.The stack origin of the stack 1 is at the base of the cone, hence the highest value of the semi -minor axis, 0.47m, on the graph in the first profile, which is approximately the base radius. The other stacks start from the apex of the cone. The shape of the graph is still similar to the ideal case with slight deviation as a result of noise.

Series 2 and 3

Series 2 and 3 represent semi minor axis from stacks with a deviation angle of 30° and 45° respectively. Stack 2 and 3 had fewer profiles due to the deviation angle. The semi minor ellipse lengths from the two series, 2 and 3, are not used to estimate the radius of the cone. This is because the semi minor axis of any ellipse which has a ratio less than one does not intersect with the axis of the cone. However, the centres of the

University of Cape Town

ellipse from these stacks are used in determining the best position of the axis through linear regression. The shape of the graph of minor axis length remains the same. Classification is therefore not affected by orientation. Outliers and ambiguity cause deviations at the base end of the cone.

6.4.5 Detecting piping elements

The algorithm was tested on piping elements composed of any of the four primitives. The results obtained are described below. The aim is to establish how piping elements are represented and classified based on results from simulated primitives. Four elements were considered.

1. Straight pipes

Straight pipes are modelled using cylinders. Therefore, detecting straight pipes is similar to detecting cylinders. Cylinder detection has been discussed in section 6.4.1. The representation and classification of straight pipes is similar to that of cylinders.

2. Elbow/Pipe bend

An elbow is generated with 8% error. The radius and point spacing of the elbow is 0.25m and 0.02m respectively. The segmentation parameters used for the pipe bend are shown in table 6-9.

University of Cape Town

Table 6-9 Segmentation parameters for pipe bend

Stack count	Method of profile segmentation	Profile width (m)	Distance threshold for proximity segmentation (m)	Curvature threshold
4	Proximity segmentation	0.05	0.04	N/A

The detected centres are shown in figure 6-26 (b).

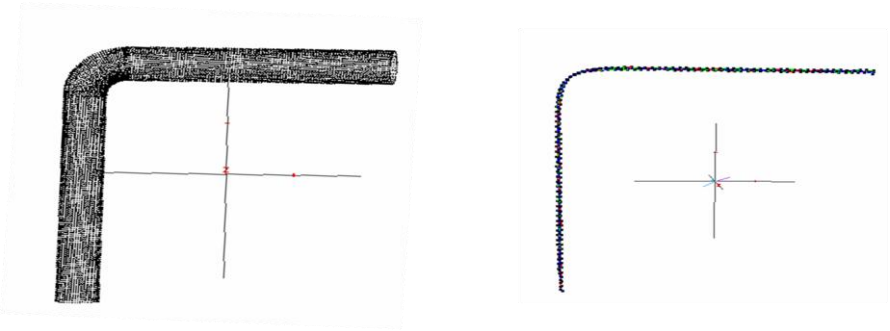

(a) Elbow – 8% error

(b) Detected centres for elbow

Figure 6-26 Detecting pipe bend – 8% error: a) point cloud before detection b) Detected axis; deviation from the true radius value increase as noise and increases and ellipse ration decreases

The results from the detection are shown in table 6-10.

Table 6-10 Detection results for elbow – 8% error

	radius(m) [Simulated elbow]	Error in elbow (%)	radius(m) [Detected elbow]	Deviation angle (°)	Minimum selection ratio (a/b)	Standard deviation from true radius (%)
All stacks	0.250	8	0.264	N/A	$1/\sqrt{2}$	6

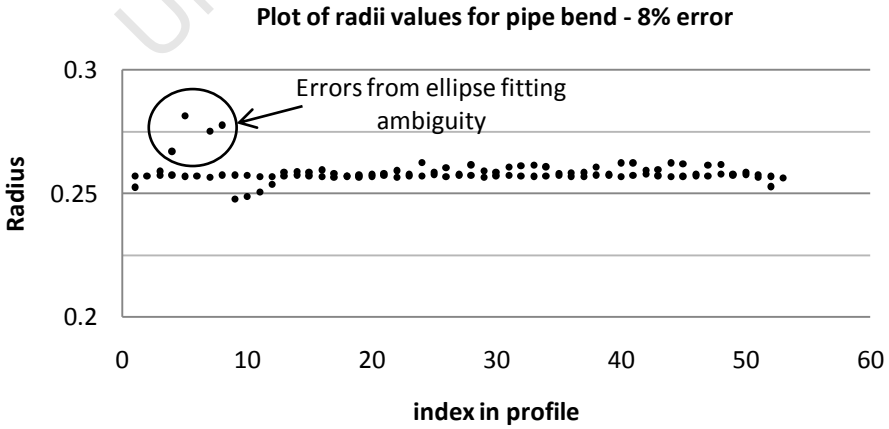

Figure 6-27 Plot of radii values for a pipe bend with 8% error:

University of Cape Town

Figure 6-27 shows the radii values obtained from selected ellipses. The pipe bend is composed of two cylinders and tori. In the ideal case, the graph of radii values for the three primitives is a line. However, deviations are expected as a result of outliers and fitting ambiguity. This is shown in figure 6-27. The error in the detected radius is 6% which is acceptable.

3. T-Junction

A t-junction is generated with 5% error. The segmentation parameters used are shown in table 6-11. The results for the detection are shown in figure 6-28.

Table 6-11 Segmentation parameters for t-junction

Stack count	Method of profile segmentation	Profile width (m)	Distance threshold for proximity segmentation (m)	Curvature threshold
4	Proximity segmentation	0.05	0.04	N/A

University of Cape Town

(a) t-junction

(b) axis of cylinders in t-junction

Figure 6-28 Detecting t-junctions a) Point cloud of a t-junction b) detected axis of t-junction

The detected axis for the cylinders which constitute the t-junction are shown in figure 6-28 (b). Thes axes form a t-shape. This shape can therefore, be used to classify t-junctions. Since the cylinders are of eqaul radii, the shape of the graph for radii values is similar to that of a cylinder. This is sohwn in figure 6-29. The axis detected do not intersect at the centre of the t-junction. This is because the line segment shapes formed were the cylinders are connected are not ellipses as discussed in section 5.4.

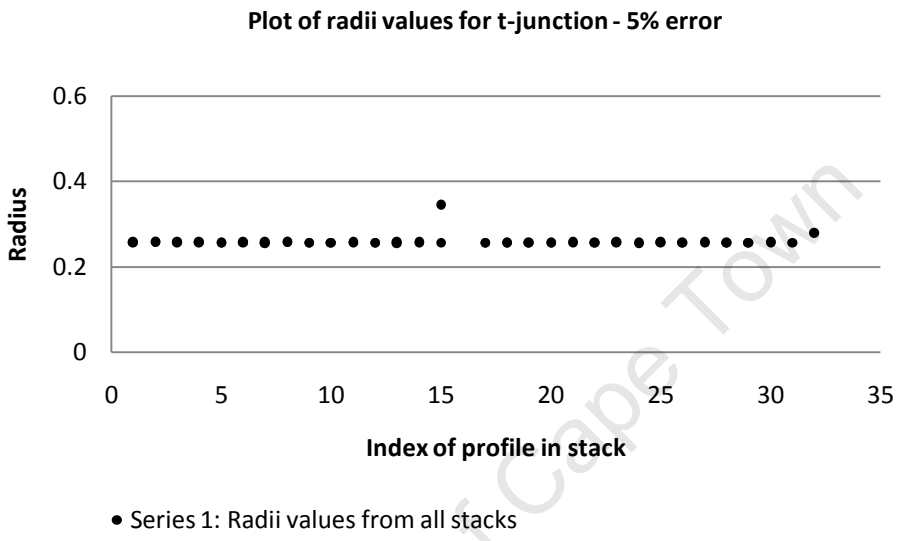

Figure 6-29 Plot of radii values for t-junction – 8% error

Table 6-12 Detection results for t-junction

	radius(m) [Simulated T-Junction]	Error in T-Junction (%)	radius(m) [Detected T-Junction]	Deviation angle (°)	Minimum selection ratio (a/b)	Standard deviation from true radius (%)
All stacks	0.250	5	0.256	N/A	$\sqrt{3}/2$	2.4

The error in the detected radius is 2.4%. The error in the detected radius is acceptable. The ellipse ratio used for this example is $\sqrt{3}/2$. This is done to avoid selecting elongated ellipses that fit to other line segment shapes which are formed at the centre of the t-junction.

University of Cape Town

4. Flanged pipe

A flange connecting two straight pipes is simulated with a 6% error. The point spacing for the piping element is 0.005m. The parameters used in the segmentation are shown in table 6-13. Figure 6-30 shows the set of centres representing the axis of cylinders which constitute the piping element.

Table 6-13 Segmentation parameters for flanged pipes

Stack count	Method of profile segmentation	Profile width (m)	Distance threshold for proximity segmentation (m)	Curvature threshold
4	Segmentation by curve fitting	0.05	0.04	10

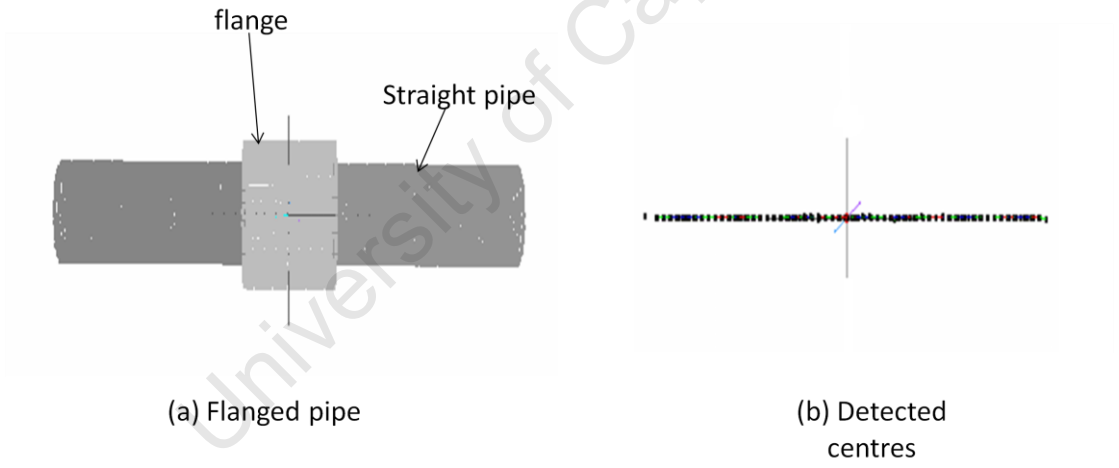

University of Cape Town

Figure 6-30 Detecting flanges a) flanged pipe point cloud b) detected centres follow straight line

Figure 6-30 (b) shows the connected centres of two straight pipes and a flange from the detection. The shape is similar to that which is obtained for cylinders and cones. From the shape of the axis, the presence of a flange cannot be established. However, a plot of the radii values obtained indicates the presence of a flange midway the graph. Since the axis is straight, the change in radius is as a result of the flange.

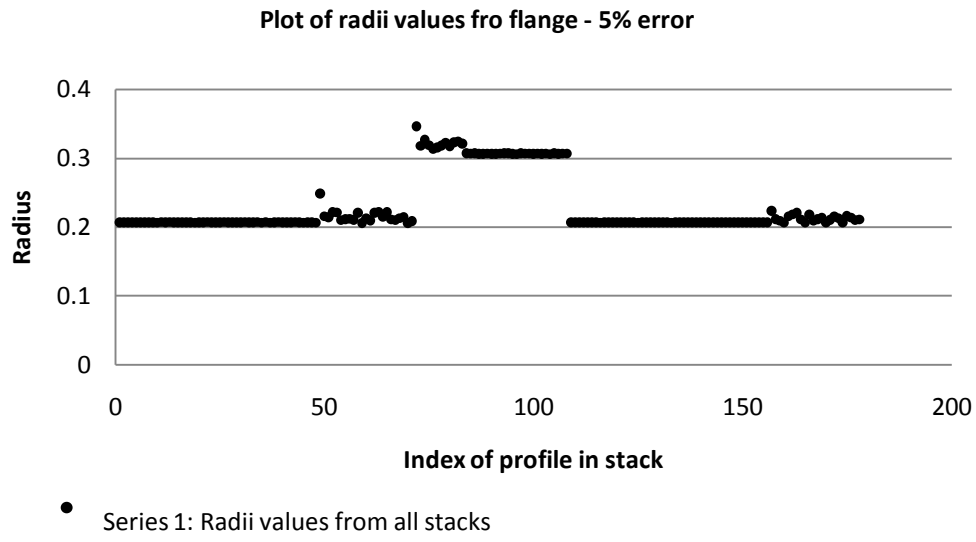

Figure 6-31 Plot of radii values for flange detection: The flange radius is larger as illustrated

Table 6-14 shows the results from the detection.

Table 6-14 Detection results for flanged pipe

	radius(m) [Simulated flange and pipes]	Error in flange and pipes (%)	radius(m) [Pipes and flange]	Deviation angle (°)	Minimum selection ratio (a/b)	Standard deviation from true radius (%)
Pipe1	0.200	6	0.209	45	$1\sqrt{2}$	5
Flange	0.300	6	0.311	45	$1\sqrt{2}$	4
Pipe 2	0.200	6	0.210	45	$1\sqrt{2}$	5

6.4.6 Classification criteria

Combining the results obtained on detecting primitives and piping elements, a summary of the detection results which can be used in the classification is of piping elements is shown in figure 6-32. The shape of the axes for the piping elements depends on the primitives that constitute the element.

University of Cape Town

Piping element	Detection and Classification Criteria		
	Plot of Radii values	Shape of axis	Description of axis
Straight pipe	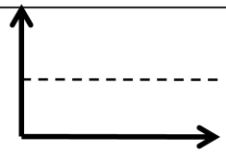		Axis: Straight Line
Elbow	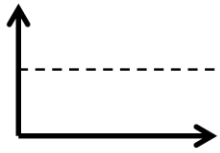		Axis: Curve
T-Junction	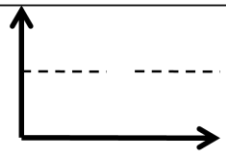		Axis: T shape
Flanged pipe	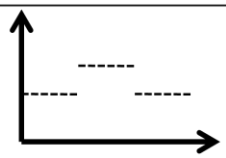		Axis: Straight Line

Figure 6-32 Detection criteria for piping elements

University of Cape Town

For piping elements that are not discussed in this section, the resulting shape of the graph of radii values and shape of axis depends on the primitives that constitute the element. This is illustrated in figure 6-33, where various primitives are connected. The resulting shape of the axis and the graph are shown in figure 6-33 (b) and 6-34. From the shape of the graph together with the set of centres, the primitives which constitute the given element are identified in figure 6-34.

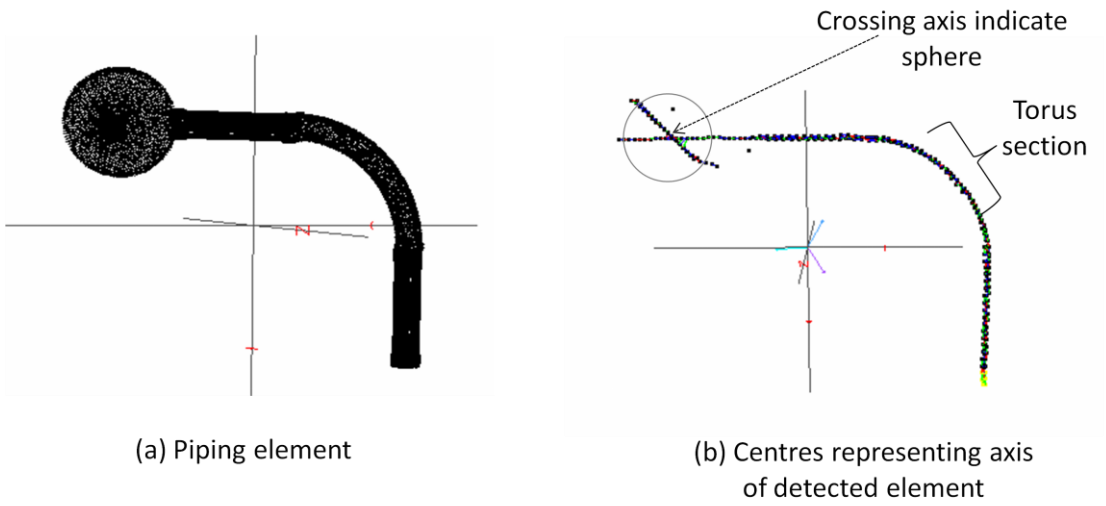

Figure 6-33 Detecting piping elements – 5 % a) Three different piping elements that are connected b) detected axes for the elements in (a)

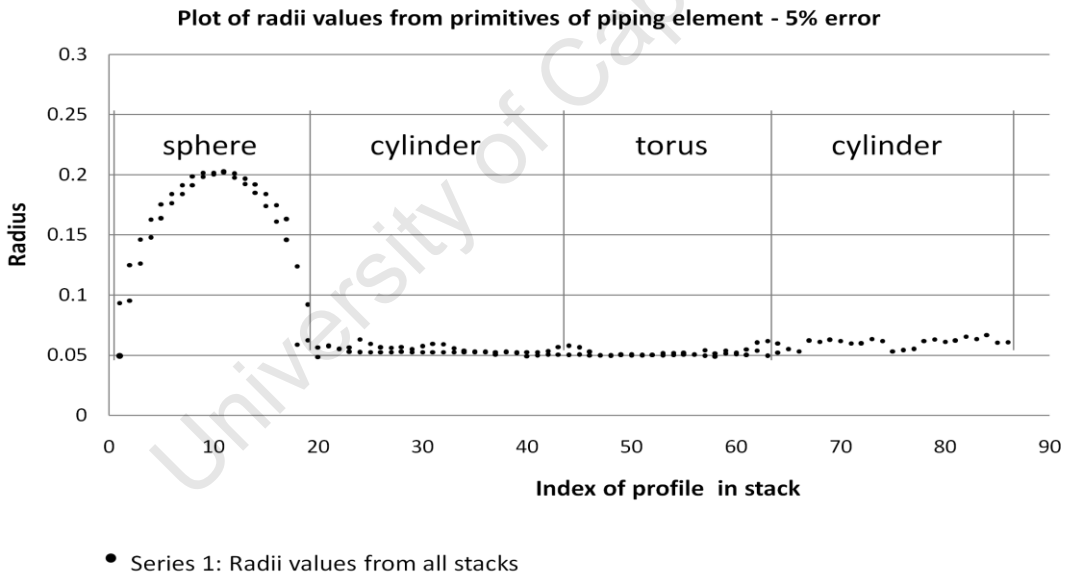

Figure 6-34 Radii values for primitives of an element

The detection of piping elements depends on the detection of the individual primitives. The pattern of the graph used in classifying elements depends on primitives which constitute the element. The graph will exhibit patterns similar to the individual primitives. These patterns are connected. Adopting this conclusion, real data is then tested on the algorithm. The results are presented in the next section.

University of Cape Town

6.5 Real data results

This section presents results on the algorithm tested using real data. Various examples are presented in this section.

Sample 1 – Straight pipe

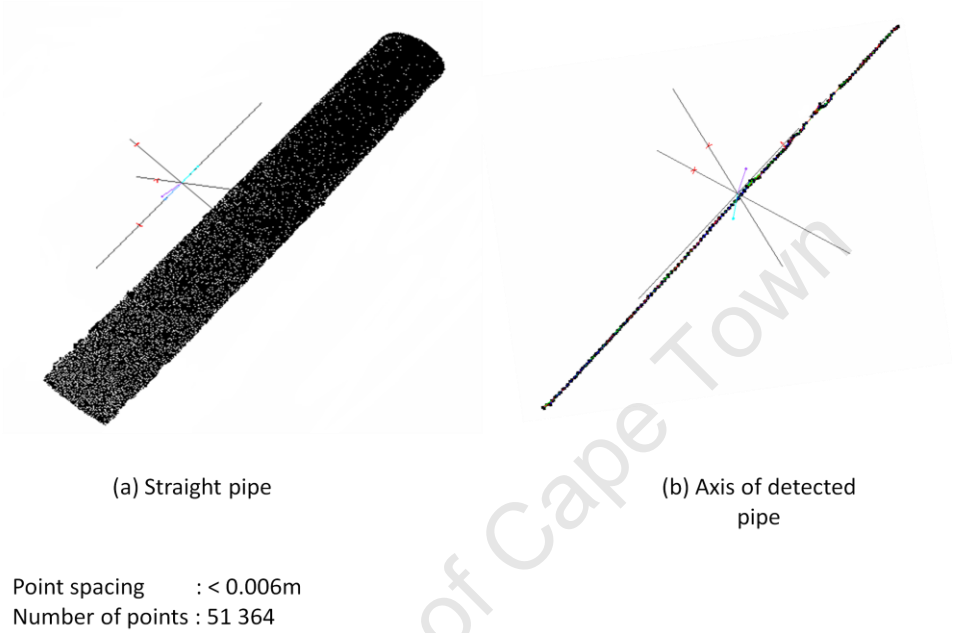

Figure 6-35 Straight pipe/Cylinder detection – point spacing < 0.006m

Table 6-15 Detection results for straight pipe (real data)

	Minimum radius value (m)	Average radius value (m)	Minimum Ratio (a/b)	Standard deviation (%)
Stack 1	0.16m	0.17	$1/\sqrt{2}$	6.25

Figure 6-35 (a) shows point data on a straight pipe. The detected centres are shown in figure 6-35 (b). The point data is a partial scan of the pipe. The distribution of points tracing out the ellipse is limited to half the ellipse since half the pipe is scanned. However, this does not affect the detection of the pipe as the distribution is approximately the same in profiles from the same stack. The centres of the ellipses trace out the pipe axis with slight deviations due to outliers as expected. A plot of the radii values across the pipe is shown in figure 6-36. This follows the same pattern as

University of Cape Town

the graph for a simulated cylinder. The average radius obtained from series 1 is 0.170m. To estimate the standard deviation of the pipe the minimum radius across all profiles is assumed to be the true value. Using this value, the standard deviation in the average radius is approximately 6%.

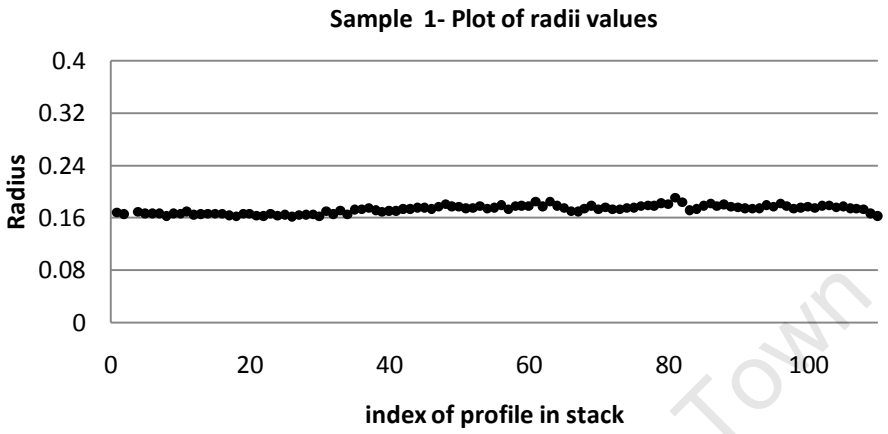

Figure 6-36 Plot of radii values from ellipses on a straight pipe (real data)

Figure 6-37 shows the reconstructed model of the straight pipe given in figure 6-37 (b). The average radius value of 0.170m is used to generate the cylinder model. The approximate length of the pipe is calculated using linear regression on the ellipse centres.

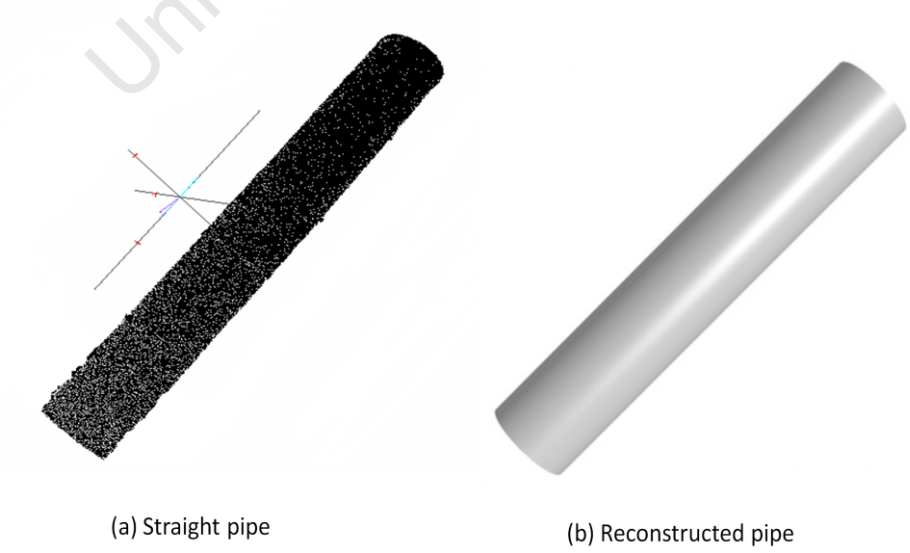

Figure 6-37 Reconstructed pipe using parameters from the detection

University of Cape Town

Sample 2 – Elbow/Pipe bend

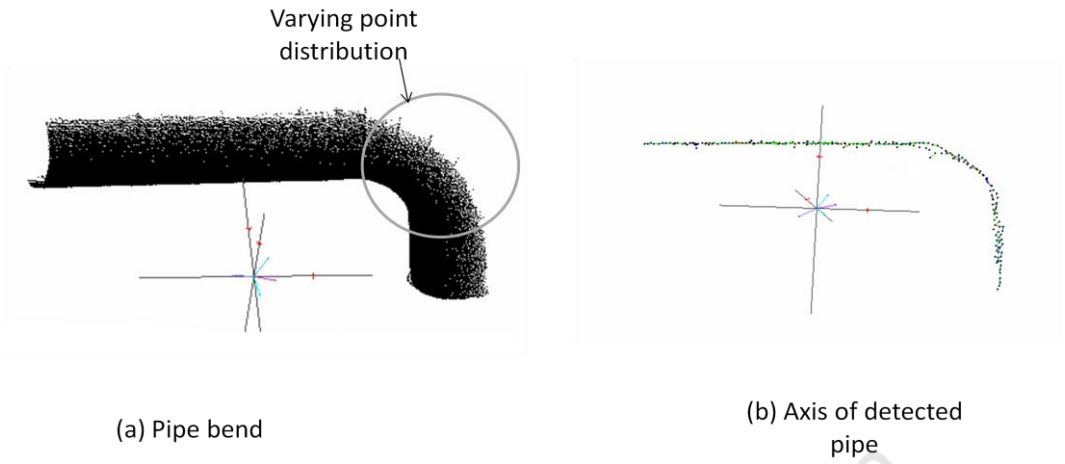

Figure 6-38 Elbow detection a) elbow point cloud b) detected axis of elbow: ellipse fitting ambiguity result in centres deviating from true axis position

Table 6-16 Detection results for pipe bend (real data)

	Minimum radius value (m)	Average radius value (m)	Minimum Ratio (a/b)	Standard deviation (%)
All stacks	0.21m	0.24	$1/\sqrt{2}$	14.28

Sample 2 shows a pipe elbow extracted from the real data. The purpose of sample 2 is to test the effect of point distribution on the detection process. Figure 6-38 (a) shows a pipe bend with varying point distribution along the surface. The point sampling around ellipses is therefore reduced in some sections of the elbow. The result is ellipse fitting ambiguity hence displaced centres; refer to chapter 5, section 5.7.1. The centres deviate from the true axis position as shown in figure 6-38 (b). As mentioned in chapter 5, section 5.5.3, proximity segmentation on the centres will connect those points that are closest to each other on the axis. Figure 6-38 (b) shows the axis after the segmentation of centres. Figure 6-39 shows the segmentation that was carried out on the centres.

University of Cape Town

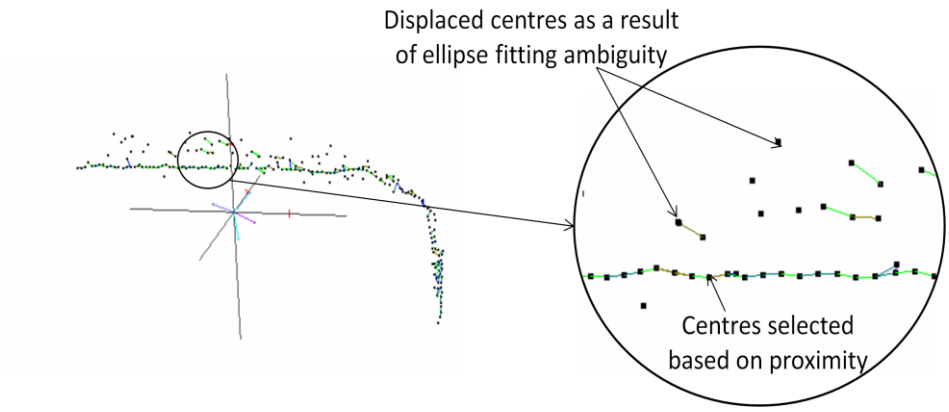

Figure 6-39 Segmentation of centres: points are connected based on proximity

The centres that are close together are connected as shown in figure 6-39. The other points that are not connected to the axis component are automatically excluded from calculations. Figure 6-40 shows a plot of the radii values from the connected centres. The average radius of the pipe from the connected centres is 0.240m. A sample reconstructed[5] pipe bend is shown in figure 6-41 (b).

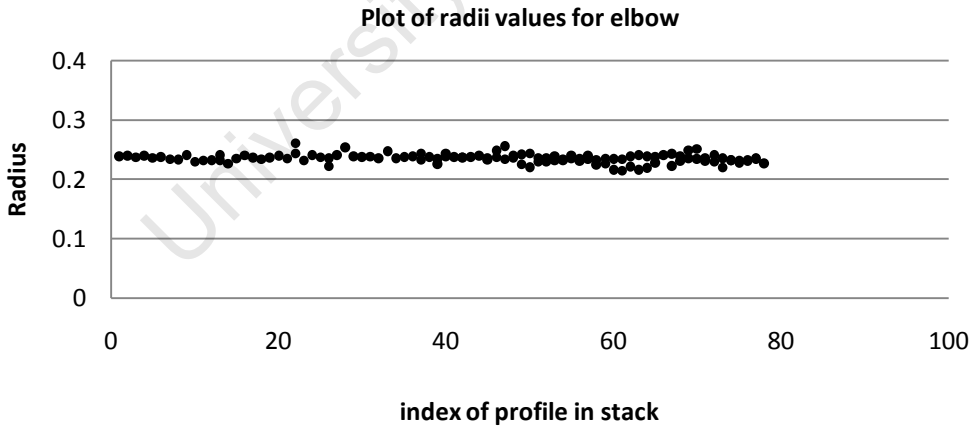

Figure 6-40 Effect of point distribution on detection: Plot of radii values from pipe elbow with varying point distribution

[5] This was reconstructed using the average radius and an approximate length of axis in blender.

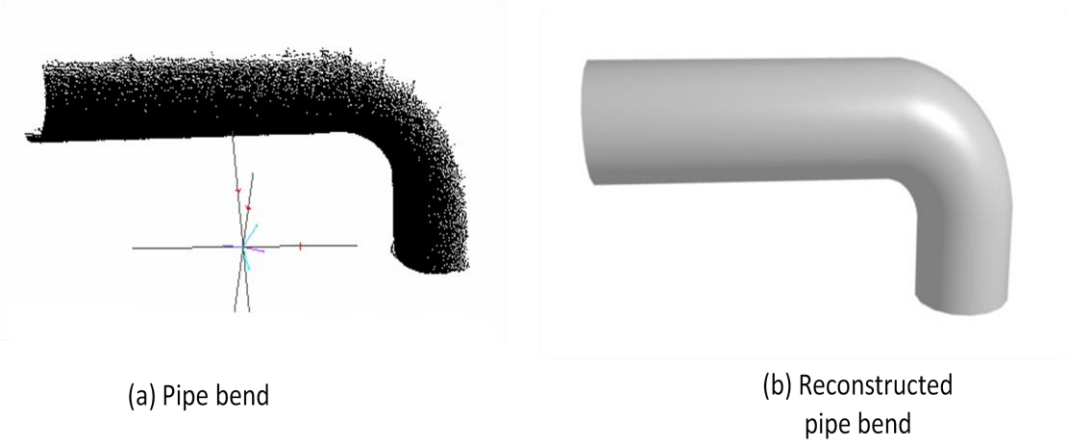

Figure 6-41 a) Pipe point cloud b) Reconstructed pipe bend/elbow

University of Cape Town

Sample 3 – Detecting deformations

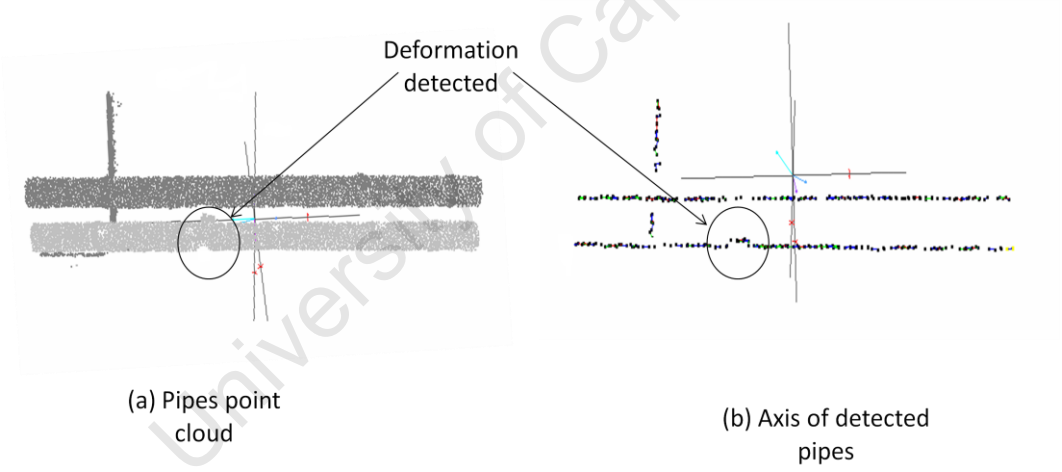

Figure 6-42 Deformation detection a) shows a pipe with a deformation and b) shows the detected deformation

The purpose of sample 3 is to test the detection of deformations. One of the pipes in figure 6-42 (a) contains a deformation. The deformation is detected in the set of centres representing the axis. The deformation will cause a discontinuity in the axis of the detected pipe as shown in figure 6-42 (b). However, the axis is still traced out correctly with the rest of the centres. This illustrates the algorithm's ability to detect deformations.

Modelling deformations using profiles

Not only are the deformations detected but they can be modelled using the profiles. The magnitude of the deformation can therefore be assessed once detected. By fitting a curve[6] to line segments in profiles that intersect with piping elements, the deformation is recreated using the curve. Figure 6-43 (a) shows a pipe free of deformations. The curves that have been fit to points on the pipe are shown in figure 6-43 (a). The change in curvature for each curve is approximately constant.

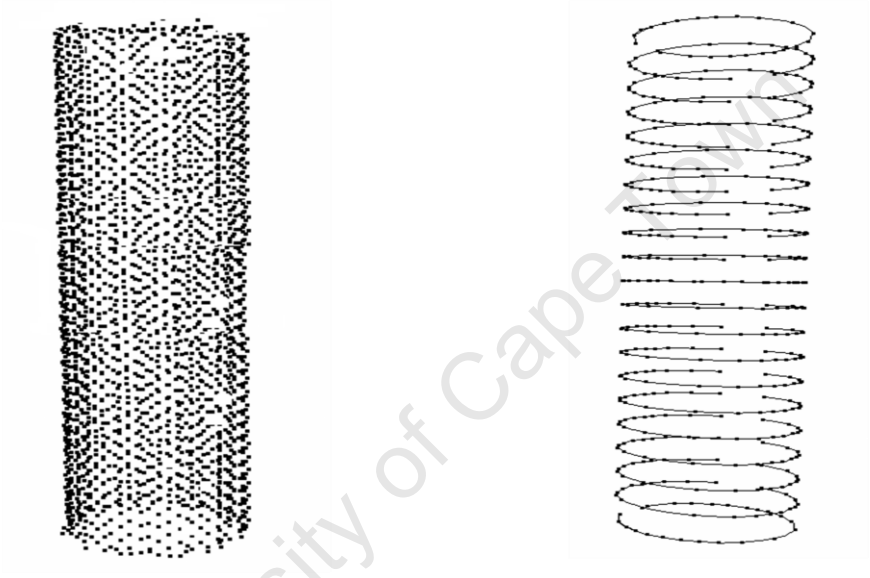

University of Cape Town

Figure 6-43 Deformation modelling using profiles a) pipe point cloud with no deformation b) curve fit to points in profiles

Figure 6-44 shows a pipe with deformations and the curves that are fit. Sharp curvature changes are encountered on the curves that are fit to points at the deformed area. However, outliers may affect the accurate modelling using curves. In the presence of outliers, the curve will not follow the form of the deformation correctly.

[6] NURBS curves are used in the fitting

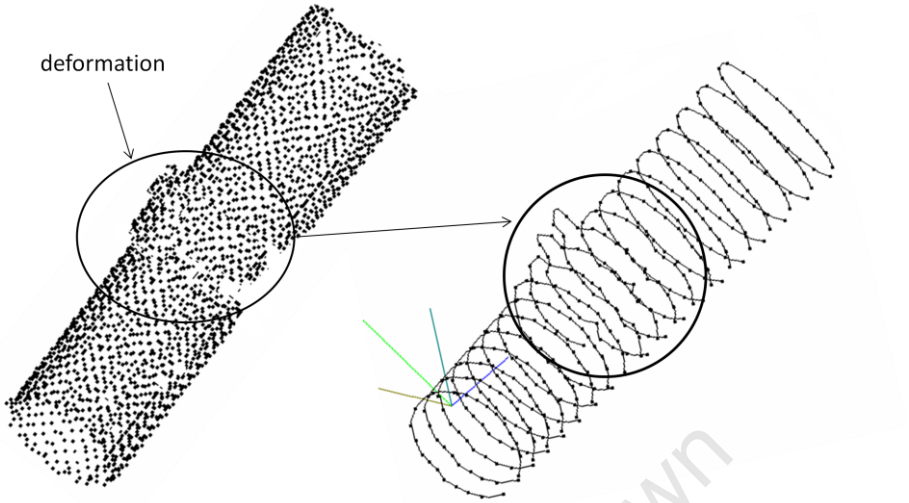

Figure 6-44 Modelling deformation using profiles: deformation modelled by curves

Figure 6-45 shows sample curves from a section of the pipe free of deformation and the deformed section. Figure 6-45 (a) and (c) show the section free of deformations. Figure 6-45 (b) and (d) show the sections that are deformed. Sharp curvature changes are encountered along the curve.

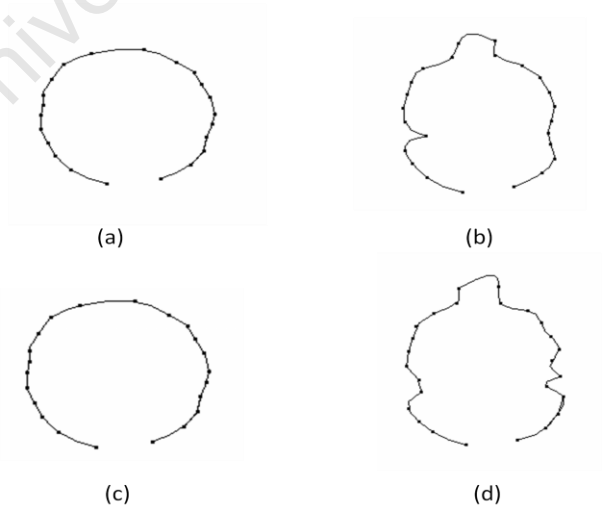

Figure 6-45 Sample curves from modelling of deformations

University of Cape Town

Sample 4 – Pipes with different radii

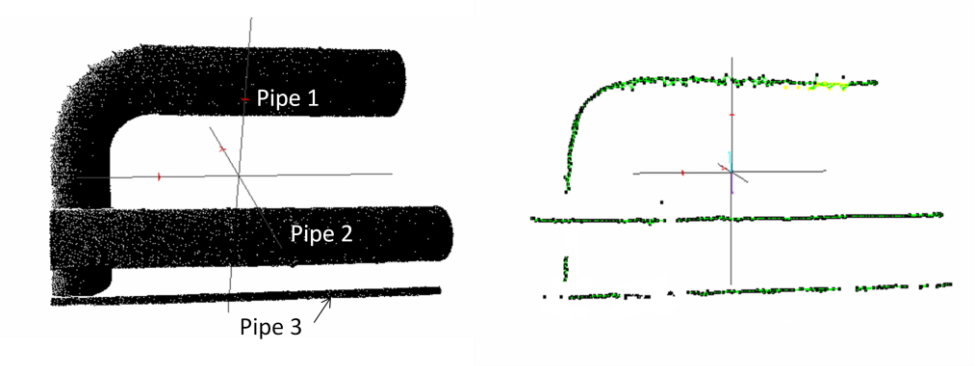

(a) Pipes with different radii

(b) Axes of detected pipes

Figure 6-46 Detecting pipes with different radii (Effects of radius on detection)

University of Cape Town

Table 6-17 Detection results for pipes with different radii values

	Minimum radius value (m)	Average radius value (m)	Minimum Ratio (a/b)	Standard deviation (%)
Pipe 2	0.160m	0.162	$1/\sqrt{2}$	1.25
Pipe 3	0.038	0.055	$1/\sqrt{2}$	45

As the ratio *point spacing/ pipe radius* increases (i.e. as the pipe radius gets smaller) the density of points around a pipe decreases if the resolution remains constant. The distribution of points therefore decreases. The result is ellipse fitting ambiguity during detection. This implies more uncertainty is encountered in the ellipse when detecting narrow pipes. This is illustrated using sample 4.

In figure 6-46 (b), more gaps are encountered in the centres representing pipe 3. Fitting ambiguity is encountered along the pipe hence more centres will not be connected as they deviate away from the axis. A plot of the radii values for pipe 2 and 3 is shown in figure 6-47. The large radius pipe (0.16m) shows slight variations in radii values (series 1) compared to the small radius pipe (series 2). The radius is

largely affected by the ratio *point spacing/ pipe radius* than the position of the axis when detecting small radii pipes. The radius value for the smaller pipe is therefore difficult to determine since the values have a lower precision. This accounts for the 45% standard deviation for the small radius pipe compared to 6% for the large radius pipe.

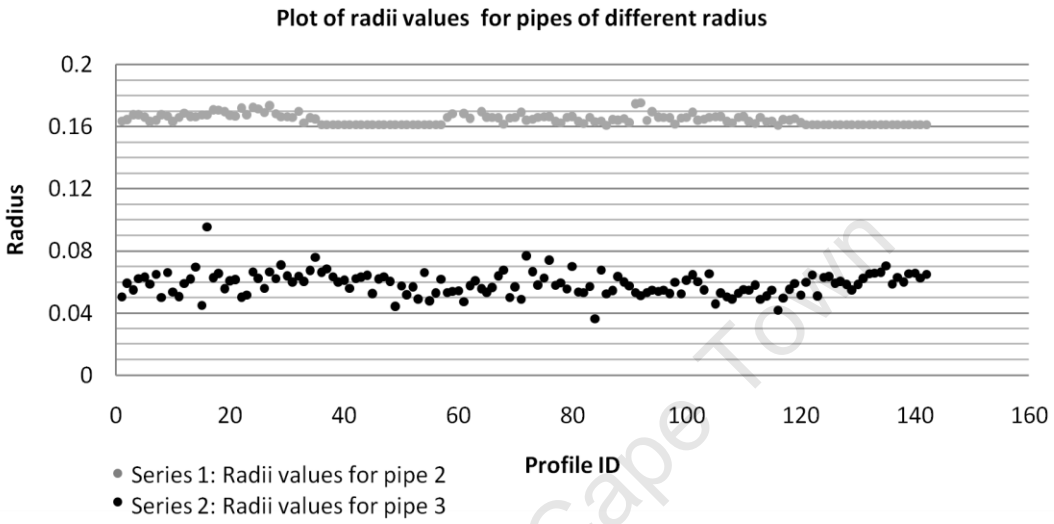

Figure 6-47 Effect of radius on detection: Series 1 shows a pipe radius of approximately 0.17 and series 2 shows a pipe radius of smaller radius which is difficult to approximate

The best radius value for the smaller pipes is the average radius. The graph above shows that as the radius gets smaller (i.e. below 0.1m[7]), the detection becomes less accurate. The radii values differ across the pipe and an accurate value is difficult to deduce. However, this depends on resolution of the point set. For a higher resolution, pipes with radius below 0.1 are detected more accurately.

[7] This applies to the resolution of the real data used in the testing. This can vary depending on resolution of point sets. From this point on, small radius refer to values less than 0.1m. This applies only to the test data used in this research. With a higher resolution point set, this value can decrease.

University of Cape Town

Sample 5 – Pipes with different radii

Figure 6-48 Pipes with different radii (Effects of pipes radius on detecting pipe axes

University of Cape Town

Table 6-18 Precision of radii values for piping elements with different radii values (< 0.1m and > 0.1m)

	Minimum radius (m)	Average radius (m)	Minimum ratio	Standard deviation (%)
Pipe1(small radius)	0.0150m	0.0179m	$1/\sqrt{2}$	20
Pipe 2 (Large radius)	0.170m	0.179m	$1/\sqrt{2}$	6

Another test using sample 5 (figure 6.48) was done to compare the precision on the values obtained from two elements with different radii values. By assuming the minimum radii value to be the accurate radii values for each pipe, the standard deviation of the average radii values are 20% for the small radius pipe and 6% for the larger radius pipe. The precision of the radii values increases with an increase in radius on condition the point density and distribution is approximately constant.

Sample 6 – Various elements in point cloud

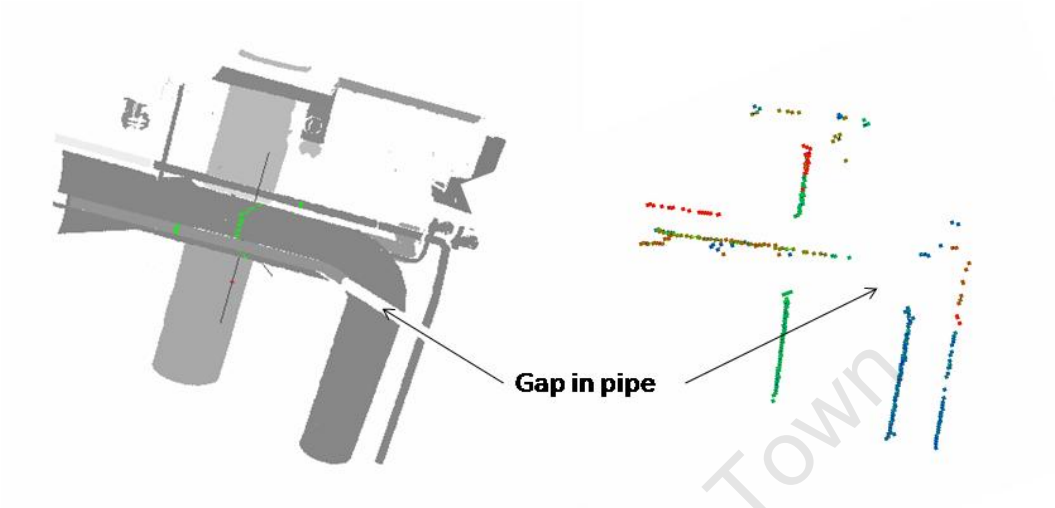

Figure 6-49 Detection of various elements: Pipes with larger radius are easily detected as compared to small radii pipes

Sample 6 (figure 6-49) shows large and smaller radii pipes in a point cloud. The axes for the large radii pipes are detected correctly without any gaps. However, this is not the same for the small radii pipes. The axes of the small radii pipes are characterised by gaps with some of the pipes not detected. This is the major drawback of the method presented in this research.

6.6 Discussion

The algorithm was able to detect primitives in the test data. The disadvantage presented with real data was that only partial scans of the elements were captured. This presents more uncertainty in ellipse fitting. For a reliable detection, at least half the surface must be captured. The effect of ellipse fitting ambiguity is reduced by proximity segmentation on the centres. The centres that deviate from the axis by a distance greater than the threshold distance used in the segmentation are excluded

University of Cape Town

As the ratio, $point\ spacing/radius$ increases and the resolution remains constant, the less accurate the detection. The radius value obtained become less precise and the axis will contain gaps. A ratio of 0.1 for $point\ spacing/radius$ is ideal for detecting piping elements at the resolution of the data used.

The main disadvantage of the algorithm is the detection of narrow pipes. At a constant resolution, the detection becomes less accurate as the radius of pipes decreases. The radius value for narrow pipes therefore, becomes less accurate. The values obtained have a lower precision as the ratio $point\ spacing/radius$ increseases.

The approximate radius of cylinders and tori can be taken to be the minimum value from the radius graphs if the precision is less than 90% otherwise the average value is adopted. For all elements, an ellipse ratio close to one would give the most accurate radius. Ellipse fitting ambiguity is the main error source in the detection algorithm when partial scans are used.

The advantages of the algorithm are the ability to detect deformations and that no information is required about the pipes prior to the detection. The deformation can be modelled from the line segments in profiles using curves. However, the presence of noise can have a negative effect on the curves in that the exact form of the deformation is not recreated. The effect of the deformations in the reconstruction of piping is that the resulting axis shape and position is shifted from the true axis position. Variations in the radii value are encountered at the deformed area and the result is a biased average radius. Ellipses fit to deformed sections of pipes are therefore not used in calculating pipe parameters for the pipes.

The detection result can be used to approximate the best set of parameters that can be used to define the piping elements. The errors obtained for large radii pipes were less than 15%. The algorithm can be used to provide information that can be used as a basis for other operations like selecting CSG models. These models can then be used to obtain better results.

University of Cape Town

7. Conclusion and Future work

7.1 Conclusion

From the study of existing literature, problems and areas of improvements in the reconstruction of piping installations from point clouds were identified. The problems identified with current algorithms are:

- Primitives are detected one a time with some algorithms. This has an extra time cost when dealing with large point sets
- Most of these algorithms do not allow for the modelling of deformations in pipes. They assume pipes that are free of deformation
- Some algorithms do not detect all the geometric primitives found in piping installations. Some detect mostly cylinders and planes.

In order to solve some of problems cited, a detection algorithm was developed. The detection algorithm requires a prior segmentation. Therefore a segmentation procedure was incorporated. The segmentation strategy is based on profile intersection. A point cloud is sliced into a series of thin parallel planes referred to as profiles. Points are connected in each profile based on proximity and surface continuity to yield connected line segments. Discontinuities in the line segments are detected using curvature. The profiles are then intersected to yield surface segments. The main advantage of the segmentation algorithm is that connected piping elements are simultaneously discriminated.

The detection algorithm proposed is based on detecting ellipses in the profiles. The ellipses are formed from the intersection of piping elements with profiles. From the ellipse parameters, the piping elements' parameters are determined. The position and orientation of the element is given by the ellipse centres. The radii values for elements are approximated using semi minor ellipse lengths. The algorithm was tested on simulated and real data and was found to work well. The algorithm developed was found to have some distinct advantages. These are listed below.

University of Cape Town

- The algorithm incorporates both the segmentation and detection of piping primitives from point clouds. No prior information is required about the scanned pipes beforehand.
- The algorithm is generic for most of piping elements which result from Boolean operations on cylinders, cones, tori and spheres. The algorithm detects geometric primitives for the piping elements regardless of whether they are connected or not. Piping elements composed of any of the four primitives are thus detected.

- The algorithm incorporates a classification strategy for piping elements. Besides detecting elements, information regarding the type of element is deduced. This is based on the radii values obtained from different sections of the elements. The sections are defined using profiles. A plot of these radii against the profile index produces a pattern unique to piping elements based on the primitives. The pattern forms the base of the classification. The question as to whether an element is a t-junction or elbow is thus answered using the detection results.

- Deformation in pipes can be detected. Any deformation will result in the deviation of ellipse centres from the true axis position. This allows for the position of the deformation to be deduced. The magnitude of the deformation can be deduced from the deviation

- The segmentation procedure has the advantage of simultaneously discriminating connected piping elements. Discontinuities introduced in areas where piping elements are connected. The segmentation algorithm identifies the discontinuities and demarcates segment boundaries at the points of connection. The algorithm also segments flanges.

The algorithm was tested on different primitives with different parameters. The algorithm was able to detect most piping elements. However, given a point set with constant point spacing, as the ratio $point\ spacing/radius$ increases, the detection becomes less accurate due to ambiguity. The ambiguity increases when the scanned

University of Cape Town

surface is less than half. The radius value for an element with small radii becomes difficult to approximate. However, the axis is still detected accurately using regression.

7.2 Future work

The algorithms performance with different data resolutions was not robustly investigated. Further testing is required. Improvements can be made on both the segmentation and detection procedures. This was not done due to time constraints. The following improvements are recommended:

- The algorithm does not detect pipes of small radius accurately. An iterative approach (RANSAC) or Hough Transform could be used to efficiently detect small pipes.

- Ellipse fitting ambiguity poses a problem as the ratio $point\ spacing/radius$ increases. This mostly affects the detection of pipes that have at most half the surface area scanned. As the ratio increases, point sampling around the ellipse decreases hence ambiguity is encountered. Robust ellipse detection methods using RANSAC or Hough Transform can be employed.

- The segmentation algorithm was not efficient in detecting flanges except those with a larger radius relative to pipes connected by the flange. Detecting the exact flange boundaries was not done correctly. Flange detection based on point distance from a surface using the detected parameters can be developed.

- The algorithm has the potential to model deformation in pipes. Further improvements can be made in the modelling of deformations in small radii pipes.

University of Cape Town

BIBLIOGRAPHY

Acka, D. (2003) 'Full Automatic Registration of Laser Scanner Point Clouds', O*ptical 3D measurement techniques VI, September 22-25, Zurich, Switzerland*, pp. 330-337.

Amenta, N., Bern, M. and Kamvysselis, M. (1998) 'A New Voronoi-Based Surface Reconstruction Algorithm', *Proceedings of the 25th annual conference on Computer graphics and interactive techniques,*pp 415-421.

Attene, M., Falcidieno, B. and Spagnuolo, M. (2006) 'Hierarchical mesh segmentation based on fitting primitives', *The Visual Computer*, vol. 22, no. 3, February, pp. 181-193.

Bae, K.-H. (2006) 'Automated Registration of Unorganised Point clouds from Terrestrial Laser Scanners', PhD Thesis, Curtin University of Technology, Perth, Australia, pp 38-74.

Bae, K.-H. and Lichti, D.D. (2004) 'Automated registration of unorganised point clouds from terrestrial Laser scanners', *International Archives of Photogrammetry and Remote Sensing*, vol. 35, B5, pp. 222-227.

Besl, P. and McKay., N. (1992) 'A method for registration of 3-d shapes.', *IEEE Transactions on Pattern Analysis and Machine Intelligence*, vol. 14, no. 2, February, pp. 239-256.

Boehler, W., Bordaz Vincent, M. and Marbs, A. (2003) 'Investigating laser scanner accuracy', *XIXth CIPA Symposium, October, Antalya, Turkey,* pp 13 pages.

Bohm, J. and Brenner, C. (2000) 'Curvature based range image classification for object recognition', *SPIE proceedings series: Intelligent Robots and Computer Vision XIX: Algorithms, Techniques, and Active Vision, November 7-8, Boston,* pp 211-220.

University of Cape Town

Bookstein, F. (1981) 'Fitting Conic Sections to Scattered Data', *Computer Graphics and Image ProcessingFitting conic sections to scattered data*, vol. 9, no. 1, January, pp. 56-71.

Burnham, K.P. and Anderson, D.R. (2004) 'Multimodel Inference: Understanding AIC and BIC in Model Selection', *Sociological Methods & Research*, vol. 33, no. 2, pp. 261-304.

Cazals, F. and Giesen, J. (2004) 'Delaunay Triangulation Based Surface Reconstruction: Ideas and Algorithms', *Rapport de recherche*, November 2004, p. 42 pages.

Chaperon, T. and Goulette, F. (2001) 'Extracting cylinders in full 3D data using a random sampling method and the Gaussian image', *Proceedings of the Vision Modeling and Visualization Conference 2001, November 21 - 23, Stuttgart, Germany*, pp. 35-42.

Chen, Y. and Medioni., G. (1992) 'Object modeling by registration of multiple range images.', *Image and Vision Computing*, vol. 10, no. 3, April, pp. 145-155.

Curless, B. and Levoy, M. (1996) 'A Volumetric Method for Building Complex Models from Range Images', P*roceedings of the 23rd annual conference on Computer graphics and interactive techniques, August*, pp. 303 - 312.

Dell'Acqua, F. and Fisher, R. (2002) 'Reconstruction of planar surfaces behind occlusions in range images', *Pattern Analysis and Machine Intelligence, IEEE Transactions*, vol. Volume 24, no. 4, April, pp. 569-575.

Dey, T.K., Giesen, a.J. and Goswam, a.S. (2004) 'Shape Segmentation and Matching from Noisy Point Clouds', *Proc. Eurographics Sympos. Point-Based Graphics (2004)*, pp. 193-199.

University of Cape Town

Dey, T.K., Li, G. and Sun, J. (2005) 'Normal Estimation for Point Clouds: A Comparison Study for a Voronoi Based Method', *Eurographics Symposium on Point-Based Graphics, June 20 -21, New York, USA.*, pp. 39-46.

Diestel, R. (2005) 'Graph Theory' New york: Springer-Verlag Heidelberg 2005.

Ermes, J., van den Heuvel, F. and Vosselman, G. (1999) 'A Photogrammetric Measurement Method using CSG Models', *International Archives of Photogrammetry and Remote Sensing*, vol. 32, no. part 5/W11, July, pp. 36-42.

Fidera, A., Chapman, M.A. and Hong, J. (2004) 'Terrestrial lidar for industrial metrology applications modelling, enhancement and reconstruction', *ISPRS Congress Istanbul 2004, Proceedings of Commission V, July 12-23, Instanbul*, pp. 4 pages.

Fitzgibbon, A., Maurizio, P. and Fisher, R.B. (1999) 'Direct Least Square Fitting of Ellipses', *Pattern analysis and machine intelligence*, vol. 21, no. 5, May, pp. 476-480.

Fröhlich, C. and Mettenleiter, M. (2004) 'Terrestrial laser scanning –New perspectives in 3D surveying', *International Archives of Photogrammetry, Remote Sensing and Spatial Information Sciences*, vol. 36, no. 8/W2, October, pp. 7–13.

Gander, W., Golub, G. and Strebel, R. (1994) 'Least-Square Fitting of Circles and Ellipses', *BIT Numerical Mathematics*, vol. 43, no. 4, December, pp. 558-578.

Gao, S. and Lu, H.-Q. (2003) 'A Fast Algorithm for Delaunay based Surface Reconstruction', *Proc. 11th Int. Conf. in Central Europe on Computer Graphics, Visualization and Computer Vision (WSCG 2003), Beijing*, pp. 4 pages.

Godin, G., Laurendeau, D. and Bergevin, R. (2001) 'A Method for the Registration of Attributed Range Images', *Proceedings of the Third International Conference on 3D Digital Imaging and Modeling (3DIM), May 23 - June 1, Québec City, Québec, Canada*, pp. 179-186.

University of Cape Town

Gorte, B. and Pfeifer, N. (2004) 'Structuring laser-scanned trees using 3D mathematical morphology', *Conference proceedings ISPRS conference in Istanbul, Instanbul*, pp. 929-933.

Holies, R.C. and A.Fischler, M. (1981) 'A RANSAC-based approach to model fitting and its application to finding cylinders in range data', *7th International Conference on Artificial Intelligence, September 22-24, Hagenberg, Austria* , pp. 637--643.

Hoppe, H., DeRose, T., Duchampy, T., Halsteadz, M., Jinx, H., McDonaldx, J., Schweitzer, J. and Stuetzlex, W. (1994) 'Piecewise Smooth Surface Reconstruction', *Proceedings of the 21st annual conference on Computer graphics and interactive techniques: International Conference on Computer Graphics and Interactive Techniques*, pp. 295 - 302.

Hoppe, H., DeRose, T., Duchampy, T., McDonaldz, J. and Stuetzlez, W. (1992) 'Surface Reconstruction from Unorganized Points', *Computer graphics*, vol. 26, no. 2, pp. 71 - 78.

Jagannathan, A. and E.L, M. (2007) 'Three-Dimensional Surface Mesh Segmentation Using Curvedness-Based Region Growing Approach', *IEEE Transactionson pattern analysis and machine intelligence*, vol. 26, no. 12, December, pp. 2195-2204.

Jiang, X. and Bunke, H. (1994) 'Fast segmentation of range images into planar regions by scanline grouping', *Machine vision and applications*, vol. 7, no. 2, June, pp. 115-122.

Kang, Z., Zlatanova, S. and Gorte, B. (2007) 'Automatic Registration of Terrestrial Scanning Data Based on Registered Imagery', *Strategic Integration of Surveying Services, FIG Working Week 2007*, May, pp. 1-7.

Khalifa, I., Moussa, M. and Mohamed, K. (2003) 'Range image segmentation using local approximation of scan lines with application', *Machine Vision and Applications (2003) 13: 263–274*, vol. 13, 263–274.

University of Cape Town

Leal, N.E., Lobo, O.O. and Branch, J.W. (2007) 'Improving NURBS Surface Sharp Feature Representation', *International Journal of Computational Intelligence Research*, vol. 3, pp. 131-138.

Liu, Y., Pottmann, H. and Wang, W. (2005) 'Constrained 3D Shape Reconstruction Using a Combination of Surface Fitting and Registration', *Technical Report*, vol. 38, no. 6, August, p. 21 pages.

Luckas, G., Martin, R. and Marshall, D. (1998) 'Faithful least squares fitting of spheres, cones, cylinders and tori for reliable segmentation', *Proceedings of the 5th European Conference on Computer Vision,* pp. 671-686.

Lukacs, G., Marshall, A.D. and Martin, R.R. (1997) 'Geometric Least-Squares Fitting of Spheres, Cylinders, Cones and Tori', *Working paper of the Computer Science Department, University of Wales,* May, pp. 20.

Marc, L., Kari, P., Brian, C., Szymon, R., David, K., Lucas, P., Matt, G., Sean, A., James, D., Jeremy, G., Jonathan, S. and Duane, F. (2000) 'The Digital Michelangelo Project: 3D Scanning of Large Statues', July, pp. 131-144.

Merry, B., Marais, P. and Gain, J. (2006) 'Compression of dense and regular point clouds', *Proceedings of the 4th International Conference on Computer Virtual Reality, Visualisation and Interaction in Africa, February 4-6, Cape Town, South Africa*, pp. 709-716.

Min, J., Powell, M.W. and Bowyer, K.W. (2004) 'Automated Perfomance Evaluation of Range Image Segmentation', *Systems, Man, and Cybernetics, Part B, IEEE Transactions*, vol. 34, no. 1, February, pp. 263- 271.

Mitra, N.J., Gelfand, N., Pottmann, H. and Guibas, L. (2004) 'Registration of Point Cloud Data from a Geometric Optimization Perspective', *Proceedings of the 2004 Eurographics/ACM SIGGRAPH symposium on Geometry processing, June 8-10, Nice, France,* pp. 22 - 31.

University of Cape Town

Mitra, N.J. and Nguyen, A. (2003) 'Estimating Surface Normals in Noisy Point Cloud Data', *Proceedings of the nineteenth annual symposium on Computational geometry: Annual Symposium on Computational Geometry, June 8-10, San Diego, California, USA*, pp. 322 - 328.

Moenning, C. and Dodgson, N.A. (2003) 'Fast Marching Farthest Point Sampling for point cloud and Implicit surfaces', *Technical Report*, pp. 15.

Moenning, C. and Dodgson, N.A. (2004) 'Intrinsic Point cloud Simplification', *Proceedings of the 14th GraphiCon '04, September 6 - 10, Moscow, Russia*, pp. 461-468.

Natonek, E. (1998) 'Fast range image segmentation for servicing robots', *Proceedings. 1998 IEEE International Conference on Robotics and Automation*, pp. 406-411.

Nonlinear Regression and Curve Fitting (2009) 'Website: http: //www.nlreg.com', Last accessed - 27 March 2009

Ohtake, Y., Belyaev, A. and Seidel, H.-P. (2005) 'An Integrating Approach to Meshing Scattered Point Data', *Proceedings of the 2005 ACM symposium on Solid and physical modeling, June 13-15, Cambridge, Massachusetts*, pp. 61 - 69.

Papadimitriou, S., Kitagawa, H., Gibbons, P. and Faloutsos, C. (2003) 'Fast outlier detection using the local correlation integral', *Proceedings. 19th International Conference on Data Engineering, March 5-8, Pittsburgh*, pp. 315-326.

Petitjean, S. (2002) 'A Survey of Methods for Recovering Quadrics in Triangle Meshes', *ACM Computing Surveys*, vol. 34, no. 2, July, pp. 1-61.

Pottman, H., Leopoldseder, S. and Hofer, M. (2004) 'Registration without ICP', *Computer Vision and Image Understanding*, vol. 94, no. 1, pp. 54-71.

Pottmann, H., Leopoldseder, S., Wallner, J. and Peternell, M. (2003) 'Recognition And Reconstruction Of Special Surfaces From Point Clouds', *Archives of the*

University of Cape Town

Photogrammetry, Remote Sensing and Spatial Information Sciences, vol. 36, no. 3A, pp. 271–276.

Pratt, V. (1987) 'Direct Least-Squares Fitting of Algebraic Surfaces', *ACM SIGGRAPH Computer Graphics* , vol. 21, no. 4, June, pp. 145 - 152.

Pulli, K. (1999) 'Multiview Registration for Large Data Sets', 3-D Digital Imaging and Modeling, 1999. *Proceedings. Second International Conference on, October 4-8, Ottawa, Ont., Canada,* pp. 160-168.

Rabbani, T. and van den Heuvel, F. (2004) '3D Industrial Reconstruction by fitting CSG models to a combination of images and point clouds', *Conference proceedings ISPRS conference, Istanbul*, pp. 7-12.

Rabbani, T. and van den Heuvel, F. (2004) 'Methods for Fitting CSG Models to Point Clouds and their Comparison', *Proceedings of Computer Graphics and Imaging, Instanbul*, pp. 279-284.

Rabbanni, T. and van den Heuvel, F. (2005) 'Efficient hough transform for automatic detection of cylinders in point clouds', *Workshop "Laser Scanning 2005"*, September 12-14, p. 6 pages.

Rabbanni, T., van den Heuvel, F. and Vosselman, G. (2006) 'Segmentation of point clouds using smoothness constraint', *ISPRS Commission V Symposium 'Image Engineering and Vision Metrology, September 25-27, Dresden, Germany*, pp. 248-253.

Sappa, A. and Devy, M. (2001) 'Fast range image segmentation by an edge detection strategy', *Third International Conference on 3-D Digital Imaging and Modeling, Quebec City, Que., Canada,* pp. 292 - 299.

Schall, O., Belyaev, A. and Seidel, H.-P. (2005) 'Robust Filtering of Noisy Scattered Point Data', *Point-Based Graphics, 2005. Eurographics/IEEE VGTC Symposium Proceedings, June 20-21,* pp. 171-144.

University of Cape Town

Schnabel, R. and Klein, R. (2006) 'Octree-based Point-Cloud Compression', I*n proceedings of Symposium on Point-Based Graphics 2006, Eurographics, June 21 - 22, New York, USA.*, pp. 11 pages.

Schnabel, R., Wahl, R. and Klein, R. (2007) 'Efficient RANSAC for Point-Cloud Shape Detection', *Computer Graphics Forum*, vol. 26, no. 2, May, pp. 214-226.

Sharp, G.C., Lee, S.W. and Wehez, D.K. (2000) 'ICP Registration using Invariant Features', *Pattern Analysis and Machine Intelligence, IEEE Transactions on*, pp. 90-102.

Sithole, G. (2005) 'Segmentation and classification of airborne Laser Scanner Data', *Phd Thesis, TU Delft*, pp. 65-92.

Sotoodeh, S. (2006) 'Outlier detection in laser scanner point clouds', *ISPRS Commission V Symposium 'Image Engineering and Vision Metrology, September 25-27, Dresden*, pp. 6 pages.

Süßmuth, J. and Greiner, a.G. (2007) 'Ridge Based Curve and Surface Reconstruction', *Proceedings of the fifth Eurographics symposium on Geometry processing: ACM International Conference Proceeding Series, Vol. 257, July 4-6, Barcelona, Spain*, pp. 243 - 251.

Tangelder, J., Ermes, P., Vosselman, G. and van den Heuvel, F. (1999) 'Fitting parameterised object models to gradient Images', *Prooceedings of the 5th ASCI Conference, June 15-17, Heijen, Netherlands*, pp. 449-456.

Tangelder, J.W., Ermes, P., Vosselman, G. and Van den Heuvel, F.A. (2003) 'CAD Based Photogrametry for Reverse Engineering of Industrial Installations', *Computer-Aided Civil and Infrastructure Engineering*, vol. 18, no. 4, pp. 264-274.

Tangelder, J., Vosselman, G. and van den Heuvel, F.A.v.d. (2000) 'Object-Oriented measurement of pipe systems using edge matching and CSG models with constraints',

University of Cape Town

International Archives of Photogrammetry, Remote Sensing and Spatial Information Sciences, vol. 33, part B5/2, pp. 132-139.

Teutsch, C., Berndt, D., Trostmann, E. and Weber, M. (2005) 'Efficient Reconstruction of Nurbs Surfaces for Shape Analysis and Surface Inspection', *Proc. of Optical 3-D Measurement Techniques VII, October 3-5, Vienna, Austria,* pp. 144-153.

Theory and practice on Terrestrial Laser Scanning, *Training material based on practical applications: 3D Risk Mapping, 2008*.

van den Heuvel, F.A. (2000) 'Trends in cad-based photogrammetric measurement', *International Archives of Photogrammetry and Remote Sensing*, vol. 33, pp. 852-863.

Veldhuis, H. and Vosselman, G. (1998) 'The 3D reconstruction of straight and curved pipes using digital line photogrammetry', *ISPRS Journal of Photogrammetry & Remote Sensing*, vol. 52, no. 1, February, pp. 6-16.

Vieira, A.W., Velho, L., Lopes, H., Tavares, G. and Lewiner, T. (2003) 'Fast Stellar Mesh Simplification', *Brazilian Symposium on Computer Graphics and Image Processing, October 12-15, Rio de Janeiro*, pp. 27-34.

Vosselman, G. (2001) 'Semi-Automatic CAD Based reconstruction of Industrial Installations', *Künstliche Intelligenz 4*, pp. 23-27.

Vosselman, G., Gorte, B., Sithole, G. and Rabbani, T. (2004) 'Recognising structure in laser scanner point clouds', *The International Archives of the Photogrammetry, Remote Sensing and Spatial Information Sciences*, vol. 46, part 8/W2, October, pp. 33-38.

Wang, W., Pottmann2, H. and Liu, Y. (2004) 'Fitting B-Spline Curves to Point Clouds by Squared Distance Minimization', *Technical Report*, p. 16 pages.

University of Cape Town

Wendt, A. (2004) 'On the automation of the registration of point clouds using the metropolis algorithm', *ISPRS Congress Istanbul 2004, Proceedings of Commission III, Instanbul*, pp. 106-111.

Werghi, N., Fisher, R., Ashbrook, A. and Robertson, C. (1999) 'Faithful recovering of quadric surfaces from 3D range data', *Second International Conference on 3-D Digital Imaging and Modeling, Ottawa, Ont., Canada*, pp. 280 - 289.

Witzgall, C. and Cheok, G.S. (2002) 'Experience with Point Cloud Registration', *International Symposium on Automation and Robotics in Construction, 19th (ISARC). Proceedings, September 23 -25, Gaithersburg*, pp.349-355.

Yang, L., Helmut, P. and Wenping, W. (2005) 'Constrained 3D Shape Reconstruction Using a Combination of Surface Fitting and Registration', *Technical Report*, September 2005.

Zhou, X. and Lu, J. (2005) 'NURBS-based Galerkin method and application to skeletal muscle modeling', *Proceedings of the 2005 ACM symposium on Solid and physical modeling*, pp. 71 - 78.

Ziuriene, R. (2004) 'Representation and Modelling of 3D objects in Different CAD Systems', *The Journal of Polish Society for Geometry and Engineeering Graphics*, vol. 14, pp. 70-75.

University of Cape Town

APPENDICES

Appendix A: Segmentation results

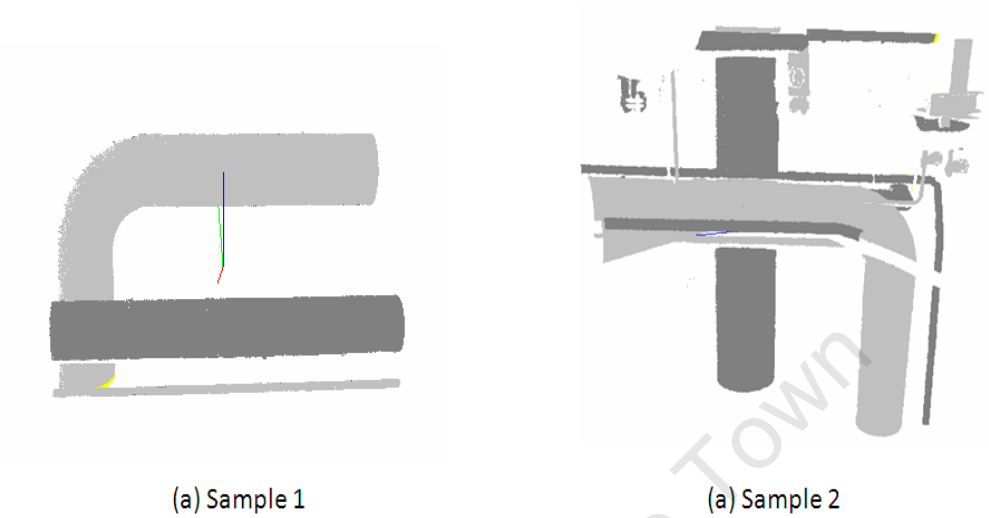

Figure 1 Sample 1 and 2

Sample 1

Point spacing	Stack count	Method of profile segmentation	Profile width (m)	Distance threshold (m)	Curvature threshold
<0.006m	4	Proximity segmentation	0.01	0.008	N/A

Sample 2

Point spacing	Stack count	Method of profile segmentation	Profile width (m)	Distance threshold (m)	Curvature threshold
<0.006m	4	Proximity/ Curve fitting	0.01	0.008	10

University of Cape Town

(c) Sample 3 (d) Sample 3

Figure 2 Samples 3 and 4

Sample 3

Point spacing	Stack count	Method of profile segmentation	Profile width (m)	Distance threshold (m)	Curvature threshold
<0.006m	4	Proximity/ Curve fitting	0.02	0.01	10

Sample 4

Point spacing	Stack count	Method of profile segmentation	Profile width (m)	Distance threshold (m)	Curvature threshold
<0.006m	4	Proximity/ Curve fitting	0.02	0.01	10

University of Cape Town

Appendix B: Effect of radius on detecting pipe axis

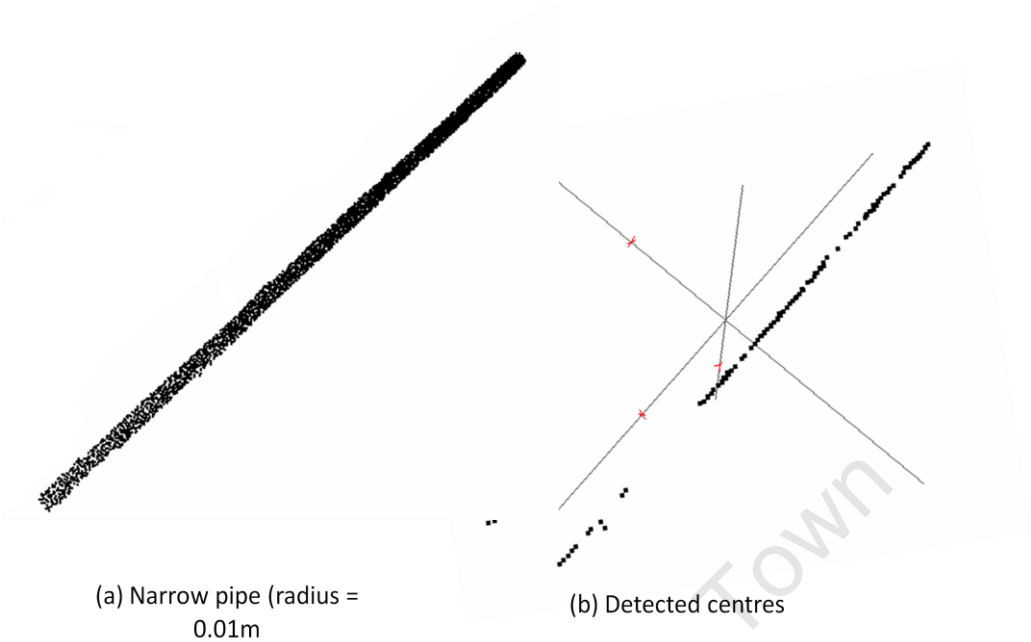

Figure 1 (a) Small radius pipe (b) Detected centres: Fewer centres as a result of ellipse fitting ambiguity

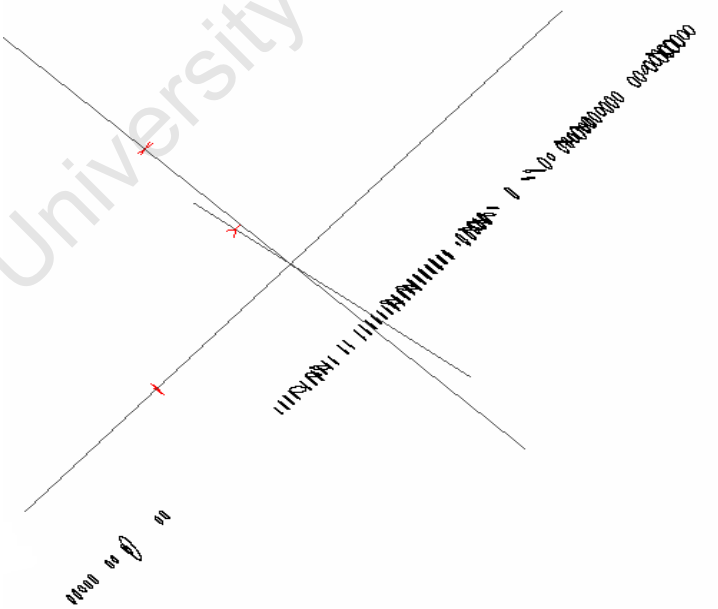

Figure 2 Fewer ellipses selected

University of Cape Town

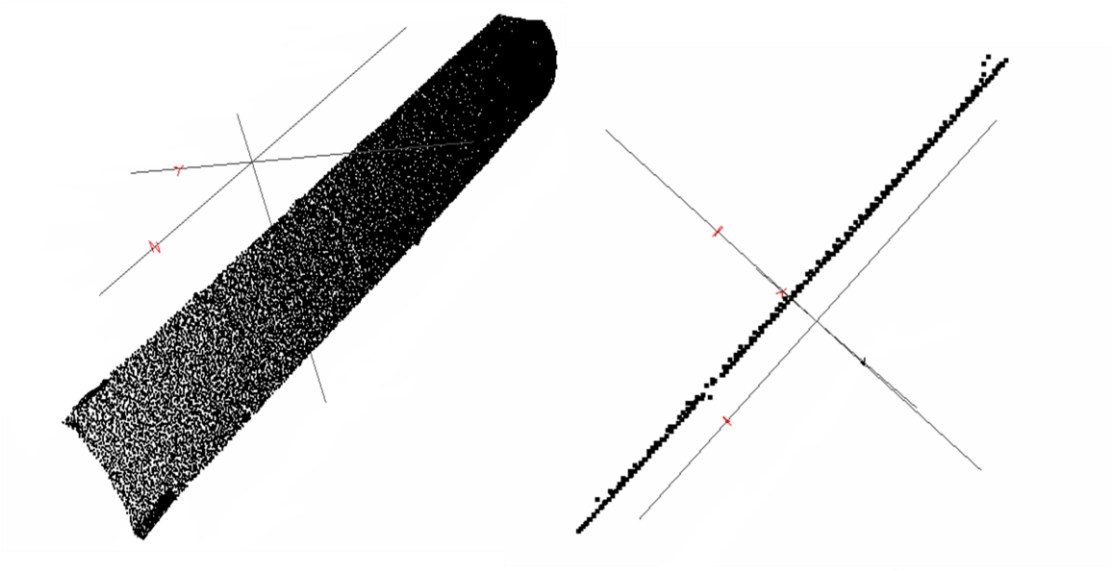

(a) Larger radius pipe (radius = 0.17m)

(b) Detected centres

Figure 3 (a) large radius pipe (b) Detected centres: More centres selected compared to narrow pipe

Figure 4 Selected ellipses: more ellipses selected.

University of Cape Town

Appendix C: Effect of narrow pipes on approximating radii values

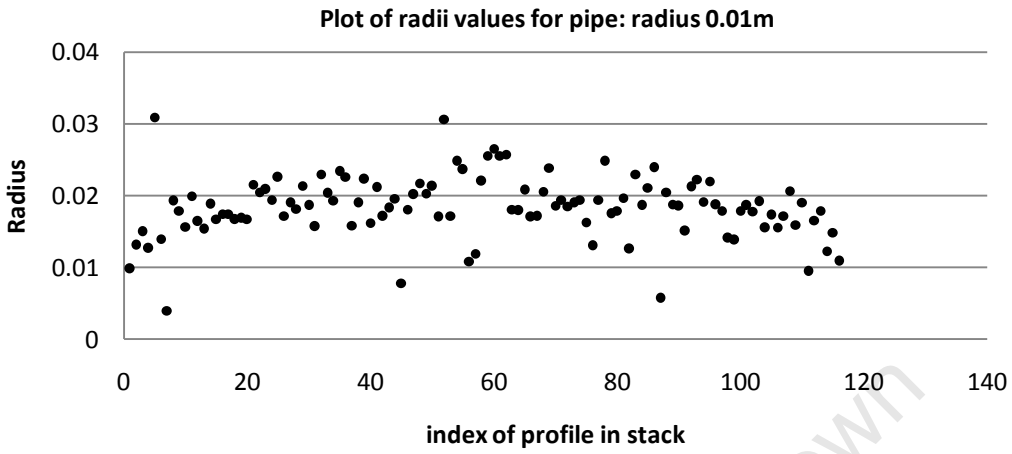

Figure 1 Plot of radii values for narrow pipe (radius = 0.01m): Radius unstable

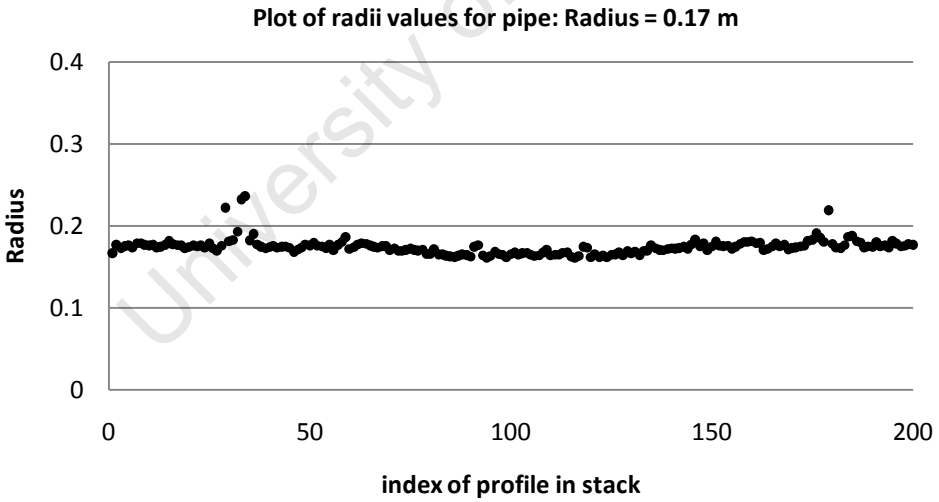

Figure 2 Plot of radii values for larger pipe (radius = 0.17m): Radius values more precise

University of Cape Town